Chain dynamics as a measure for internal friction in the intrinsically disordered protein alpha-synuclein

Master thesis at the department of Biomedical Engineering
Faculty of Science and Technology
Nanobiophysics group
University of Twente
30-06-2022

Author:
Anamaria Boamfa

Graduation Committee:
Prof. dr. M.M.A.E. Claessens
Dr. C. Blum
Dr. C. Otto
Dr.ir. S.A. Semerdzhiev
Msc. G. Heesink

UNIVERSITY OF TWENTE.

Abstract

Intrinsically disordered proteins (IDPs) are proteins that lack a fixed three-dimensional structure, there is no folding of the protein into a secondary or tertiary structure. In general, IDPs have a dynamic conformation flexibility, meaning that their shape changes over time. The conformational dynamics of IDPs are still poorly understood.

The protein alpha-synuclein (αS) is an IDP that is linked to neurodegenerative diseases such as Parkinson's and dementia with Lewy bodies. It is known that many mechanisms are of influence on the aggregation behaviour of αS, however, the exact cause or trigger that originates the formation of αS aggregates is not yet clearly understood. One factor of influence is the change in conformational dynamics of the protein due to environmental factors.

This thesis aims to obtain more fundamental insight into the chain dynamics of αS monomers, in order to get a better understanding of the protein and its aggregation behaviour.

The dynamics of αS are investigated with nanosecond Fluorescence Correlation Spectroscopy (nsFCS) in combination with single-molecule Forster Resonance Energy Transfer (smFRET). With these techniques, the reconfiguration time of the protein is determined for the N-terminus, NAC region and the C-terminus of the protein. The reconfiguration time is used to study the conformation dynamics of the protein and its change in different solvents. This is a useful tool to better understand the initiation of αS aggregation.

Experimentally it is shown that αS exhibits different behaviour in chain dynamics for different regions of the protein. For the N-terminus, it is observed that the reconfiguration time decreases with increasing viscosity, a fact that could not be explained by the theory. For the NAC region, the reconfiguration time does increase with increasing viscosity. This part of the protein behaves like a random coil where solvent-dependent friction increases with increasing solvent viscosity. The C-terminus shows no overall change in reconfiguration time for increasing viscosity. This could be the result of less surface exposure to the solvent, leading to a minimal or absence of change in solvent-dependent friction. Additionally, it is shown that denaturation of αS leads to faster chain dynamics and induction of secondary structure leads to slower chain dynamics.

These results give insight into the reconfiguration time of αS. It is proven that the technique of nsFCS in combination with smFRET poses a promising way to study the effect of different solvents and situations on the dynamics of the intrinsically disordered protein alpha-synuclein.

In the future, this technique can be used to couple conditions or binding partners that induce protein aggregation to a change in protein chain dynamics.

Acknowledgements

During my thesis I had the opportunity to work in the NBP group, a very diverse and interesting group. Apart from the interesting research topic and beautiful technologies that I worked with, I also had the opportunity to work together with great people.

First of all my great thanks to my daily supervisors Gobert Heesink and Slav Semerdzhiev. I appreciate all your assistance and all the advice that you have given me during my thesis. Thank you for all the good discussions and for having the patience to listen to all of my questions. You really helped me a lot.

I would like to thank Mireille Claessens and Christian Blum for their great insights and guidance during my thesis. You helped me to look further, you gave new insights and suggested other experimental approaches when I got stuck in surprising and seemingly unlogic results. You pushed me to look and dig further into the how's and whys of everything.

I also want to thank Cees Otto for being the external member of my graduation committee.

I want to thank Kirsten van Leijenhorst-Groener who helped me around the chemical lab and Robert Molenaar for his assistance in the optics lab.

Many thanks to my family who are my greatest support and always believe in me.

Last, I want to thank everyone from the NBP group for making me feel at home, I have learned a lot from many good discussions and talks with many of you.

Table of contents

Abstract 3
Acknowledgements 5
List of abbreviations 9
1. Introduction 11
2. Theoretical background 13
2.1 The intrinsically disordered protein αS 13
2.2 Polymer physics 14
2.3 Influence of solvent additives on protein dynamics 16
2.4 Rouse model 18
2.5 Fluorescence 20
2.6 Förster resonance energy transfer 23
2.7 Fluorescence correlation spectroscopy 26
2.8 Nano second FCS 27
2.9 nsFCS and smFRET 28
3. Materials and Methods 31
3.1 Samples 31
3.2 Sample preparation 31
3.3 General measurement setup 33
3.4 General notes 35
3.5 FCS measurements 35
3.6 FCCS measurements 36
3.7 smFRET measurements 36
3.8 nsFCS measurements 37
4. Data analysis 39
4.1 FCS analysis 39
4.2 FCCS analysis 39
4.3 Processing of raw data in Python 41
4.4 smFRET analysis 41
4.5 nsFCS analysis 46
5. Validation of setup and data analysis for smFRET and nsFCS 51
5.1 smFRET 51
5.2 nsFCS 52
6. smFRET and nsFCS on FRET labelled αS 61
6.1 Sample FRET labelling efficiency 61
6.2 Determining the mean FRET efficiency of αS with smFRET 62

6.3 Determining the reconfiguration time of αS with nsFCS 64
7. Chain dynamics of αS 69
7.1 Internal friction of αS 69
7.2 Influence of glycerol on protein compactness 70
7.3 Viscosity of αS environment 72
7.4 Viscosity corrected influence on chain dynamics 74
7.5 Influence of solvent additives on protein dynamics 75
8. General conclusion and discussion 81
9. Outlook and recommendations 83
Bibliography 85
Appendix A - Labelling of PEG 91
Appendix B - Influence of glycerol on αS aggregation 95

List of abbreviations

αS	Alpha synuclein
AF	Alexa Fluor
BSA	Bovine serum albumin
dsDNA	Double stranded DNA
DTT	Dithiothreitol
HFIP	Hexafluoroisopropanol
IDP	Intrinsically disordered protein
FCCS	Fluorescence cross correlation spectroscopy
FCS	Fluorescence correlation spectroscopy
FRET	Förster resonance energy transfer
PBS	Phosphate-buffered saline
PIE	Pulse-interleaved excitation
nsFCS	Nano second FCS
smFRET	Single molecule FRET
ssDNA	Single stranded DNA
TCSPC	Time-correlated single photon counting
ThT	Thioflavin T

1. Introduction

Alpha-synuclein (αS) is a protein that is present in the human body, it is mainly found in the brain[1]. Its function and behaviour are poorly understood, however, it is shown to be linked to neurodegenerative diseases such as Parkinson's disease and dementia with Lewy bodies[2]. A pathology that is often expressed in patients who suffer from these diseases is the presence of αS aggregates, deposits of many αS proteins that have clumped together. The αS aggregates lead to the impairment of neuronal functions and thus lead to neurodegeneration. This can affect the functionality of the brain, leading to the classical symptoms that are seen in patients, such as motor dysfunction and memory problems. Parkinson's disease and Lewy body dementia are the second most common neurodegenerative disease, after Alzheimer's disease. Nowadays there exist various drugs and treatments that relieve the symptoms and improve or maintain the quality of life for patients. However, due to the complexity and lack of knowledge on the underlying molecular mechanisms of disease and αS aggregation onset, there is not yet a cure for these diseases.
It is known that many mechanisms are of influence on the aggregation behaviour of αS. One of them is the conformational dynamics of the protein, which is affected by certain solvents, solvent additives and the presence of certain proteins[3,4]. It is speculated that changes in the conformational dynamics of the protein create a more favourable or unfavourable condition for aggregation initiation and progression.
The knowledge of the dynamics and dynamical changes in αS is minimal. Therefore, this thesis aims to obtain more fundamental insight into the protein dynamics of αS monomers to better understand the protein and its aggregation behaviour.

The conformational dynamics of the αS protein arise from its nature, αS is an intrinsically disordered protein (IDP). An IDP lacks a fixed three-dimensional structure, so there is no folding of the protein into a secondary or tertiary structure. In general, IDPs have a dynamic conformation flexibility, meaning that their shape changes over time.
A protein, or IDP, can show internal motion on different time and length scales. It has been shown that for αS three types of internal motion can be distinguished[3]. First of all, there are fast motions present, in the timescale of sub 2ns. These are caused by local fluctuations of the backbone orientation of the protein. The second order of motion is related to segmental dynamics. This means that the chain of the protein moves differently in some parts than others, it is in the order of 10ns.
The third order of motion is the global chain reconfiguration time of the protein structure. This gives the time until complete decorrelation of the end-to-end positions of the protein occurs. The average time before the protein reconfigures is in the order of 60ns but is highly dependent on environmental factors.
This last timescale of dynamics gives information about the internal friction of the protein. The subject of this thesis focuses on using the chain reconfiguration time of αS to quantify and map the internal friction along the αS protein chain to get more insight into its dynamics. This is done with the use of nanosecond Fluorescence Correlation Spectroscopy (nsFCS) in combination with single-molecule Forster Resonance Energy Transfer (smFRET).

In this thesis, first information is provided on the structure of the αS protein and the physics behind the behaviour, followed by the aforementioned microscopic techniques. In the following chapters, information is given on the experimental setup, measurement procedures and data analysis. Finally, the results of the experiments are shown and provided with a discussion.

2. Theoretical background

In this chapter, all underlying theory that is of interest for this thesis will be explained. First, background information is given on the αS protein together with a brief introduction to polymer physics. This is followed by the principles of fluorescence and the techniques which use fluorescence to study single molecules and protein dynamics.

2.1 The intrinsically disordered protein αS

The αS protein consists of 140 amino acids where three regions can be identified; the N-terminus, the NAC-region and the C-terminus[1], see Figure 1 and Figure 2.

The N-terminus carries both positive and negative charges but is net positively charged. This region can interact with cell membranes by binding to lipid bilayers, it contains amino acids 1 to 60.

The hydrophilic NAC-region contains amino acids 61 to 95. This is the region that is most associated with aggregation and fibril formation due to the formation of β-structures which is a precessor of aggregation[1].

The C-terminus, amino acid 96 to 140, has a low hydrophobicity and a high net negative charge. This causes it to have a random coil structure. It is speculated that interaction between the C-terminus and the NAC-region inhibits aggregation[1].

When studying the dynamics of several regions of the αS protein it is important to keep the nature of the chemical structure of the protein backbone in mind, since each region can express a different behaviour due to chemical and structural differences.

Figure 1: Schematical representation of the regions of alpha synuclein[5]

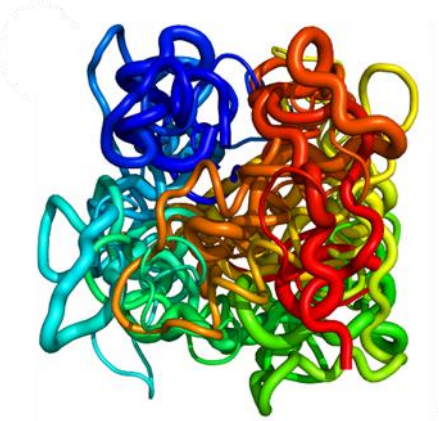

Figure 2: Conformational ensemble of αS in solution as determined by simulations[6]

Experiments have shown that αS is not an ordered protein since it lacks a fixed three-dimensional structure, and undergoes conformational changes over time[7]. Therefore, the αS protein is considered an IDP.

Very globally said an IDP has a certain conformation, then undergoes a slight conformational change and has another configuration. The conformation of a protein does not change instantly, the correlation of the end-to-end position of the protein changes constantly. The time until complete decorrelation of motion occurs is denoted as the reconfiguration time, t_r.

2.2 Polymer physics

2.2.1 Gaussian chain model

Because αS is assumed to be an IDP, which is a polymer consisting of amino acids. Therefore, models that have been developed to describe the behaviour of homopolymers can also be applied to IDPs.
The most simple polymer model is the Gaussian chain model, which gives an approximation of the end-to-end distance of a protein[8]. This model describes a polymer as an ideal chain which consists of a fixed number of monomers that are modelled as rigid rods, see Figure 3. The orientation of a monomer is independent of its neighbouring monomers. The excluded volume effect is not taken into account, and it is assumed that there are no attractive or repulsive interactions within the chain. The motion of the monomers is thus only a result of Brownian motion where the probability to move in a direction is thus equal for all directions.
This random nature of the monomers gives rise to a global structure of the overall polymer that changes with t_r.

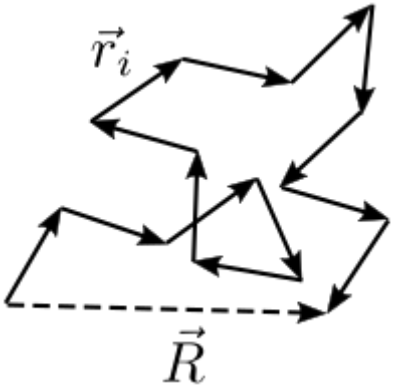

Figure 3: Graphic representation of the Gaussian chain model, with $\vec{r}$ the vector of a monomer and $\vec{R}$ the total end-to-end vector [9]

The Gaussian chain model gives the probability that a polymer chain has a certain end-to-end distance between two locations on the chain[10]:

$$P(r) = 4\pi r^2 \left(\frac{3}{2\pi\langle r^2\rangle}\right)^{\frac{3}{2}} \exp\left(-\frac{3}{2}\frac{r^2}{\langle r^2\rangle}\right) \quad (1)$$

With P(r) the probability density, r the end-to-end distance and $\langle r^2\rangle$ is the mean squared end-to-end distance between two locations on the polymer.

2.2.2 Internal friction

The αS protein is shown to be in good agreement with the Gaussian chain model[7]. However, αS does not behave strictly like a Gaussian chain, due to the occurrence of interactions along the chain between monomer segments. For repulsive interaction this causes dissipation of energy to the solvent that results in the dynamics of the polymer chain to be slowed down in certain positions, this is denoted as internal friction.
It is good to note that two types of friction can be distinguished for a protein, solvent-dependent and solvent-independent friction. The solvent-independent friction is of interest for this thesis, since it is a result of transient intra-molecular interactions.
Solvent-depended friction is caused by different solvents that interact with or alter the protein structure and cause a change in the overall chain dynamics. The viscosity of a solvent also plays a role in the dynamics, the relation between viscosity and dynamics is inversely linear. A more viscous environment slows down the overall motion of the polymer chain because with the same energy less solvent can be displaced due to the higher deformation resistance of the viscous fluid.
The solvent-independent friction, or internal friction, is the friction present at zero viscosity[11]. The cause of this friction component is quite complex and not completely understood. New insights

based on different polymer models speculate that internal friction is caused by a collection of events. These are mainly the dihedral angle transition and the intrachain interaction, of which the relative contribution is influenced by the compaction of the protein[12,13,14].

For the understanding of the two principles that cause internal friction, some understanding is needed of the chemical structure of a protein. The protein backbone is a three-dimensional structure, where atoms are bound to each other in a certain manner, see Figure 4. This structure consists of different two-dimensional planes, created by the backbone and its side groups. The angles between the different planes of the protein backbone are called dihedral angles, they represent the torsion angles between different bonds. Dihedral angle transition or rotation is the movement in a twisting motion between the covalent bonds of the protein backbone.
Intrachain interaction arises from collisions of the protein with itself, or the formation and breaking of physical intrachain interaction. When a protein is more compact, the backbone is partially shielded from the solvent, which causes physical intrachain interactions to occur more easily. The collision of the protein with itself causes small motions where some solvent is displaced.
The compaction of the protein is altered by the goodness of the solvent that the protein resides in. A good solvent is a solvent where it is energetically favourable for the monomers of the protein to interact with the solvent, so expansion of the polymer occurs. In a poor solvent, it is more energetically favourable for the monomers to interact with each other, resulting in compaction.
At higher protein compaction the intrachain friction dominates, while at low compaction the chain interacts less with itself and the friction arising from dihedral angle transitions dominates. An additional phenomenon for more compact proteins is that the solvent interacts less with the protein since less surface area is exposed to the solvent, causing a decrease in solvent friction[13].

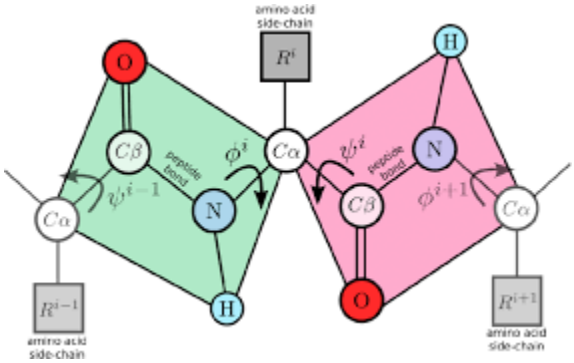

Figure 4: Schematic representation of the three-dimensional molecule structure, the coloured areas show the two-dimensional planes within the molecule, φ and ψ represent two dihedral angles between planes[15]

Induction of secondary structure in αS, due to a different solvent or a binding partner, can alter the internal friction and thus the chain dynamics. It is speculated that a change in the dynamics of the αS protein in certain positions facilitates or inhibits aggregation. Localizing and quantifying the friction and the relation of these parameters when αS is introduced to a different solvent or binding partner can give insight into the process of aggregation. In this thesis, the influence of different solvents on the change of αS dynamics is investigated.

2.3 Influence of solvent additives on protein dynamics

Different molecules can influence the secondary structure of a protein. When a protein resides in a solvent consisting of water and certain additional molecules, these can interact with each other and result in a change in protein chain dynamics.

Solvents can cause the breaking of hydrogen bonds, leading to the loss of the secondary protein structure. This leads to unfolding of the protein, and thus to faster dynamics where dihedral angle transition dominates. Other solvents can cause compaction of the protein, which stiffens the protein due to an increase in intrachain reactions, which leads to slower dynamics. In this chapter, the influence of several solvent additives on αS is explained.

2.3.1 Glycerol

Glycerol or propane-1,2,3-triol, see Figure 5, is a highly viscous polyol compound[16]. It can be added to a solvent to increase its viscosity and is commonly used to slow down molecular dynamics in dynamical studies[17]. It has been shown that solvents containing below 5M of glycerol, equal to 41v%, have little effect on the secondary structure of αS[18]. However, at higher concentrations, glycerol induces folding or compaction of the protein[18]. With the addition of glycerol, below 5M, it is expected that only the solvent friction increases, causing the dynamics of αS to be slowed down due to the higher viscosity of the environment, while no structural changes occur.

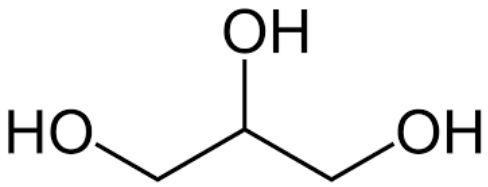

Figure 5: Molecular structure of glycerol[19]

2.3.2 Urea

Urea is an organic compound, see Figure 6, that can denature proteins by binding to their backbone and form hydrogen bonds with water. It disrupts hydrogen bonds that form the secondary structure of a protein and it acts as a surfactant, causing the denaturation of hydrophobic regions[20]. These phenomena cause a protein to lose any form of secondary structure present and as a result, the protein expands. The denaturing effect of urea is linear with increasing concentration.
For an ordered protein the effect of urea is large, it transits from a completely folded to an unfolded state. However, for an intrinsically disordered protein, the effect is smaller since there is originally no or little secondary structure present.
αS has some secondary structure, in presence of urea, the present hydrogen bonds will be broken. This can result in an expansion of the structure, which causes a decrease in internal friction. This in turn leads to a different dynamical behaviour of the protein. When hydrogen bonds are broken, the monomers of the protein can move more freely, thus faster dynamics are expected.

When performing dynamical studies with urea, not only the denaturation properties need to be taken into account, but also an increase in viscosity. Solvents containing 8M urea have a higher viscosity than pure water, at 20°C it is equal to 1.26 mPa·s[21]. For the best comparison in dynamical change, the effect of a solvent that contains urea should be compared to a water-glycerol mixture that is equal in viscosity.

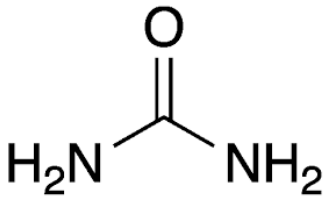

Figure 6: Molecule structure of urea[22]

2.3.3 Hexafluoroisopropanol

Hexafluoroisopropanol (HFIP) is a polar fluoralcohol, see Figure 7 for its molecular structure[23]. It has strong hydrogen bonding properties, meaning that it can easily form hydrogen bonds with molecules or polymers. This also causes an increased dissolution of hydrogens bond acceptors, such as amides and ethers. Its strong hydrogen bonding properties make HFIP suitable to solubilize peptides and monomerize beta-sheet aggregates.

A property of HFIP is that it induces alpha-helix formation in ordered and disordered protein monomers[24]. A hydrophobic part of a protein finds itself in a compact state when exposed to a watery environment, HFIP can bind to such a hydrophobic part due to its hydrogen bonding properties. HFIP is thus a molecule that can induce conformational changes in a protein and alter the chain dynamics.

When the αS protein is introduced to a solvent containing HFiP it also undergoes a structural change[25]. At 0 to 3% of HFIP the protein transitions from unfolded to partially folded. At a 3 to 10% it transitions from partially folded to an α-helical conformation. For higher concentrations there occurs rearrangement of the α-helical species. The partially folded structure of αS is highly prone to aggregate. At HFIP concentration of 0 to 5%, there is a decrease in aggregation lag time. However, for concentrations of 20% or above of HFIP αS monomers stabilise and do not aggregate at all.

The structural change induced by HFIP is strongest in the hydrophobic part of the protein, where the protein is most likely to form hydrogen bonds with HFIP, for αS this is the NAC-region.

When secordary structure in αS is induced due to helix formation upon the introduction of HFIP, the internal friction increases. It is expected to see slower dynamics with the addition of HFIP to αS.

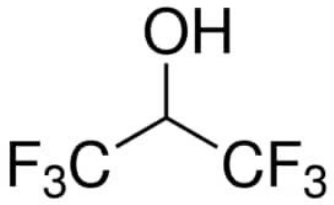

Figure 7: Molecule structure of HFIP[26]

2.4 Rouse model

The Rouse model with some additional extensions can be used to model the dynamics of a protein[12]. The dynamics are defined by the reconfiguration time of the protein, which can be separated into two components, corresponding to the two types of friction that the protein experiences, solvent and internal friction.

The classical Rouse model describes the conformational dynamics of an ideal polymer chain. Like the Gaussian chain model, it describes the polymer as a fixed number of segments, N+1, that are connected by N bonds that can be modelled as harmonic springs[12]. Each segment consists of multiple monomers that follow Gaussian chain statistics. The length of a segment is taken to be equal to the Kuhn length, it is the hypothetical length that can be considered as freely joined.
Because of this, the mean squared end-to-end distance of two locations on the polymer is defined as follows:

$$\langle r^2 \rangle = N\, b^2 \tag{2}$$

With $\langle r^2 \rangle$ the mean squared end-to-end distance, N the number of Kuhn segments and b the length of the segment.

On each segment a force is exerted:

$$\boldsymbol{f_{bk}} = \boldsymbol{f_{ek}} + \boldsymbol{f_{sk}} \tag{3}$$

Where k is the position of the monomer, $\mathbf{f}_{bk}$ is the Brownian motion force which is due to the collision of monomers with solvent molecules, $\mathbf{f}_{ek}$ is the elastic force between the monomers and $\mathbf{f}_{sk}$ is a frictional force that arises due to the diffusion of the monomers.

The frictional force is given by stokes law, under the assumption that the interaction due to solvent friction is only localized in individual monomers:

$$\boldsymbol{f}_{sk} = \zeta_s \boldsymbol{r}_k \tag{4}$$
$$\text{with } \zeta_s = 6\pi\eta a \tag{5}$$

Where $\mathbf{r}_k$ is the position and ζ_s the solvent friction coefficient, which is determined by the solvent viscosity, η, and the hydrodynamic radius, a, of the monomer.

The reconfiguration time of the system is described as:

$$\tau_q = \frac{\zeta_s}{\alpha q^2} \tag{6}$$

With τ_q the mode-dependent reconfiguration time of the chain, α the stiffness of harmonic bond potentials between two neighbouring monomers and q the inverse wavelength of the mode that the polymer resides in. The mode is used to describe the relative vibrational motion of the atoms within a molecule, which have a vibrational wavelength.

Since the classical Rouse model takes only the solvent friction into account, the model can be extended to include internal friction, giving the Rouse model with internal friction (RIF)[27]. The RIF model assumes that internal friction arises from bond rotation processes between monomers, and only acts on individual bonds. The internal friction is therefore an accumulation of the bond rotations along the polymer chain.
In the RIF model the solvent friction coefficient ζ_s, is replaced by an effective friction coefficient, ζ_{eff}, that includes both the solvent- and internal friction, ζ_s and ζ_i:

$$\zeta_{eff} = \zeta_s + q^2 \zeta_i \tag{7}$$

The vibrational mode-dependent reconfiguration time of the chain can be described in terms of internal friction:

$$\tau_q = \frac{\zeta_s}{\alpha q^2} + \frac{\zeta_i}{\alpha} \quad (8)$$

For the quantification of internal friction, the longest relaxation time is of interest. This corresponds to a mode number of one, q=1. The solvent friction is viscosity dependent and the internal friction not, therefore equation (8) can be written to:

$$\tau_r = \frac{\eta}{\eta_0}\tau_s(\eta_0) + \tau_i \quad (9)$$

With τ_r the reconfiguration time η viscosity of the solvent and η_0 the viscosity of water, τ_s the solvent-dependent time and τ_i the internal friction time[17].

In the theoretical situation where the viscosity of the solvent would be equal to zero, the reconfiguration time of the polymer chain is equal to the internal friction component. However, it is not possible to obtain a solvent with a viscosity of zero. To obtain the reconfiguration time at zero viscosity for a protein in solution, the reconfiguration time can be measured for different solvent viscosities. When plotting τ_r against the solution viscosity, see Figure 8, the fit of the data points can be extrapolated to a viscosity of zero to obtain τ_i:

$$\tau_r = a \langle r^2 \rangle \frac{\eta}{\eta_0} + \tau_i \quad (10)$$

Where a is a global fit parameter.

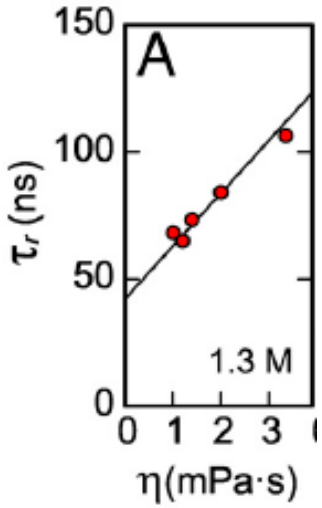

Figure 8: determining of internal friction timescale[17]

A manner to measure the reconfiguration time of a polymer, and determine its internal friction, is by combining the technique of nanosecond Fluorescence Correlation spectroscopy (nsFCS) with single-molecule Forster resonance energy transfer (smFRET)[17].
In the following chapters, the underlying theory of the techniques is explained in detail. First, the principle of fluorescence is explained, followed by the smFRET and nsFCS techniques and the combination thereof that is used to investigate the chain dynamics of a protein.

2.5 Fluorescence

Fluorescence is a physical phenomenon, it is the emission of light by molecules that have absorbed energy in the form of electromagnetic radiation[28]. Molecules that fluoresce are called fluorophores, when they are shown upon with light of a certain wavelength, an electron present in the molecule can absorb the energy of the light and is excited to a higher energy state. However, for the fluorophore, it is thereafter energetically favourable to go back to the original ground state. For this to happen, the excited electron needs to lose its energy. It generally first returns to the ground state of the excited state by vibrational relaxation, see Figure 9. Then the electron falls back to the ground state through non-radiative decay, the energy is transformed to heat or vibrational energy, or through radiative decay, by emitting a photon. This last phenomenon is denoted as fluorescence.
Another possibility for the electron to lose its energy is by quenching, its energy is transferred to another electron on another molecule. The last possibility for the electron for deexcitation is delayed fluorescence. The electron undergoes intersystem crossing and resides in its triplet state. Thereafter phosphorescence occurs or the electron loses its energy non-radiatively. The probability of transition to the triplet state is low and decreases with decreasing laser power.

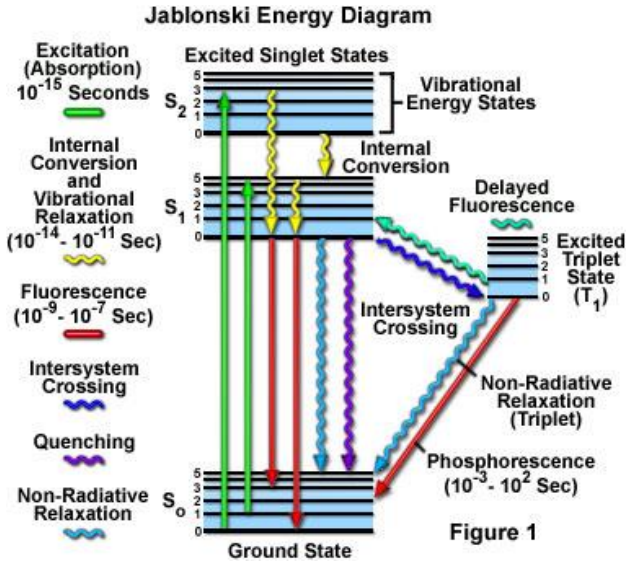

Figure 9: Principle of fluorescence containing excitation, non-radiative and radiative decay and excitation to the triplet state[29]

2.5.1 Fluorophores

There exist many different fluorophores that each can be excited with a different wavelength range. The energy of the emission photons is always lower than the excitation photons, due to internal energy loss in the form of vibrational energy. Subsequently, the emission wavelength is always higher than the excitation wavelength. Figure 10 shows a schematical representation of the excitation and emission spectrum of a fluorophore.

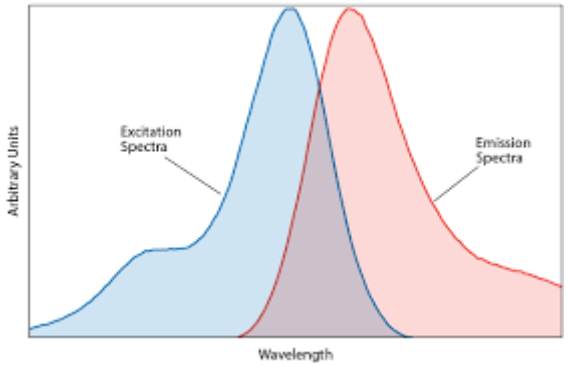

Figure 10: Schematical representation of the spectrum of a fluorophore[30]

Fluorophores are characterised by two properties, their quantum yield, η, and fluorescence lifetime, τ.
The quantum yield defines the ratio between the number of photons that are absorbed and emitted by the fluorophore. It is the efficiency of the energy loss by radiative energy transfer:

$$\eta = \frac{\#\ emitted\ photons}{\#absorbed\ photons} \tag{11}$$

The fluorescent lifetime is the average time that a fluorophore spends in the excited state. Since fluorescence is a stochastic process, the fluorescent lifetime has a small distribution. When exiting a large number of the same fluorophores, the resulting emission intensity can be plotted over time, see Figure 11. The decay of the resulting curve is used to determine the mean lifetime of the fluorophore present in a sample:

$$I(t) = I(0)e^{-\frac{t}{\tau}} \tag{12}$$

With I intensity, t time and τ the lifetime.

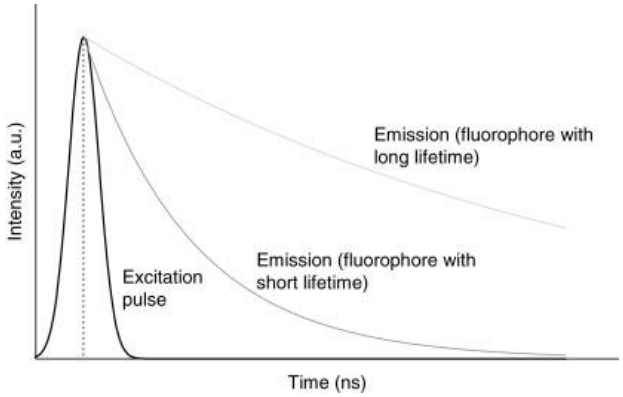

Figure 11: Representation of fluorescent lifetime[31]

The lifetime of a fluorophore is independent of the excitation wavelength and intensity but does depend on the environment. The lifetime of a fluorophore depends on the radiative and the nonradiative decay, k_{rad} and k_{nonrad}:

$$\tau = \frac{1}{k_{rad}+k_{nonrad}} \tag{13}$$

The radiative decay depends on the natural lifetime, under the circumstance of an ideal condition where no energy is lost through non-radiative decay. Under certain circumstances and environmental factors, nonradiative decay can increase. For example due to the presence of or interaction with molecules, a change in pH or temperature. One additional environmental factor that

can play a role in the lifetime, is the dye-chain interaction between the fluorophore and the molecule to which it is attached. This can lead to quenching. Therefore, it is important to choose the right fluorophore for a certain application, since some are more stable than others in different environments. It is also important to keep the fluorophore under the same conditions while performing the same experiments due to this environmental susceptibility. On the other hand, environmental susceptibility can also be used to study and characterise changes in cells, proteins or other molecules when they are subjected to different environments.

2.5.2 Fluorescence microscopy

In fluorescence microscopy, the imaging principle relies on attaching fluorophores to the molecule of interest, exiting the sample and detecting the emitted photons. One thus looks at the fluorophore instead of at the specimen itself. The phenomenon that the excitation and emission wavelengths differ is used to easily separate the excitation from the emission photons with the use of optical filters, see Figure 12.

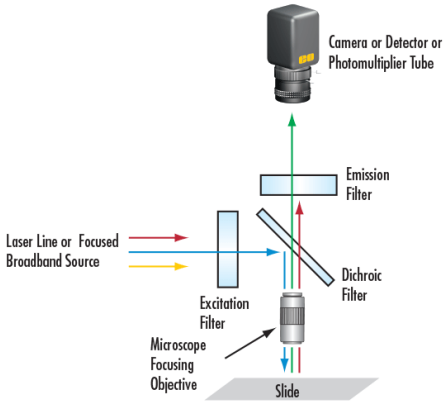

Figure 12: Schematical representation of a fluorescence microscope[32]

In a fluorescence microscope, a sample is excited with laser light of a certain wavelength. The laser light is reflected towards the sample by a dichroic mirror. The fluorophores present in the sample are excited by the laser light and emit photons. Then, the emitted photons pass the dichroic mirror and are detected by a detector or camera.
A dichroic mirror has the property to reflect a small range of wavelengths while letting through all other wavelengths. In fluorescence spectroscopy, the dichroic mirror is chosen such that it reflects the wavelength of the excitation laser light and lets through the wavelength of the photons emitted by the sample. To make sure that only the light emitted by the sample ends up at the detector, a filter is placed in front of the camera. This filter lets through only light of a small wavelength range. This filter is chosen such that the wavelength range matches the emission spectrum of the fluorophore present in the sample.

With different fluorescent techniques, different information can be extracted from the fluorescent signal emitted by a sample. One can for example localize structures, perform lifetime measurements or define the diffusion and correlation of molecules. In this thesis, fluorescence microscopy is used to determine the reconfiguration time of the αS protein by combining the techniques of single-molecule Förster resonance energy transfer (smFRET) and nanosecond fluorescent correlation spectroscopy (nsFCS).

2.6 Förster resonance energy transfer

Förster resonance energy transfer (FRET) is a physical phenomenon where energy transfer occurs between two fluorophores, a so-called donor and acceptor[33]. The emission spectrum on the donor overlaps the excitation spectrum of the acceptor fluorophore. When the donor fluorophore is excited, and the acceptor is in close proximity, the excited donor can lose its energy through energy transfer to the acceptor due to dipole-dipole coupling, and excite the acceptor fluorophore, see the Jablonski diagram in Figure 13.

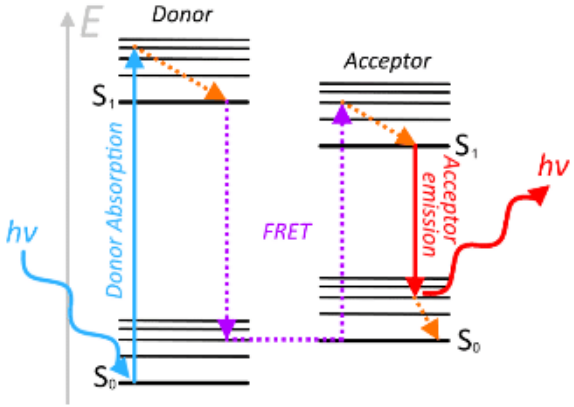

Figure 13: Jablonski diagram showing FRET principle[34]

In the case where FRET is possible, the excited electron can lose its energy in three manners, through radiative decay by emitting a photon, through non-radiative decay or non-radiative energy transfer to the acceptor fluorophore. The lifetime of the fluorophore changes due to the extra decay component in comparison to equation (13):

$$\tau = \frac{1}{k_{rad}+k_{nonrad}+k_{FRET}} \tag{14}$$

Here k_{FRET} is the decay due to FRET. The efficiency of the energy transfer from the donor to the acceptor fluorophore is determined by the decay constants, denoted as the FRET efficiency:

$$E_{FRET} = \frac{k_{FRET}}{k_{rad}+k_{nonrad}} \tag{15}$$

The FRET efficiency (E_{FRET}) is highly dependent on the inter-dye distance (r). When the distance between the donor and the acceptor decreases, the transfer of energy from the donor to the acceptor increases, increasing E_{FRET}. This causes a decrease in the donor emission intensity (I_D), and an increase in the acceptor emission intensity (I_A). Accompanying these phenomena, the lifetime of the donor in presence of the acceptor (τ_{DA}) decreases with decreasing distance between donor and acceptor. The E_{FRET} can be calculated based both on the donor lifetime, equation (16) and the observed intensity, equation (17). From the determined E_{FRET}, the distance between the donor and acceptor fluorophore can be calculated following equation (18).

$$E(\tau) = 1 - \frac{\tau_{DA}}{\tau_D} = 1 - \tau_{relative} \tag{16}$$

$\tau_{DA} = donor\ lifetime\ in\ presence\ of\ acceptor$
$\tau_D = donor\ lifetime\ in\ absence\ of\ acceptor$

$$E(I) = \frac{I_A}{I_D+I_A} \tag{17}$$

$I_A = fluorescence\ intensity\ of\ acceptor$
$I_D = fluorescence\ intensity\ of\ donor$

$$E(r) = \frac{R_0^6}{R_0^6 + r^6} \quad (18)$$

$R_0 = Forster\ radius, the\ distance\ where\ E\ is\ 0.5$
$r = distance\ between\ donor\ and\ acceptor$, *inter-dye distance*

The use of FRET allows for real-time spatial and temporal measurement of molecule interaction and conformation[35]. A donor and acceptor fluorophore are attached to a macromolecule on different sites or to two different molecules. By observing the photon emission intensities and lifetime of the donor and the acceptor fluorophore, one can determine inter-dye distances, which correspond to the intramolecular distances of the macromolecule.
FRET can be studied with a fluorescence microscope. Here the sample is placed above the objective and is excited with laser light of the wavelength corresponding to the excitation wavelength of the donor fluorophore. Depending on the proximity of the donor to the acceptor fluorophores, there occurs energy transfer and the acceptor fluorophores become excited. The emitted light from the donor and acceptor fluorophores passes a dichroic mirror, which splits the two wavelengths such that the emission of the donor and acceptor are detected on two separate detectors. Based on the measured emission, the mean relative lifetime and intensity of the sample can be determined. In FRET studies the mean FRET efficiency of a sample is determined since single events cannot be captured.

2.6.1 Single-molecule FRET

To study single molecules the microscopy setup is slightly altered. An additional confocal pinhole is used, this creates a tightly focussed light beam and creates a small, confocal detection volume in the order of femtoliter. In combination with the use of low sample concentrations, in the picomolar range, it is possible to have maximally one molecule at a time in the detection volume. When this method is used in combination with a sample that is FRET labelled it is called single-molecule FRET (smFRET).

With smFRET it is possible to study the intramolecular dynamics of a molecule and determine if a molecule is static or dynamic. It is important to note that the time that a molecule spends in the confocal volume, on the order of microseconds, is longer than the time in which conformational changes occur, in the order of nanoseconds.
In situations where the macromolecule is rigid, there is no change in the intermolecular distances. This causes the FRET efficiency to be equal by calculation with equations (16), (17) and (18). In situations where the donor and acceptor fluorophore move relative to each other, in dynamic macromolecules, the FRET efficiency based on lifetime and intensity differ. This inequality arises because the lifetime is calculated from the decay of multiple fluorescence events during the measurement time, however, the lifetime changes over time due to the movement of the fluorophores. Thus the lifetime is overestimated. The observed intensity is not averaged and thus not overestimated.
The FRET efficiency based on lifetime can be plotted over the relative lifetime for many FRET events of the same sample, see Figure 14. For a static molecule, the mean FRET efficiency resides on the static reference line. For a dynamic molecule the mean FRET efficiency deviates from this line, the trend is shown for a molecule that behaves like a gaussian chain.

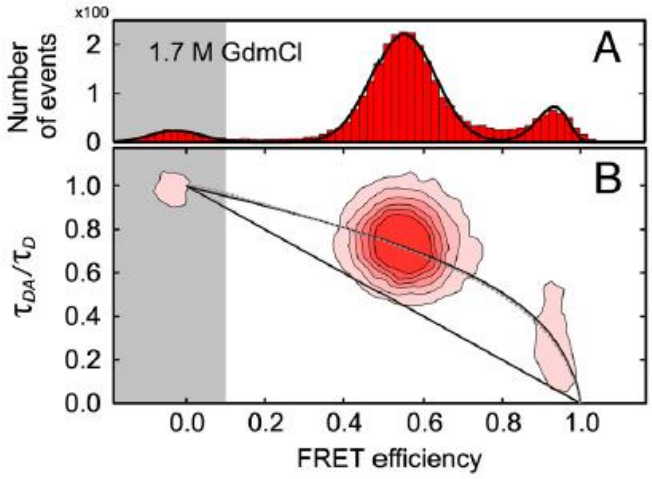

Figure 14: A. FRET efficiency histogram B. relative donor fluorescence lifetime versus FRET efficiency, the straight line shows the theoretical dependence for a static sample, the curved line for a sample that behaves like a gaussian chain[17]
The cloud at E_{FRET} zero are molecules with only a donor attached, the cloud at E_{FRET} equal to one are molecules with only an acceptor attached and the cloud around an E_{FRET} of 0.55 is due to FRET labelled molecules

smFRET is a suitable technique to study the conformational dynamics of αS. Since αS is an IDP, its chain configuration is not static over time, its mean FRET efficiency deviates from the static reference line. The mean FRET efficiency of an IDP is given as follows:

$$\langle E \rangle = \int_0^\infty E(r)P(r)dr \qquad (19)$$

Here E(r) is the FRET efficiency given by equation (18) and P(r) is the probability density of the inter-dye distance. The probability of the inter-dye distance depends on the model with which the dynamics of the molecule can be modelled. Since αS can be modelled by the Gaussian chain model, as discussed in chapter 2.2.1 Gaussian chain model, P(r) follows equation (1). The resulting mean FRET efficiency over relative lifetime is expected to reside on the Gaussian chain curve, similar to Figure 14.
With smFRET only the average conformational changes in a protein can be studied. This is because conformational changes that occur in proteins are typically in a timescale of tens of nanoseconds, but the time resolution of detectors is in the order of 100 nanoseconds. For studying conformational changes that occur sub 100 nanoseconds, another technique needs to be used in addition to smFRET, namely nanosecond fluorescence correlation spectroscopy (nsFCS). This method will be explained in the following chapters.

2.7 Fluorescence correlation spectroscopy

Fluorescence correlation spectroscopy (FCS) is a technique that is used to study molecule concentration, mobility, transport, and diffusion processes[36].

FCS makes use of a tightly focussed, confocal, light beam, see Figure 15a. Only the fluorophores that reside within a small sub-femtoliter excitation volume, will be excited. The fluorescence signal from the confocal volume is measured over time, see Figure 15b.

Due to the motion of the molecules, fluorophores diffuse in and out of the confocal volume, this causes the intensity of the emission signal to fluctuate over time. The first-order correlation of this signal over time can be calculated following:

$$G(\tau) = \frac{<\delta I(t)\delta I(t+\tau)>}{<I(t)^2>} \qquad (20)$$

With G(τ) the correlation, I(t) the intensity over time and δI(t) the intensity fluctuation over time. This can be represented in an autocorrelation graph see Figure 15c.

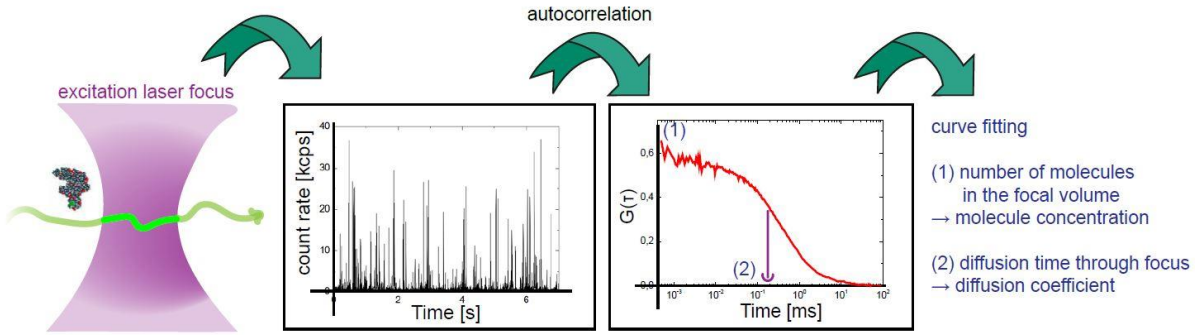

Figure 15: a. the confocal volume of the FCS where fluorophores are detected b. the measured counts over time c. the autocorrelation graph of the signal[37]

The autocorrelation graph shows the correlation of the signal at a certain time with the original signal, at time zero. The time at a correlation of 0.5 is the diffusion time of the molecule, this is the time a molecule spends in the excitation volume. This is used to define the diffusion coefficient of the molecule. These parameters are used to determine the diffusion and other kinetic parameters of the molecule.

When there are two different fluorophores present, for example when a molecule is FRET labelled, the cross-correlation between the donor and acceptor emission signal can be determined. The cross-correlation gives information about the movement of one fluorophore in regard to the other. This technique is called fluorescence cross-correlation spectroscopy (FCCS). Figure 16 shows an example of an FCCS graph. This technique can be used to assess the FRET labelling efficiency of a sample.

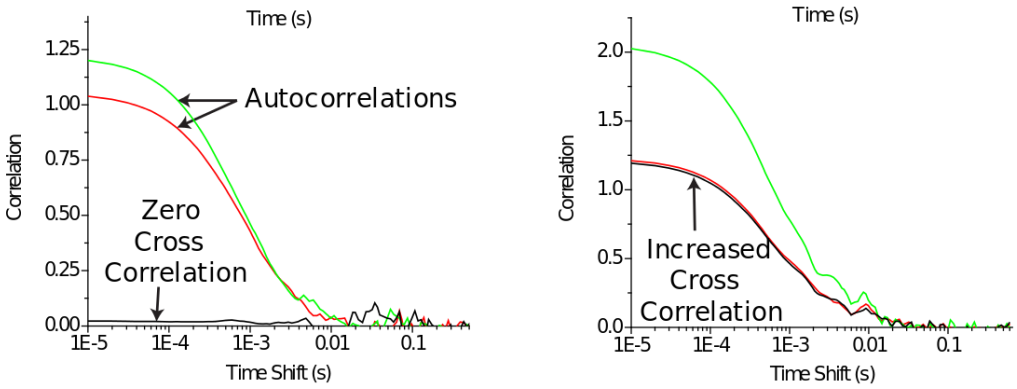

Figure 16: Example of an FCCS graph, the back line is the cross-correlation, the green line the correlation of the donor signal and the red line of the acceptor signal. On the left, a situation is shown where the donor and acceptor fluorophore does not correlate, on the right, a situation is shown where they do correlate[38]

2.8 Nano second FCS

Normal FCS measurements are limited to the range of microseconds, this is because the detectors have a dead time of about 100ns[39]. The dead time is the time that the detector cannot record a second signal after having received the first signal, due to the properties of the detector. If a photon is detected by the detector, for about 100ns it cannot detect a second photon, see Figure 17. This means that for a normal FCS setup the time resolution is limited to 100ns. Conformational changes in a protein occur in a shorter timescale, around 50 ns, so an adjustment is needed to omit the dead time of the detector and improve the time resolution.

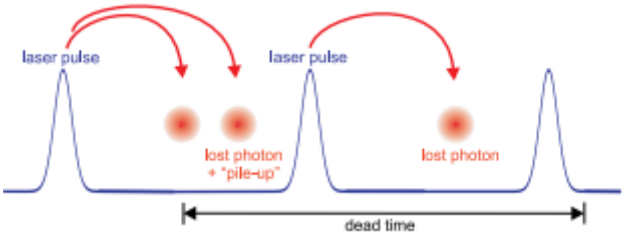

Figure 17: The principle of detector deadtime[40]

A solution is to split the emission signal of the sample by a beam splitter and detect the signal of both donor and acceptor on two separate detectors[41]. See Figure 18 and Figure 19 for a comparison between conventional FCS and nsFCS setups for smFRET measurements.

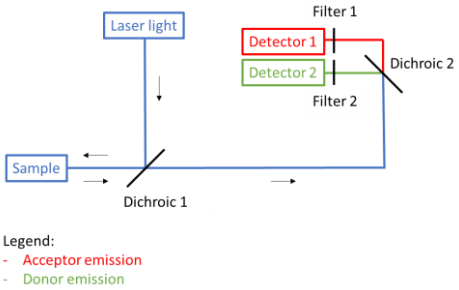

Figure 18: Schematical representation of the setup for conventional FCS, all emitted photons are guided to one detector pair

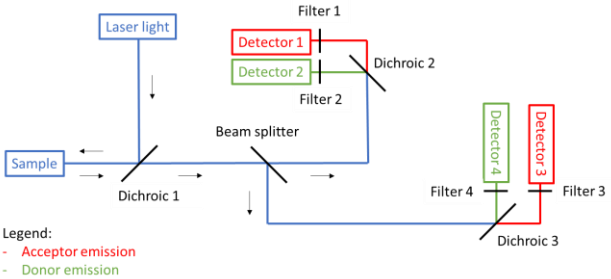

Figure 19: Schematical representation of the setup for nsFCS, the emitted photons are spitted by a beam splitter and guided to one of the two detector pairs

By the use of the nsFCS setup, the chance that a photon ends up at the first detector pair is 50%, and the chance that it ends up at the other is also 50%. In this manner, successive photons do not all end

up at one detector, but either at detector one or two. By cross-correlating the signal obtained from two detectors, the deadtime of the detector is circumvented. This leads to a higher detection time resolution which is only limited by the timing accuracy of the counting electrons and the jitter of the detectors, this is limited to 80ps[42]. This sort of experiment is called a Hanbury Brown and Twiss experiment.

To obtain a correlation from the measured signal, a second-order correlation is used:

$$G_{ij}^{(2)} = \frac{<I_i(t)I_j(t+\tau)>}{<I_i(t)><I_j(t+\tau)>} \quad (21)$$

With I the intensity of successive events over time, t and t+τ.

The combined signal from the two acceptor detectors is correlated, as well as the combined signal from the two donor detectors. The combined acceptor signal can be correlated with the combined signal of the donor, this gives the cross-correlation. For each calculation, $G_{ij}^{(2)}$gives the probability of detecting a second photon after having detected the first photon.

Another method to determine the second-order correlation is to use the interphoton time (Δt), the time between two successively detected photons on different detectors. The histogram of the interphoton times gives the interphoton distribution, ϕ(Δt). In the situation that the interphoton time is much smaller than the mean interphoton time, the interphoton time distribution is directly related to the intensity correlation function[43]:

$$\phi(\Delta t)=G^{(2)}(\tau) \quad (22)$$

For the type of experiments where the sample is in the single-molecule regime, the time between successive molecules that are present in the confocal volume is much larger than the time that a molecule is present in the detection volume. This causes the mean interphoton time to be much larger than the interphoton time of single events. Thus it can be stated that the interphoton distribution is equal to the intensity correlation function for nsFCS measurements. The histogram of the interphoton times is the nsFCS curve[43].

2.9 nsFCS and smFRET

By combining the techniques of smFRET and nsFCS, information can be obtained about the conformational changes of a protein. When a protein that diffuses through the confocal volume undergoes a conformational change, the distance between the donor and acceptor fluorophore changes, thus the FRET efficiency changes accordingly. With the combination of smFRET and nsFCS, the average conformational changes are determined for a large number of events.

In Figure 20 a typical nsFCS graph of a FRET-labelled IDP is shown. The three graphs result from the same sample, from top to bottom they give the donor, acceptor and cross-correlation of the detected signal. Three phenomena can be distinguished in time for all nsFCS graphs.
First, a sharp negative peak at time zero is seen, this is denoted as antibunching[44]. Antibunching is a characteristic of a two-level quantum system, a single fluorophore cannot emit two photons simultaneously, therefore, the correlation is zero at time zero and increases with longer timescales. The decay of this negative peak is equal to the average lifetime of the fluorophore. This occurs in a range of 1 to 5 nanoseconds.

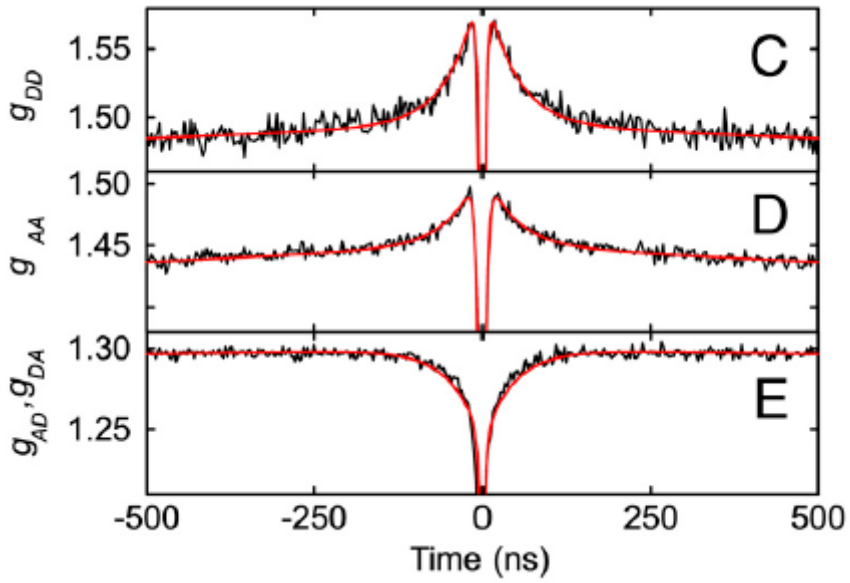

Figure 20: nsFCS graph, C donor cross-correlation, D acceptor cross correlation, E donor-acceptor cross-correlation

Second, a positive peak at the donor and acceptor correlation and a negative peak at the cross-correlation is seen around 50ns. The phenomenon is denoted as photon bunching. In situations with non-rigid FRET labelled structures, for example IDPs. Due to conformational changes in the protein, the energy transfer of donor to acceptor fluctuates over time. The bunching peak is positive for the donor and acceptor since the probability that a second photon is emitted is increased in a certain timescale. For the cross-correlation, the bunching is negative, since the donor and acceptor intensity are anti-correlated.
The decay of the photon bunching peak corresponds to the reconfiguration time of the protein, t_r. For timescales larger than t_r a conformational change has occurred thus the chance of emitting a second photon is not increased anymore but is determined by the average transfer efficiency.
Photon bunching is absent in samples with free dye, rigid FRET labelled structures or structures labelled with single dye where no dye-strand interaction occurs. Since the photon emission is not changed by any interaction, there is no increased probability of emitting a second photon in any timescale.

The last component is the triplet state, this occurs in the microsecond timescale. The triplet state causes a slight overall decay in the nsFCS graph, this results that the correlation at timescales above t_r does not stabilise but decreases slightly over time. This can be seen in the donor and acceptor correlation in Figure 20.

A phenomenon that also occurs is dye reorientation, this affects the photon count rate through the second factor in the energy transfer rate. It is assumed that this factor is averaged out by rapid rotational diffusion of the dyes. The dye reorientation can affect the antibunching part of the correlation function, but not the bunching part of the correlation function since that is in a larger timescale than dye reorentation[43].

The nsFCS curve can be fitted as follows[17]:

$$g_{ij}(\tau) = 1 + \frac{1}{N}\left(\left(1 - c_{AB}e^{-\frac{t}{\tau_{AB}}}\right)\left(1 + c_{CD}e^{-\frac{t}{\tau_{CD}}}\right)\left(1 + c_{T}e^{-\frac{t}{\tau_{T}}}\right)\right) \quad (23)$$

Where τ_{AB} is the antibunching correlation time, equal to the fluorescent lifetime. τ_{CD} is the chain dynamics timescale and τ_T is the triplet timescale. The c factors are weighting factors of the three

timescale components. N is the mean amount of molecules present in the confocal volume For nsFCS there should be only one emitter present at the time in the confocal volume, therefore, N needs to be smaller than 1.

To be able to extract accurate data, the signal-to-noise ratio (SNR) of the nsFCS curve should be high. The SNR is proportional to the number of photon counts, more photon counts lead to better statistics, thus to a higher SNR. The photon counts depend on multiple factors; the quantum yield and the concentration of the fluorescent dye and the measurement time. So for a high SNR, it is beneficial to use a sample containing a fluorophore with a high quantum yield and to measure for a long time. In addition, the concentration can be chosen such that it is the highest concentration where maximal one molecule is simultaneously present in the confocal volume. This ensures that the measurement is performed in the single-molecule regime while having a high number of molecule passages per unit of time.

3. Materials and Methods

In the following chapter, a description is given of all samples used during this thesis, together with an overview of the measurement setups and procedures.

3.1 Samples

For this thesis several samples have been used, see Table 1. DNA and PEG samples are used for measurement and analysis validation. Single labelled αS proteins are used to investigate dye-chain interaction. Double labelled αS samples with different FRET labelling positions are the object of study.

Table 1: Samples

Sample	Fluorescent dyes
DNA-19[45]	ATTO 550 647N
DNA-23[45]	ATTO 550 647N
DNA-31[45]	ATTO 550 647N
ssDNA	ATTO 488-565
PEG	ATTO 550-647N
αS 140	Alexa Fluor 488
αS 140	Alexa Fluor 568
αS 140	Alexa Fluor 584
αS 6-69	Alexa Fluor 488-594
αS 42-90	Alexa Fluor 488-594
αS 90-140	Alexa Fluor 488-594

3.2 Sample preparation

3.2.1 dsDNA samples

Double-stranded DNA is chosen to be used for setup and analysis validation. The DNA sample consists of a single-stranded DNA where the donor fluorophore is conjugated and it is hybridised with its complementary strand where an acceptor fluorophore is conjugated, see Table 2 for an overview of the sequences. The DNA is identical to the DNA used in a benchmark study by Hellenkamp et al.[45]. The donor dye is ATTO550 and the acceptor dye is ATTO647N. The difference between the three samples used is the location where the donor dye is conjugated to the DNA strand, creating samples with different FRET efficiencies. The samples used are referred to as hi-1, mid-1 and lo-1 by Hellenkamp et al., in this thesis they are referred to as DNA-19, DNA-23 and DNA-31, the numbers represent the amount of nucleotides between the labels. The buffer described by Hellenkamp et al. is used, consisting of 20mM $MgCl_2$ 5mM NaCl 5mM tris pH 7.4 in milli-Q[45]. The single-stranded DNA is hybridised by using a 2:1 ratio of acceptor to donor strand.

Table 2: Nucleotide sequences of the single-strand DNA's used for the hybridised DNA samples, the green and red colour represent the location where consecutively a donor and acceptor fluorophore is attached

Sample	Sequence
Acceptor	3'- CTC GAC TTT CAC AGC TCA AAC AAA CTC ACA AAC AGA CC - 5' - biotin
Donor - 19	5'- GAG CTG AAA GTG TCG AGT TTG TTT GAG TGT TTG TCT GG - 3'
Donor - 23	5'- GAG CTG AAA GTG TCG AGT TTG TTT GAG TGT TTG TCT GG - 3'
Donor - 31	5'- GAG CTG AAA GTG TCG AGT TTG TTT GAG TGT TTG TCT GG - 3'

3.2.2 ssDNA sample

Single-stranded DNA (ssDNA) is chosen as a control for a non-rigid structure. The sample consists of an ssDNA strand where a donor and an acceptor fluorophore are conjugated at the first and last nucleotide, a distance of 25 nucleotides apart, see Table 3. The donor dye is ATTO488 and the acceptor dye is ATTO565. The buffer used for this sample is PBS pH 7.4.

Table 3: Nucleotide sequences of the single-strand DNA's used for the hybridised DNA samples, the green and red colour represent the location where consecutively a donor and acceptor fluorophore is attached

Sample	Sequence
ssDNA	5'-TTT GAG AGA TTT GAG AGA TTT GAG AGA-3'

3.2.4 Alpha-synuclein samples

The αS samples used are single or double labelled with fluorescent dye following the synthesis as described by Fakhree et al.[46]. To attach the fluorescent dyes to the protein, first an amino acid at a selected point of the protein is replaced by a cysteine. Then the fluorophore is attached to the protein by the cysteine. For the FRET labelling of αS, αS samples are used that have two reaction sites. For single labelling, αS samples with only one reaction site are used.
The labelling is performed in two steps, first the dye, or the FRET dyes, and αS are incubated for 1 hour at room temperature. This allows the dyes to bind to αS. Next, any unbound dye is removed from the sample with a Zeba spin desalting column[47]. For single labelled samples the ratio of protein to dye is 1:1. For FRET labelling the ratio of protein to donor dye to acceptor dye is 1:1:1.4.

In this thesis, 3 different FRET-pair labelling positions of αS are used. In this study, these samples are named: αS n-m where n and m are the positions of the amino acids which are replaced by cysteines and hence labelling positions. The three combinations are αS9-69, αS42-90 and αS90-140. These locations are chosen such that they probe the N-term, NAC and C-term respectively.

For all experiments with αS, the used buffer is 10mM tris pH 7.4, 10mM NaCl and 0.1 mM EDTA in milli-Q, unless stated otherwise. For experiments with FRET labelled αS, Alexa Fluor 488 is used as the donor dye and Alexa Fluor 594 as the acceptor dye. Therefore, it can be assumed for the following chapters that the sample in question is labelled with the mentioned dye pair unless stated otherwise.

3.2.5 Different solvents and additives

For the investigation of the internal friction component of αS, the buffer with different concentrations of added glycerol is prepared. The used buffer is 10mM tris pH 7.4, 10mM NaCl, 0.1 mM EDTA in milli-Q. Table 4 shows the volume percentage and corresponding molarity and viscosity of the series.

Table 4: Glycerol- buffer series

V% glycerol	Molarity (M)	η at 21.2°C (mPa·s)
10	1.4	1.3
20	2.7	1.9
25	3.4	2.3
30	4.1	2.9
35	4.8	3.6

3.3 General measurement setup

For all measurements performed for this thesis, the PicoQuant MT confocal 200 is used. This is a semicommercial setup and is based on confocal microscopy. The advantage of this setup is that it is robust and not prone to misalignment. A schematical representation of the general setup and its components is shown in Figure 21. For certain applications alterations are made, the exact setup will be shown for each application in their corresponding chapter.

The detectors used are avalanche photodiode detectors 'SPCM-AQRH-14-TR' from Excelitas[48]. All measurements are performed at 21.2°C.

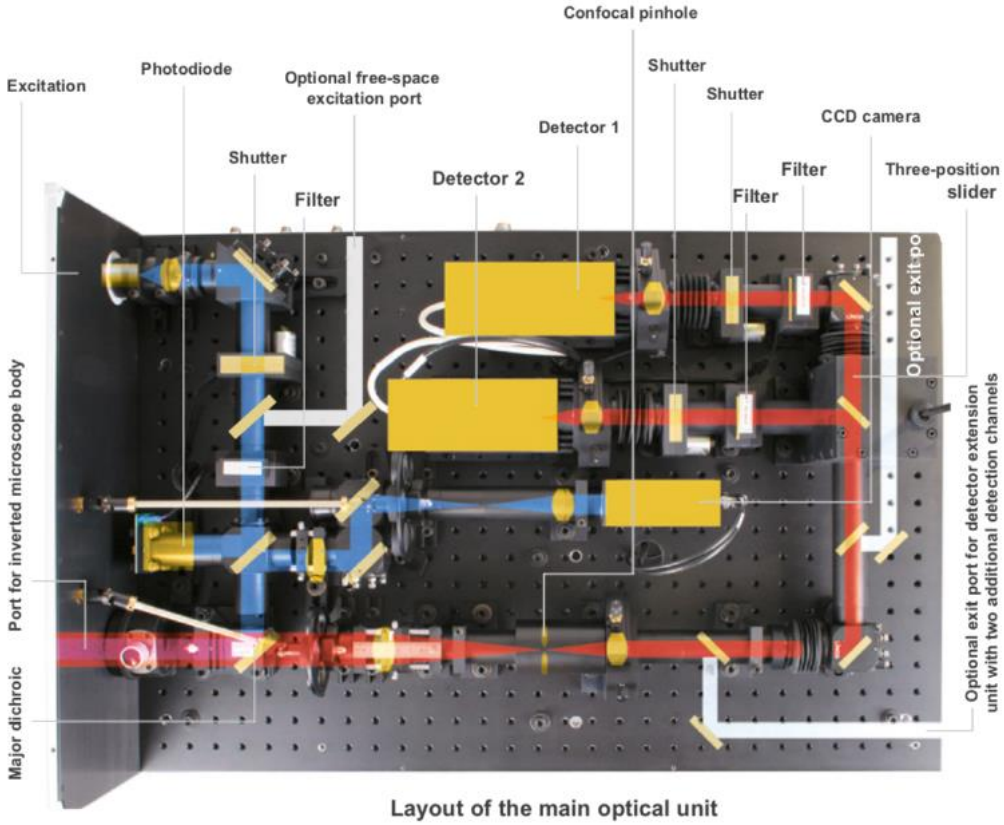

Figure 21: Layout of the main optical unit of the PicoQuant MT200[49]

3.3.1 Pulsed interleaved excitation

In the traditional setup for smFRET studies, only the donor fluorophore is excited and the resulting emitted signal is analysed. For smFRET studies only the signal resulting from FRET is of interest. However, during a measurement not all detected signal is the result of FRET due to the presence of noise, signal leakage or direct excitation of the acceptor. The signal needs to be corrected for these factors. Therefore, nowadays the use of pulsed interleaved excitation (PIE) is preferred since this determines the presence of the acceptor and donor fluorophore separately[50]. This allows for better correction of the signal and determination of FRET.

For PIE two lasers with different wavelengths are pulsed with a high frequency one after the other. One laser excites the acceptor fluorophore while the other excites the donor fluorophore, see Figure 22. To avoid crosstalk between excitation from both lasers at the detector site, the repetition frequency is such that the fluorescence of the excited fluorophores has decayed before a second laser pulse occurs.

Figure 24 shows an example of the resulting time trace. For smFRET and nsFCS studies only the signal due to FRET is of interest. FRET occurs when a signal is detected simultaneously during donor excitation at both the donor and acceptor channel and during acceptor excitation at the acceptor

channel. PIE allows for better determination of FRET which leads to better correction of the signal during data analysis, the exact corrections will be discussed in chapter 4.4.1 Correction factors .

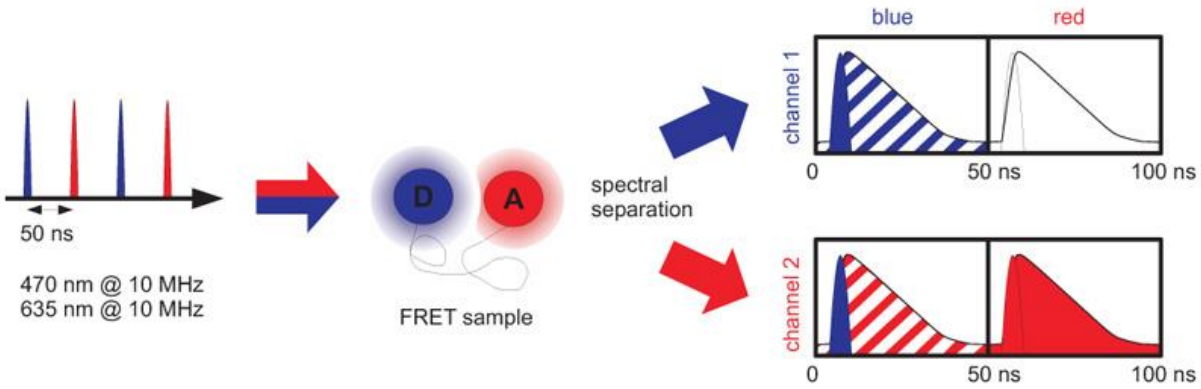

Figure 22: Graphical representation of PIE excitation. In the most left panel, it is seen that first the donor fluorophores are excited with the blue laser pulse then the acceptor fluorophores are excited with the red laser. In the right panel, the laser pulse is shown as a short peak and the resulting signal at the detectors is shown as a broader peak. Channel 1 detects the donor fluorophores, and channel 2 the acceptor fluorophores[50]

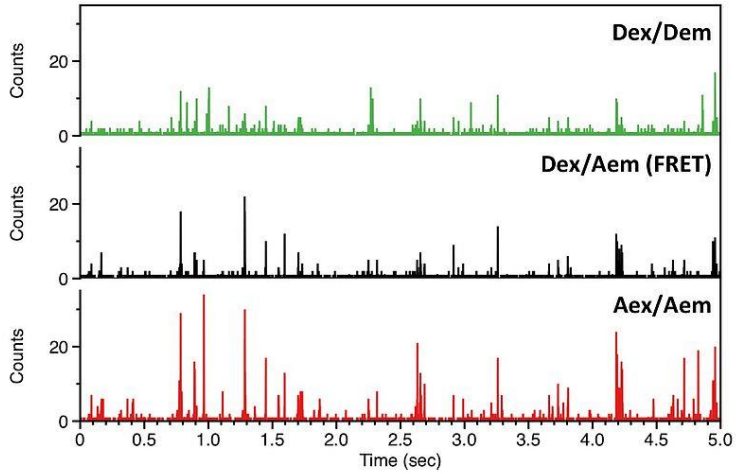

Figure 23: Time trace of a PIE measurement of a FRET labelled molecule[50]
The top graph shows the donor signal detected during donor excitation
The middle graph shows the acceptor signal during donor excitation, the FRET events
The bottom graph shows the acceptor signal during acceptor excitation

3.3.2 Time correlated single photon counting

Time correlated single photon counting (TCSPC) is a technique to determine fluorescence lifetime. The sample is excited with a pulsed laser. The time between the laser pulse and the detection of a photon at the detector, the arrival time, is recorded, see Figure 24. The arrival time is recorded for all detected photons, and a histogram is constructed from all arrival times. The decay rate of the resulting curve corresponds to the mean lifetime of the fluorophore present in the sample.

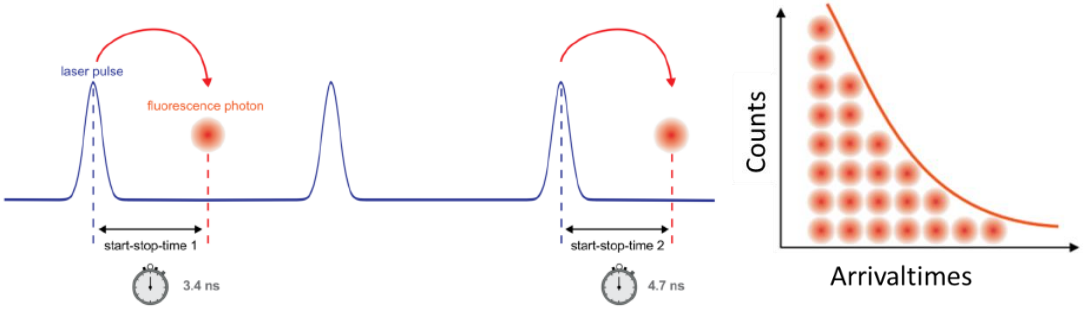

Figure 24: Schematic representation of the TCSPC time recording principle[40]

3.4 General notes

For all measurements performed on the PicoQuant MT confocal 200 a sample volume of 30 to 50 microliter is pipetted on a 20x20mm, high precision cover glass unless stated otherwise.

The αS protein binds to the cover glass causing a rapid decrease in sample concentration. To minimise or prevent the attachment of the sample to the cover glass, which leads to a decrease in sample concentration, the microscopy cover glass is coated with a high concentration of unlabelled wild-type αS. This is done as follows, a 40µL droplet of 5µM αS wildtype is pipetted on the cover glass and left for five minutes. Then the solution is pipetted of the cover glass, and the glass is washed 2x with buffer. Then the αS sample of interest is pipetted on the cover glass and can be used to conduct experiments.

Measurements on the PicoQuant MT confocal 200 are performed The Time-Tagged Time-Resolved T3 mode unless stated otherwise.

3.5 FCS measurements

FCS measurements are used to determine different parameters of the sample, such as the number of molecules in the volume, N, the triplet lifetime, τ_T, its contribution, c_T, and the diffusion coefficient, D. These values are needed for the analysis of nsFCS measurements.

3.5.1 Setup

For FCS measurements of FRET labelled samples, the PicoQuant MT confocal 200 is used, following the setup shown in Figure 25. The sample is excited in pulsing mode with 20MHz by one laser, corresponding to the donor excitation wavelength. For each investigated FRET pair the set of filters differs to achieve the best spectral separation. In Table 5 the exact combinations are shown based on the used FRET labelling pair.

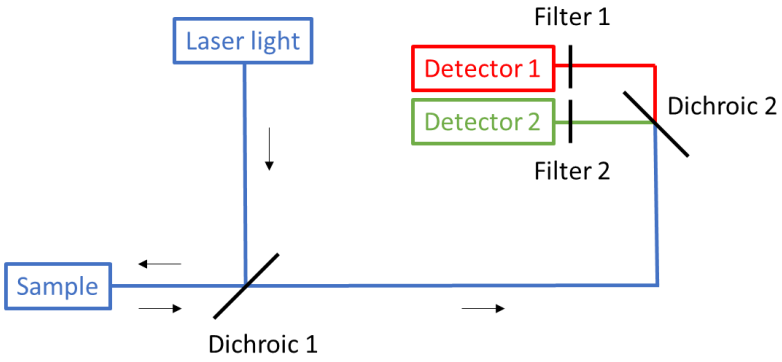

Figure 25: Schematical representation of the PicoQuant setup used for FCCS, the red lines represent the acceptor emission, and the green the donor emission

Table 5: Filter selection for different FRET pairs

FRET pair	Lasers	Dichroic 1	Dichroic 2	Filter 1	Filter 2
AF488-AF594	488+560	488+560	560LP	620/60	520/35
ATTO550-647N	560+640	405+488+560+640	635LP	690/70	620/60

3.5.2 Measurement procedure

For making a correct FCS measurement of a FRET labelled sample first the detection volume V_{eff}, and its ratio between length and height of the volume, k, needs to be calibrated. These parameters are wavelength and laser power-dependent. Calibration is performed with an FCS measurement of free dye that has a known diffusion coefficient. Calibration with free dye is performed separately for each

dye that is present in the sample of interest, in the case of a FRET-labelled sample thus with the donor and acceptor dye. In the case no free dye is available that is the same as in the sample of interest, a dye with a similar fluorescence spectrum is also suitable for calibration.

A 40µL sample containing free dye, with a concentration in the order of 2nM, is placed on a cover glass above the objective. Then the corresponding excitation laser is turned on in pulsed-wave mode at 20MHz and with an intensity of 30µW. The focus of the microscope is placed 35µm above the glass-sample interface and typically a 30 to 60 second measurement is made. The measurement is analysed in the PicoQuant FCS calibration module, where a classical FCS curve is obtained and fitted, based on the known diffusion coefficient of the dye. By fitting this curve V_{eff} and k of the confocal are calculated and set as the calibration values for the donor and acceptor detection channels.

For the FCS measurement, the sample of interest is placed on the cover glass and the corresponding excitation laser is turned on in pulsed-wave mode at 20MHz and with the same intensity as during the calibration measurement. The excitation beam is focused 35µm above the glass-sample interface and a 300 second measurement is made. The measurement is analysed in the PicoQuant FCS module, where a classical FCS curve is obtained and fitted based on the defined calibration values of V_{eff}, and k.

3.6 FCCS measurements

The determination of the labelling ratio of the αS proteins is used to determine if a sample contains sufficient FRET labelled molecules for the application of smFRET and nsFCS measurements. FCCS provides a relatively robust way to determine the fraction of FRET-labelled proteins in a sample. The same setup is used as in FCS measurements, see Figure 25 and Table 5.

3.6.1 Measurement procedure

For a correct FCCS measurement, first an FCS calibration measurement needs to be performed to define V_{eff}, and k for both the donor and acceptor channels. This is performed as stated in the previous chapter.

Before the determination of the labelling ratio, first, a positive and negative control measurement is performed. For the positive control, a rigid sample with a known high labelling FRET efficiency is needed, with the same dyes attached as in the sample of interest. A rigid sample is a sample that does not change its conformation over time, the distance between the donor and acceptor dye remains fixed. Therefore, hybridised DNA-31 is used as the positive control. For the negative control, a sample is made consisting of an equal concentration of donor and acceptor free-dye, 1nM is used. The concentration used for samples in FCCS is relatively high because for a good FCS a large number of fluorescent events need to be detected.

A 300 second PIE measurement is performed at 40MHz with both controls, followed by a 300 second PIE measurement with a 5nM sample containing the αS sample of interest. 500 seconds is chosen since during this time sufficient molecules have passed the confocal volume to achieve good statistics

3.7 smFRET measurements

In smFRET measurements, the mean FRET efficiency of the sample is determined based on both lifetime and intensity. For extraction of this information a burst analysis is performed where the methods of TCSPC and PIE are applied.

3.7.1 Setup

For smFRET measurements, the PicoQuant MT confocal 200 is used, following the setup shown in Figure 25. The sample is excited in PIE mode by two pulsing lasers, corresponding to the donor and

acceptor excitation wavelength. The photons emitted from the sample follow the same path as described in chapter 3.5 FCS measurements. For each FRET pair, a different set of filters is used to achieve the best spectral separation, see Table 5.

3.7.2 Measurement procedure

To achieve single-molecule events the concentration of molecules in the sample of interest is low, 0.3nM. For an accurate mean lifetime and FRET efficiency, it is necessary to have a high number of events to ensure good statistics. This requirement is met by choosing a relatively long measurement time, of 1800 seconds. This time is chosen since during this time sufficient molecules have passed the confocal volume to achieve good statistics. Shorter measurements could result in an inaccurate determination of the mean lifetime and FRET efficiency, whereas measuring for a longer time does not lead to more accurate results.

The sample of interest is placed on the cover glass above the objective. Both lasers corresponding to the excitation wavelengths of the used dyes are turned on in PIE wave mode at 40MHz and with an intensity of 30µW. The focus of the microscope is placed 35µm above the glass-sample interface and an 1800 second measurement is performed.

3.8 nsFCS measurements

nsFCS is used for the investigation of the conformational dynamics of the αS protein.

3.8.1 Setup

For the nsFCS measurements, the PicoQuant MT confocal 200 is used. A schematic representation is shown in Figure 26. In Table 6Table 5 the exact filter combinations are shown based on the used FRET labelling pair.

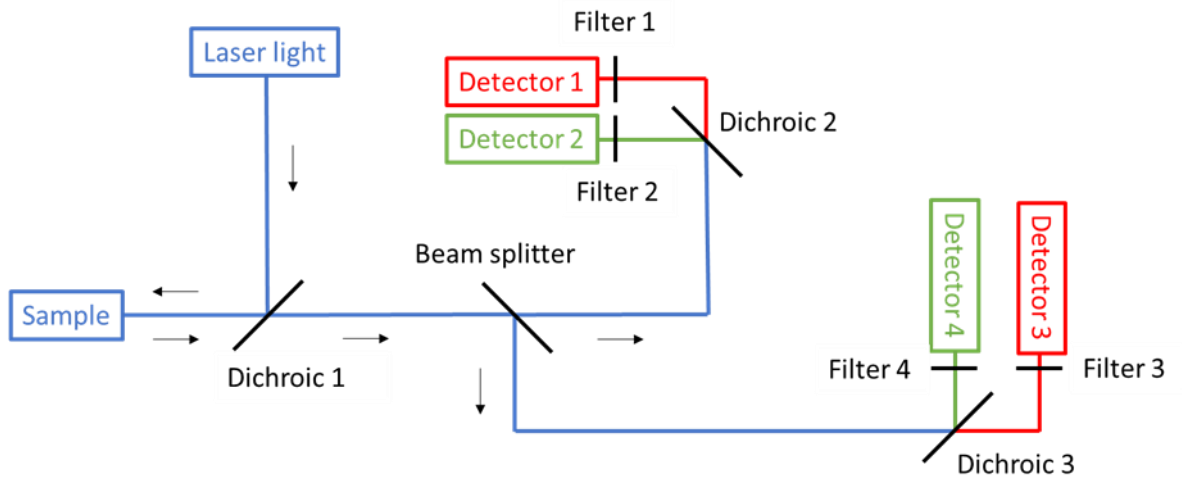

Figure 26: Schematical representation of PicoQuant setup for nsFCS measurements, the red lines represent the acceptor emission, and the green the donor emission

Table 6: Filter selection for different FRET pairs

FRET pair	Laser	Dichroic 1	Dichroic 2 & 3	Filter 1 & 3	Filter 2 & 4
AF488-AF594	488	488+560	560LP	620/60	520/35
ATTO550-647N	560	405+488+560+640	635LP	690/70	620/60

3.8.2 Measurement procedure

Before performing an nsFCS measurement, an FCS measurement is performed to determine certain parameters that are needed for data analysis, namely the diffusion coefficient, the average number

of molecules present in the sample and the contribution and lifetime of triplet state occurrences. This is performed as stated in chapter 3.5 FCS measurements.

For nsFCS measurements the sample is placed above the objective in an airtight chamber, to prevent evaporation during the measurements. In Figure 27 the different components of the chamber are shown.

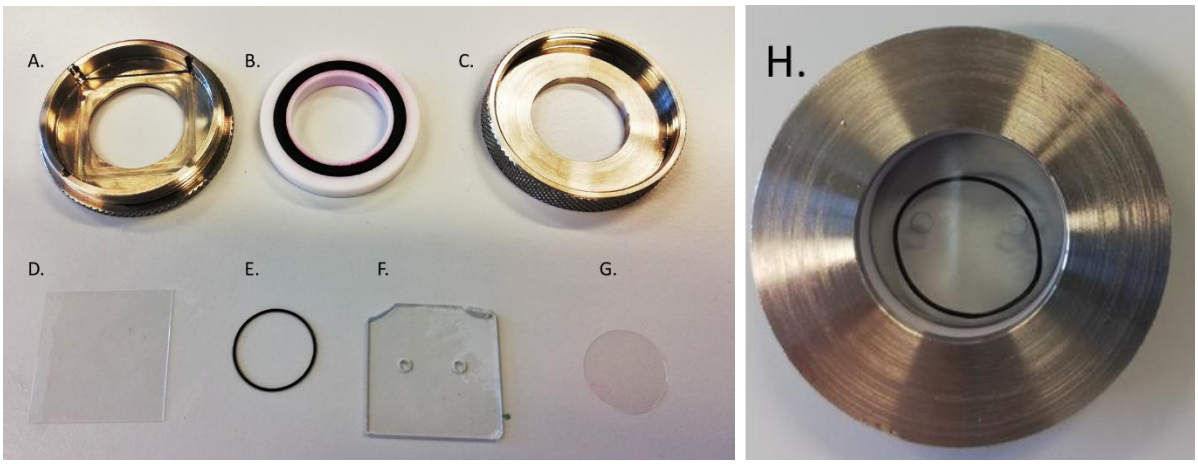

Figure 27: Components to create an airtight chamber for microscopy experiments
A. Bottom plate where a 24x24 mm cover glass can be placed
B. Plastic element C. Top plate that allows for screwing the chamber components tightly
D. 24x24 cover glass E. Small rubber band F. 24x25 cover glass with two 1mm holes
G. Small cover glass to close off the chamber H. Final airtight chamber

Prior to assembly, all cover glasses and the rubber are cleaned with distilled water, ethanol and again with distilled water, to ensure that they are clean. To assemble the chamber, first, a cover glass (D) is placed on the bottom plate(A), the rubber band (E) is placed on top, followed by the second cover glass that contains two small holes (F). To secure the chamber, the plastic element is placed (B) on top and the second metallic plate (C) is screwed tightly onto the ensemble. This creates a chamber of approximately 80µL, with two small holes that allow for pipetting the sample in (H). The chamber is closed off with a small round cover glass (G) and sealed with nail polish at the edges. Nail polish is used since it dries quickly and closes the chamber off airtight, on top of that it is also easily removed when the chamber needs to be used for a new sample.

For measurements with αS, the chamber is coated with a high concentration of αS wild-type to prevent or reduce the sticking of the sample of interest to the chamber. 80µL of 5µM unlabelled wildtype αS is pipetted into the chamber. This is incubated for 5 to 10 minutes. Then the solution is pipetted out and the chamber is washed twice with buffer. The chamber is let to dry, to speed up the process a small tissue can be used. Then the sample of interest is pipetted into the chamber and the chamber is sealed.

The nsFCS measurements are performed in the Time-Tagged Time-Resolved T2 mode of the PicoQuant. The laser power is set to 150µW in continuous wave mode for each measurement. One measurement consists of twelve hours. After six hours the sample concentration decreases significantly, therefore, the sample is replaced with a fresh one. The whole measurement is saved in separate parts of one hour since this is computationally easier to process than one long measurement of multiple hours.

4. Data analysis

This chapter describes how data from FCS, FCCS, msFRET and nsFCS measurements are analysed.

4.1 FCS analysis

FCS measurements are performed as described in chaper 3.5 FCS measurements. The data is analysed in the FCS analysis module provided by PicoQuant. The autocorrelation of the fluorescence intensity fluctuation is calculated and fitted with:

$$G(t) = \left[1 + T\left[exp\left(-\frac{t}{\tau_{Trip}}\right) - 1\right]\right] \sum_{i=0}^{n_{Diff}-1} \frac{\rho[i]}{\left[1+\frac{t}{\tau_{Diff}[i]}\right]\left[1+\frac{t}{\tau_{Diff}[i]\kappa^2}\right]^{0.5}} \quad (24)$$

With G(t) the correlation over time, T the triplet fraction, τ_{Trip} the lifetime of the triplet state, k the legth to diameter ratio of the confolcal volume, n_{Diff} the number of independently diffusing species and ρ the contribution of the diffusing molecule.

With FCS the diffusion coefficient, the average number of molecules present in the sample and the contribution and lifetime of triplet state occurrences are defined by the fit.

4.2 FCCS analysis

FCCS is used to investigate the ratio of FRET labelling of αS, measurements are performed as described in chapter 3.6 FCCS measurements. Due to the double labelling procedure of αS as described in chapter 3.2 Sample preparation, the sample contains four different labelled populations, see Figure 28. For FRET studies only the FRET labelled populations of αS are of interest, Figure 28 C. and D.

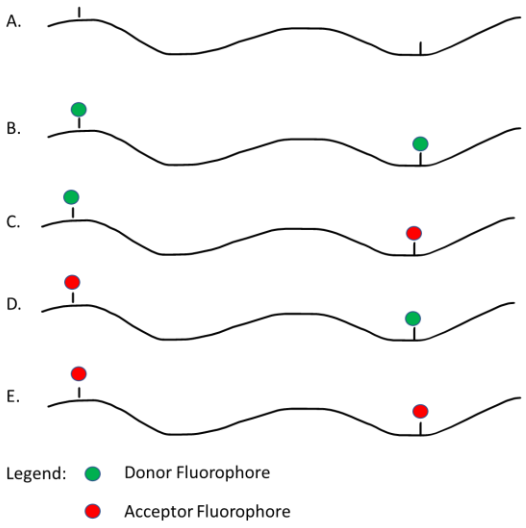

Figure 28: Graphic representation of αS with labelling options, A. αS strand with labelling positions B. Donor-donor labelling C. Donor-acceptor labelling D. acceptor-donor labelling E. Acceptor-acceptor labelling

FCCS is performed to determine the actual labelling ratio of the sample. The measurement procedure is similar to a conventional FCS measurement but the analysis is different. For FCCS in addition to the autocorrelation, also the cross-correlation between the two fluorescent dyes is determined. The calculation for the correlations is performed in the FCS analysis module provided by PicoQuant.

After obtaining the FCCS curves, the fraction of molecular binding in a sample can be determined by calculating the relative cross-correlation (RCC). The RCC is the ratio between the concentration of the population of interest and the concentration of fluorophore present[51]:

$$RCC = \frac{[complex]}{[fluorophore]} \quad (25)$$

Only the FRET-labelled populations cause a positive cross correlation. In an ideal labelling situation the RCC is 0.5, since half of the fluorophores present are attached as depicted in situation C. and D. in Figure 28. For determining the RCC several computational steps are required.

The concentration of the amount of double labelled population and fluorophores is defined as follows:

$$[complex] = \frac{G_{cross}(0)}{G_{donor}(0) * G_{acceptor}(0)} \frac{1}{N_A} \frac{1}{V_{eff}} \quad (26)$$

$$[Donor\ fluorophore] = \frac{1}{G_{donor}(0)} \frac{1}{N_A} \frac{1}{V_{eff}} \quad (27)$$

$$[Acceptor\ fluorophore] = \frac{1}{G_{acceptor}(0)} \frac{1}{N_A} \frac{1}{V_{eff}} \quad (28)$$

With G(0) the correlation at time zero, N_A Avogadro's number and V_{eff} the effective measurement volume of the confocal microscope.

To determine the RCC of the acceptor fluorophore, equation (25) is rewritten using equation (26) and (27) to obtain:

$$RCC_{acceptor} = \frac{[complex]}{[acceptor\ fluorophore]} = \frac{\left(\frac{G_{cross}(0)}{G_{donor}(0) * G_{acceptor}(0) N_A V_{eff}}\right)}{\left(\frac{1}{G_{acceptor}(0) N_A V_{eff}}\right)} \quad (29)$$

This can be simplified to:

$$RCC_{acceptor} = \frac{G_{cross}(0)}{G_{donor}(0)} \quad (30)$$

Similarly, the RCC for the donor fluorophore is determined:

$$RCC_{donor} = \frac{G_{cross}(0)}{G_{acceptor}(0)} \quad (31)$$

The RCC value needs to be corrected for detector noise and setup inaccuracies, for this a positive and a negative control measurement is performed. The relative cross-correlation values of the positive control are regarded as the value in the case of 100% binding and the negative control in the case of 0% binding. The cross-correlation for the positive control is expected to be close to one, and for the negative control it is expected to be close to zero.
The RCC donor and RCC acceptor for the negative and positive control are calculated following equations (30) and (31). Then these values are used to determine the corrected RCC values[51]:

$$cRCC_{acceptor} = \frac{RCC_{acceptor} - RCC_{acceptor_{NC}}}{RCC_{acceptor_{PC}} - RCC_{acceptor_{NC}}} \quad (32)$$

$$cRCC_{donor} = \frac{RCC_{donor} - RCC_{donor_{NC}}}{RCC_{donor_{PC}} - RCC_{donor_{NC}}} \quad (33)$$

cRCC are the corrected RCC values, with PC the positive control and NC the negative control. The cRCC is a value between 0 and 1. The higher the cRCC, the higher the double labelling ratio.

4.3 Processing of raw data in Python

For the analysis of smFRET and nsFCS data, the programming language Python is used. All scripts are self-written[52]. To better understand both analysis methods, de general manner of raw data handling from PicoQuant is explained.

Each detected photon carries information about the time between the start of the measurement and the detection of each photon, the macro time. The raw data of the PicoQuant gives the macro time of the detected photons, per detector. Any difference between the offset of the detectors is corrected by the PicoQuant software.
To relate the data consisting of only time to intensity, all detected photons are separated into bins of 1ms. Within the 1ms bins, the photon count determines the intensity of that bin.
When a fluorescently labelled molecule passes the excitation volume, it is exited and emits photons. Generally, the time that a molecule spends in the confocal volume is shorter than 1ms. In single-molecule experiments, there is at maximum only one molecule present in the excitation volume. Therefore, during the whole timespan of the measurement, some bins will contain signal, and some not. The bins that contain a high photon count are linked to the passage of fluorescently labelled molecules through the confocal volume, these are denoted as bursts.
By calculating the intensity per bin, per detector, it can be determined at what time a burst occurs. This information is used to calculate the intensity time trace and the FRET efficiency per burst.

The separation of the data into 1ms bins allows to correct the data for noise and select the bursts of interest for further analysis, in smFRET and nsFCS these are the bursts resulting from FRET labelled molecules. The exact manner of data correction and analysis will be explained separately for smFRET and nsFCS in their respective chapters.

4.4 smFRET analysis

The goal of smFRET analysis is to determine the mean FRET efficiency and mean relative lifetime of a sample. smFRET experiments are performed as described in chapter 3.7 smFRET measurements. In this chapter, it is explained how burst data is corrected for noise and used for smFRET analysis.

For a PIE measurement, it can be distinguished between bursts detected by the donor and acceptor channel, but also if a burst takes place during the acceptor or donor excitation. For a PIE measurement this gives three possibilities:

- Acceptor excitation with acceptor emission (I_{AexAem})
- Donor excitation with donor emission (I_{DexDem})
- Donor excitation with acceptor emission (I_{DexAem})

With this information it is possible to define which bursts are due to FRET and which consists of donor only (DO) or acceptor only (AO) emission, Figure 29 shows an example of an intensity timetrace of a FRET labelled protein. Technically there is a fourth signal, the acceptor excitation with donor emission, since this intensity is very close to zero it is not of interest.

FRET occurs when signal is detected simultaneously during donor excitation at both the donor and acceptor channel and during acceptor excitation at the acceptor channel. The bursts that do not suffice this criterium are not FRET bursts, they are not of interest and thus removed from the dataset.

Figure 29: Time trace of FRET labelled αS, the top panel is I_{DexDem} the middle pannel is I_{DexAem} and the bottom panel is I_{AexAem},
A FRET burst occurs if there is a signal detected in all three time traces simultaneously, for example at t=199.75s
A donor-only burst occurs when only a signal at I_{DexDem} is detected, there is no example for this in the time trace
Leakage of donor signal to the acceptor channel can be detected by the presence of I_{DexDem} and I_{DexAem} while signal is absent at I_{AexAem}, for example at t=200.70s
An acceptor only bust occurs when only signal is detected at I_{AexAem}, for example at t=200.50s
Direct acceptor excitation occurs when a signal is detected at I_{DexAem} and I_{AexAem} while there is no signal at I_{DexDem}, for example at t=200.25s

4.4.1 Correction factors

Several factors need to be taken into account to correct the raw data so that it gives the actual occurring FRET bursts. The burst analysis method and the corrections thereof are performed following a multilibrary benchmark study by Hellenkamp et al. on smFRET studies [45].

First of all the signal needs to be corrected for background noise. An upper and lower threshold is set. The bursts with an intensity lower than the lower threshold are seen as background signal. The photons with an intensity higher than the upper threshold are most likely not single emitters. They do not give relevant information for this analysis, so they are disregarded.

The mean of the intensity of the photons below the lower threshold is calculated. This value is seen as the background signal (BG). The value of the background signal is then removed from the signal:

$$I_{DexDem} = I_{DexDem} - BG_{DexDem} \quad (34)$$

$$I_{DexAem} = I_{DexAem} - BG_{DexAem} \quad (35)$$

$$I_{AexAem} = I_{AexAem} - BG_{AexAem} \quad (36)$$

To further correct the signal first the apparent FRET efficiency and stoichiometry need to be determined per bin, based on the background-corrected signal:

$$S_{app_{uncorrected}} = \frac{I_{DexAem}+I_{DexDem}}{I_{DexAem}+I_{DexDem}I_{AexAem}} \quad (37)$$

$$E_{app_{uncorrected}} = \frac{I_{DexAem}}{I_{DexAem}+I_{DexDem}} \quad (38)$$

Stoichiometry relates the donor signal to the total signal. In the case that excitation and detection are equal for donor and acceptor, the stoichiometry gives the relation between donor and acceptor signal present. In Figure 30 an example of a stoichiometry plot for the FRET efficiency is shown.

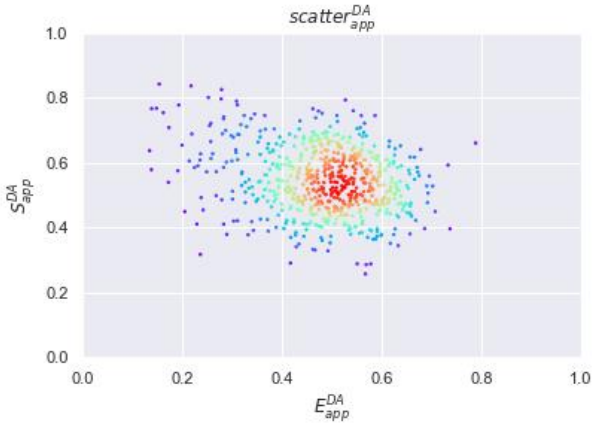

Figure 30:Stoichiometry of FRET efficiency scatter plot

Next, the signal is corrected for four common phenomena. Namely the leakage of donor fluorescence onto the acceptor detector (α), photons that arise from acceptor fluorophores that are directly excited by the donor laser (δ), the differences in the excitation intensity and cross-section of the donor and acceptor dye (β) and for the difference in quantum yields and detection efficiencies of the dyes (γ).

The α correction factor represents the leakage of donor fluorescence into the acceptor channel. They are calculated from the donor-only bursts (DO):

$$\alpha = \frac{<E_{app}^{DO}>}{1-<E_{app}^{DO}>} \quad (39)$$

The δ correction factor represents the fraction of the acceptor bursts that arise from direct excitation by the donor laser, and are thus not FRET occurrences. This is determined with the use of the stoichiometry of acceptor-only bursts:

$$\delta = \frac{<S_{app}^{AO}>}{1-<S_{app}^{AO}>} \quad (40)$$

With these values, a correction can be made to the measured I_{DexAem} and I_{DexDem} and the corrected apparent FRET efficiency and stoichiometry are calculated:

$$E_{app} = \frac{I_{DexAem}-\alpha I_{DexDem}-\delta I_{AexAem}}{I_{DexAem}-\alpha I_{DexDem}-\delta I_{AexAem}+I_{DexDem}} \quad (41)$$

$$S_{app} = \frac{I_{DexAem}-\alpha I_{DexDem}-\delta I_{AexAem}+I_{DexDem}}{I_{DexAem}-\alpha I_{DexDem}-\delta I_{AexAem}+I_{DexDem}+I_{AexAem}} \quad (42)$$

For a FRET burst, the relation between donor and acceptor signal is assumed to be 1:1, so the stoichiometry should be around 0.5. Due to differences in the excitation intensity and cross-section of the donor and acceptor dye and the difference in quantum yields and detection efficiencies of the dyes, the stoichiometry differs slightly. This can be corrected by the β and γ factors. For stoichiometries that differ largely from 0.5 the relation between donor and acceptor signal is inequal, the donor and acceptor are not present in a 1:1 relation in the confocal volume, these outliers are

removed from the dataset. A FRET burst is considered an outlier when the stoichiometry is below 0.3 or above 0.7.

The β and γ factors are determined by using the apparent FRET efficiency and stoichiometry for only bursts a donor and acceptor are detected simultaneously (DA). γ and β are determined by fitting equation (43) for bursts with stoichiometry between 0.3 and 0.7.

$$S_{app}^{DA} = \left(1 + \gamma\beta + (1-\gamma)\beta * E_{app}^{DA}\right)^{-1} \quad (43)$$

When all correction factors are calculated, the final FRET efficiency and the stoichiometry per bin are determined with the background-corrected intensity signal:

$$E_{FRET} = \frac{I_{DexAem} - \alpha I_{DexDem} - \delta I_{AexAem}}{\gamma I_{DemDex} + I_{DexAem} - \alpha I_{DexDem} - \delta I_{AexAem}} \quad (44)$$

$$S = \frac{\gamma I_{DexDem} + I_{DexAem} - \alpha I_{DexDem} - \delta I_{AexAem}}{\gamma I_{DexDem} + I_{DexAem} - \alpha I_{DexDem} - \delta I_{AexAem} + \frac{1}{\beta} I_{AexAem}} \quad (45)$$

The majority of the occurrences are due to FRET, but a small amount is due to spectral overlap, so leakage. To obtain only FRET burst, the bursts with a stoichiometry below 0.3 and above 0.7 are removed.

4.4.2 FRET efficiency histogram

A histogram can be made from the FRET efficiencies per burst. This is used to determine the mean FRET efficiency of the sample. The FRET histogram is fitted with a gaussian, in theory the histogram of the FRET efficiency has a normal distribution, in practice this is not always the case[53]. In a perfect system, the FRET efficiency is in an equal amount of bursts larger or smaller than the mean, resulting in a normal distribution. However, in some systems the distribution is more to one side, resulting in a skewed gaussian distribution. This can be due to a property of the dye, or environmental factors like interaction with side groups of the structure to which the fluorophore is attached. There can also be two populations of FRET efficiencies when two different species are present in the sample, resulting in a double Gaussian distribution. In the case of an IDP, this could also be the result of two different dominating conformations.

The histogram of the FRET efficiency is fitted with a normal distribution, skewed gaussian and a double Gaussian distribution, see Figure 31. Upon visual interpretation, the fit is chosen that best follows the data and gives the most logical mean value. In general, the skewed Gaussian distribution fits best. From the fit, the mean E_{FRET} is calculated and set as the mean FRET efficiency of that system.

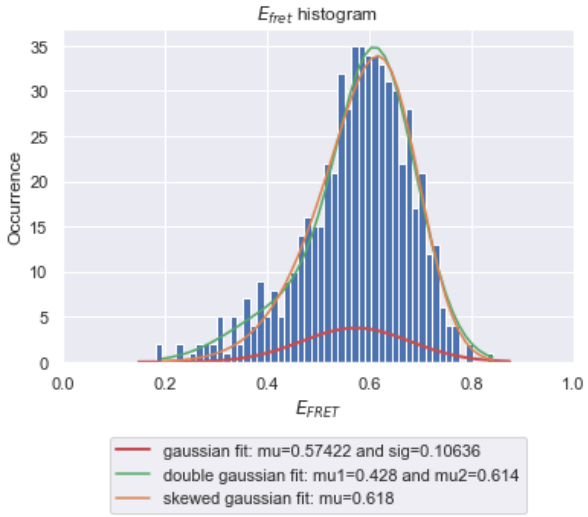

Figure 31: Example of a FRET efficiency histogram with fits

The next step is to determine the average lifetime of the donor dye in the configuration. As stated in chapter 2.6.1 Single-molecule FRET, the average lifetime of the dye and the FRET efficiency scale linearly in a rigid system, but not in a system where there occur conformational changes.

The mean arrival time of all photons within the FRET bursts equals the mean fluorescent lifetime. The arrival time of the photons is plotted in a histogram and the mean lifetime is calculated based on a skewed gaussian fit. The relative lifetime for each burst is calculated based on the average lifetime of the donor in absence of the acceptor:

$$\tau_{relative} = \frac{\tau_{DA}}{\tau_D} \tag{46}$$

To accurately assess the relative lifetime of the sample, the lifetime of the donor in absence of the acceptor dye needs to be known. Since the dye is attached to a molecule, the lifetime is not equal to the lifetime of the free dye, due to possible interactions with the sample and environmental factors that alter the dye's properties. This means that the lifetime of the donor can be slightly different for different labelling positions. The lifetime of the donor fluorophore in absence of the acceptor is determined with the donor only occurrences of the FRET labelled sample of interest.

For each FRET burst, E_{FRET} is plotted over $\tau_{relative}$, this results in a typical burst cloud that is colour coded, see Figure 32. The most frequent to least frequent bursts are coloured accordingly on a scale from red to blue.

Figure 32: Example of a 2D cloud plot of FRET efficiency against relative lifetime, colour coding is from red to blue for most to least frequent bursts

4.5 nsFCS analysis

The goal of nsFCS analysis is to determine the reconfiguration time of a protein. nsFCS experiments are performed as described in chapter 3.8 nsFCS measurements.

4.5.1 Backgroud correction and FRET burst selection

For nsFCS analysis, the second-order correlation of all photons within FRET bursts is of interest. The PicoQuant has a so-called Antibunching module, which calculates the second-order correlation of the raw data. However, this module makes use of all detected photons without any corrections to the signal. Therefore it is not suitable for nsFCS analysis.
To obtain an nsFCS curve that contains only data of interest, a custom Python script is written[52]. The structure and the outline of the Python script are explained in the upcoming chapter.

As stated before, in single-molecule experiments the histogram of the interphotontimes is equal to the second-order correlation of the signal. So, to determine the nsFCS graph the interphoton times of all photons within FRET bursts need to be determined.
Herefore, the signal of both acceptor detectors and subsequently of both donor detectors are combined, and the detected photons are sorted based on their increasing detection time. The data is separated into bins of 1ms to determine the FRET bursts and correct the raw data.

The raw data is correct for four phenomena that influence the measured signal. The first correction is for noise, detected fluorescent bursts that have a low signal intensity do not contribute to any relevant results but do add noise and decrease the SNR. The second is the α correction factor which corrects for crosstalk. The third is the γ correction factor which accounts for the difference in quantum yields and detector efficiencies of the dyes. Lastly, donor or acceptor-only bursts are removed, since only FRET bursts give relevant information about chain dynamics.

First of all, the noise is removed similarly as described in chapter 4.4.1 Correction factors :

$$I_{Donor} = I_{Donor} - BG_{Donor} \tag{47}$$

$$I_{Acceptor} = I_{Acceptor} - BG_{Acceptor} \tag{48}$$

Both the alpha and gamma correction factors determined by burst analysis are used to correct for crosstalk and the difference in quantum yields and detector efficiencies. This can be done because the corrections depend only on the detectors and dyes used, which remain the same.

The α and γ factors are used for correction of the FRET efficiency to be able to compare it to smFRET measurements:

$$I_{acceptor}corrected = I_{acceptor} - \alpha I_{donor} \tag{49}$$

$$I_{donor}corrected = I_{donor} + \alpha I_{donor} \tag{50}$$

$$E_{FRET} = \frac{I_{acceptor_{corrected}}}{\gamma I_{donor_{corrected}} + I_{acceptor_{corrected}}} \tag{51}$$

Lastly, the bursts where the FRET efficiency is more than ±0.2 of the mean FRET efficiency are discarded. This removes donor or acceptor-only bursts, which are not of interest for the nsFCS analysis. In this manner, only the FRET bursts are used for the computation of the nsFCS graph.

The arrival times of the photons within the bursts of interest, the FRET bursts, are used to calculate all interphoton times of the donor photons, acceptor photons and the cross-correlation. The histogram of the interphoton times is related to the second-order correlation, as described in

chapter 2.8 Nano second FCS. Therefore, the histogram results in the nsFCS graphs of the donor, acceptor and cross-correlated signal.

4.5.2 Pile-up correction and normalisation of nsFCS curve

After having obtained the nsFCS graph for a certain sample, the data still needs to be normalised[43]. In Figure 33 an example of an uncorrected graph is shown, here a downwards slope is observed for long interphotontimes. This thus means that the occurrence or probability of the measurement of a long interphoton time is lower than for a short interphoton time. This phenomenon is caused by the effectiveness of the excitation of the fluorophore. This depends on the laser power and the properties of the fluorophore. For the same fluorophore excited with a low excitation power, the effectiveness of exiting the fluorophore is low compared to the use of a high laser power. When the laser power is increased, the effectiveness of excitation is higher. It is easier for the electron in the fluorophore to absorb energy and move to the excited state and then fluoresce. Therefore, the photon rate increases, and with that the occurrence of short interphoton times increases while the occurrence of long interphoton time decreases, this is called a pile-up effect.

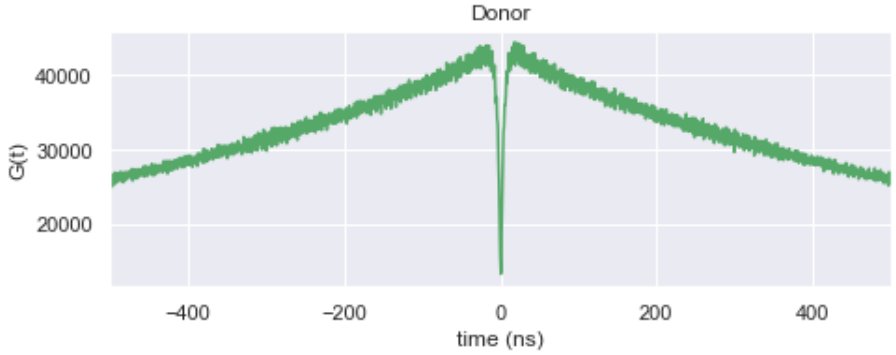

Figure 33: Example of an uncorrected nsFCS graph

The pile-up effect is in essence not bad for measurement analysis, it can be even beneficial. When studying the conformational dynamics of proteins the timescales of interest overlaps with the timeframe of the short interphotontimes mentioned above. The resolution or accuracy of the nsFCS graph is highest for the interphoton time region that is most occurring, thus a good resolution is obtained for the timescale of interest.

The data does need to be corrected for pile-up since the pile-up masks the occurring chain dynamics which causes an inaccurate fit of the data.

For the correction of pile-up the histogram of the interphoton time distribution ϕ_{ii} is fitted to[43]:

$$\phi_{ii} = A\, e^{-\frac{t_i}{\tau_i}}\, g_{ii}(\tau) \tag{52}$$

A is an overall amplitude, to account for the normalisation of the data, $e^{-\frac{t_i}{\tau_i}}$ is accounting for the pile-up effect, with t_i being the interphoton time and τ_i the mean interphotontimes of the whole dataset.

For a system where photon bunching occurs the second-order correlation, $g_{ii}(\tau)$ is given as:

$$g_{ii}(\tau) = \left(1 - c_{AB} e^{-\frac{t_i}{\tau_{AB}}}\right)\left(1 + c_{CD} e^{-\frac{t_i}{\tau_{CD}}}\right)\left(1 + c_T e^{-\frac{t_i}{\tau_T}}\right) \tag{53}$$

For a system where photon bunching does not occur, where c_{CD} is zero, for example in rigid structures or when only one dye is present, $g_{ii}(\tau)$ is given as:

$$g_{ii}(\tau) = \left(1 - c_{AB} e^{-\frac{t_i}{\tau_{AB}}}\right)\left(1 + c_T e^{-\frac{t_i}{\tau_T}}\right) \tag{54}$$

In equation (53) the first component accounts for the antibunching, the second for the chain dynamics and the last for triplet timescales. In equation (54) the first component accounts for the antibunching the last for triplet timescales. Here all 'c' components account for the contribution of the phenomena and the 'τ' for the correlation times of the phenomena. For the fit the lifetime of the triplet state is set as a constant, this value is determined by an independent FCS measurement for the same sample and in identical conditions as the nsFCS measurement. The rest of the parameters are determined by the fit. For all other parameters, a well-founded initial guess is given based on the FCS measurement or literature to assure a good fit.
The value for c_T is set as the value obtained by FCS. For $\tau_{AB,}$ the average lifetime of the dye in question is used, typically around 4ns. For τ_{CD} the theoretical timescale of the chain dynamics is used, for αS, this is equal to 60ns. C_{AB} and C_{CD} are set to 1.
For an initial guess of A, the amplitude of the uncorrected graph is used and for τ_i the mean interphotontime as calculated with the dataset.

The resulting values of the A and τ_i of the fit are used to correct the data for the pile-up effect by dividing each histogram value of the nsFCS graph by $A\, e^{-\frac{t_i}{\tau_i}}$. See Figure 34 for the resulting nsFCS graph.

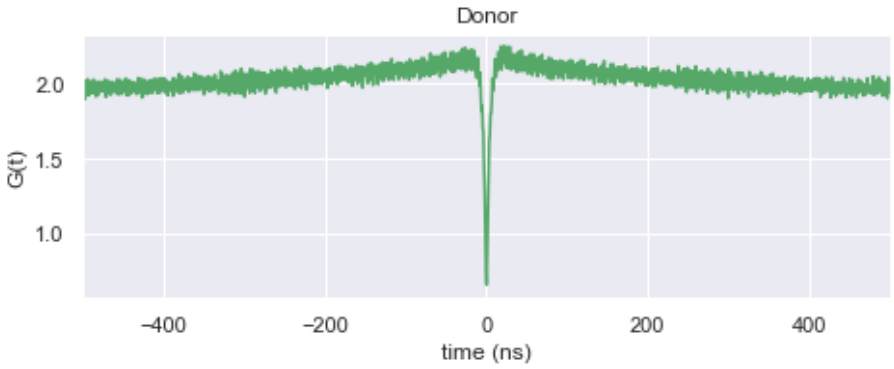

Figure 34: Example of a corrected nsFCS graph

4.5.3 Fitting of the nsFCS curve

The corrected nsFCS graph is fitted with equation (55) to obtain the values of interest, see Figure 35.

$$g_{ii}(\tau) = 1 + \frac{1}{N}\left(\left(1 - c_{AB}e^{-\frac{t_i}{\tau_{AB}}}\right)\left(1 + c_{CD}e^{-\frac{t_i}{\tau_{CD}}}\right)\left(1 + c_T e^{-\frac{t_i}{\tau_T}}\right)\right) \qquad (55)$$

For the fit, all values are set free, except for the lifetime of the triplet state (τ_T) which is fixed as the value defined by an independent FCS measurement for the same sample and in identical conditions as the nsFCS measurement. For the fit there are thus six free parameters, a well-founded initial guess is given based on the FCS measurement or literature in order to assure a good fit. The values are the same as for the pile-up correction fit. Additionally, N is the average number of molecules present in the confocal volume, which is determined by independent FCS measurements of the sample.

By fitting the nsFCS curve of the donor, acceptor and cross-correlation the free parameters can be determined separately for each curve. When the τ_{CD} is equal in all correlations, and the bunching peak is positive for the donor and acceptor and negative for the cross-correlation, this is an indication for the presence of chain dynamics.

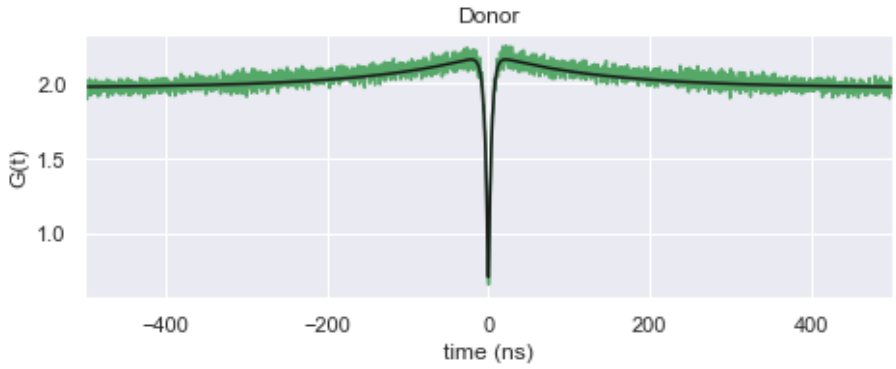

Figure 35: Example of a fitted nsFCS graph of the donor correlation for the free dye AF488, the green line represents the data and the black line is the fit of the data

5. Validation of setup and data analysis for smFRET and nsFCS

To make sure that all data is measured and analysed properly, the setup and analysis methods for the smFRET and nsFCS techniques are verified and validated. The following chapter describes the validation method and outcome for both techniques.

5.1 smFRET

For the validation of the smFRET setup and analysis method, three double-strand DNA samples are used, DNA-19, DNA-23 and DNA-31, as described in chapter 3.1 Samples. The measurement procedure and analysis method are validated by comparing the experimentally defined mean FRET efficiency to the mean FRET efficiency as determined by Hellenkamp et al.[45].

smFRET measurements and analysis are performed as described in chapter 3.7 smFRET measurements and chapter
4.3 Processing of raw data in Python
For the analysis of smFRET and nsFCS data, the programming language Python is used. All scripts are self-written52. To better understand both analysis methods, de general manner of raw data handling from PicoQuant is explained.

Each detected photon carries information about the time between the start of the measurement and the detection of each photon, the macro time. The raw data of the PicoQuant gives the macro time of the detected photons, per detector. Any difference between the offset of the detectors is corrected by the PicoQuant software.
To relate the data consisting of only time to intensity, all detected photons are separated into bins of 1ms. Within the 1ms bins, the photon count determines the intensity of that bin.
When a fluorescently labelled molecule passes the excitation volume, it is exited and emits photons. Generally, the time that a molecule spends in the confocal volume is shorter than 1ms. In single-molecule experiments, there is at maximum only one molecule present in the excitation volume. Therefore, during the whole timespan of the measurement, some bins will contain signal, and some not. The bins that contain a high photon count are linked to the passage of fluorescently labelled molecules through the confocal volume, these are denoted as bursts.
By calculating the intensity per bin, per detector, it can be determined at what time a burst occurs. This information is used to calculate the intensity time trace and the FRET efficiency per burst.

The separation of the data into 1ms bins allows to correct the data for noise and select the bursts of interest for further analysis, in smFRET and nsFCS these are the bursts resulting from FRET labelled molecules. The exact manner of data correction and analysis will be explained separately for smFRET and nsFCS in their respective chapters.

4.4 smFRET analysis, following the method proposed by Hellenkamp et al.[45]. The resulting 2D smFRET efficiency plots over lifetime are shown in Figure 36.
The plots show the FRET efficiency per burst versus associated relative fluorescent lifetime. The mean point does visually not lie in the middle of the colour cloud. This is because the mean of the total amount of bursts is based on a skewed gaussian while the colour map is based on Gaussian kernel density estimation, which estimates the probability density function[54]. The red points represent the most occurring bursts, which do not necessarily correspond to the mean value.
Both the mean FRET efficiency over relative lifetime and the peak of the colour cloud are located around the black static reference line. This shows that the DNA samples are rigid and do not behave as a Gaussian chain.
Any deviation of the mean away from the static reference is ascribed to data variation, i.e. limited accuracy, and linker flexibility. The latter introduces a small movement in the position of the

fluorescent dye that is attached to the DNA strand which causes an apparent overestimation of the lifetime.

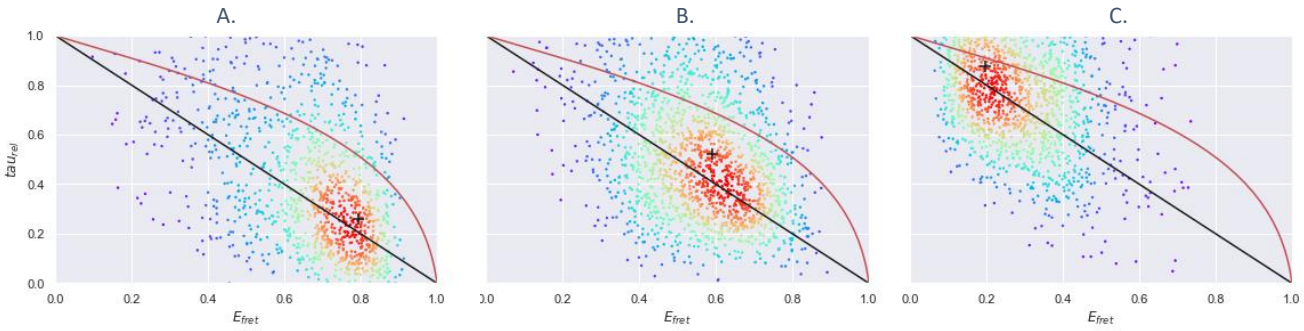

Figure 36: *FRET efficiency over the relative lifetime of DNA, colour coding is from red to blue for most to least frequent bursts, the back line is the static reference, the red line the gaussian chain line and the plus symbol marks the mean FRET efficiency over the mean relative lifetime*
A. DNA-D19, mean E_{FRET} = 0.79 and mean τ_{rel}= 0.26 B. DNA-D23, E_{FRET} = 0.59 mean and τ_{rel}= 0.52
C. DNA-D31, mean E_{FRET} = 0.20 and mean τ_{rel}= 0.15

The experimentally determined mean FRET efficiency is compared to Hellenkamp et al., see Table 7.

Table 7: FRET efficiency of DNA samples compared to Hellenkamp et al.[45]

Sample	E_{FRET} theory[45]	E_{FRET} measured
D19	0.74	0.79
D23	0.56	0.59
D31	0.15	0.20

The resulting values are close to the expected values, therefore, the used experimental setup and analysis method are validated and can be used to accurately perform burst analysis on other samples.

5.2 nsFCS

For the validation of the nsFCS setup and analysis method, there is no standard validation technique. It is chosen to validate on two different levels, with a system that should not show bunching and a system that should show bunching.
The first system uses the fact that in nsFCS curves of free dye, single labelled samples and rigid samples there should be no bunching peak present due to the absence of interaction. For the nsFCS curve, the fitted antibunching lifetime should be close to the lifetime of the dye present.
The second system makes use of an nsFCS measurement of a polymer that is behaving as an ideal gaussian chain that is known to have no internal friction.

To validate the setup and the analysis method nsFCS measurements are performed on free dye, double-stranded FRET labelled DNA, single-stranded FRET labelled DNA and FRET labelled PEG. Free dye and double-stranded DNA are expected to show no photon bunching. Single-stranded DNA and PEG are expected to behave like dynamic structures, with PEG assumed to be a random coil.
Moreover, single-labelled αS is analysed to asses if there are interactions between the dye and αS. If this is the case for any of the dyes they cannot be used further for nsFCS analysis of FRET labelled samples, since observed bunching due to dye-chain interaction cannot be distinguished from chain dynamics. Therefore, no conclusion can be drawn about chain dynamics.
After all validation experiments are performed, one FRET dye pair is chosen to use for further experiments on the dynamics of αS.

The validation measurements are performed following the method as described in chapter 4.5 nsFCS . All samples have a concentration of 0.5nM and are measured for a length of two hours. Two hours is chosen because after two hours of measurement the overall nsFCS trend is already seen. Measuring for a longer time gives only better statistics, which are not necessary for this validation step.

5.2.2 Free dye

For the validation measurement of a situation where no dynamics are present, the free dye AF488 is chosen. Figure 37 shows the resulting nsFCS curve for the donor signal. There is no acceptor present so the acceptor and cross-correlation are not shown.

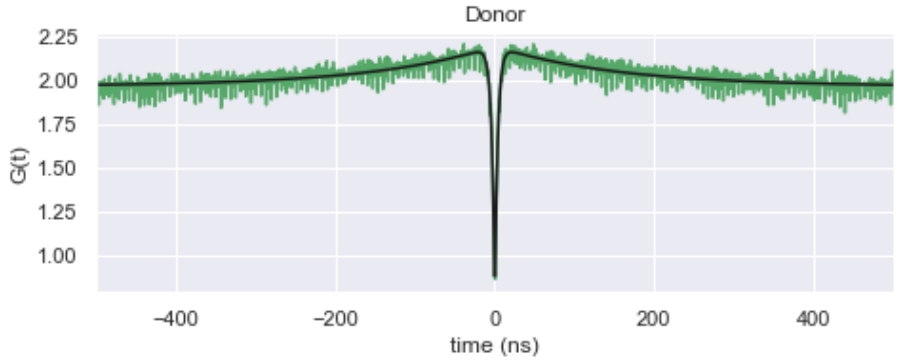

Figure 37: nsFCS curve of donor channel signal for free dye AF488 with residuals of the fit
The green line represents the data, the black line is the fit, fitted τ_{ab} = 3.8 ns and τ_{cd} = 150

In Figure 37 it can be seen that there is a clear antibunching drop present at t_0. There is no bunching peak present, only a slightly decaying slope of the correlation over time.
The lifetime of the antibunching is determined to be 3.8ns. The theoretical lifetime of AF488 is 4.1ns so it can be stated that this is a relatively accurate fit.
The lifetime of the reconfiguration time is fitted as 150ns, this is higher than the 50ns timescale associated with chain dynamics. In addition, there is no reason that the signal of free dye would fluctuate over time and give a photon bunching peak. Therefore the slight decay of the correlation over time is the result of either the triplet state of the fluorophores or an incomplete correction of the pile-up.
It can be concluded that the nsFCS setup and analysis are valid for a sample where no bunching peak is expected.

5.2.3 hybridised DNA

To further validate the setup and analysis method, a rigid FRET labelled molecule was necessary. A hybridised DNA strand, DNA-D23, is chosen, since a short, hybridised DNA strand is rigid, therefore, no bunching is expected in an nsFCS measurement.

The mean FRET efficiency obtained with nsFCS is compared to the values found with nsFCS, since it concerns the sample, the mean FRET efficiency should be equal for both measurement methods. From the nsFCS measurement, the mean FRET efficiency of the sample is determined, this is 0.59. This corresponds to the found FRET efficiency of 0.59 with smFRET measurements, see chapter 5.1 smFRET. Since the mean FRET efficiency obtained by nsFCS is equal to the mean FRET efficiency found in the smFRET experiment, it is shown that the determination of the FRET efficiency of a sample is accurate for nsFCS measurements.

Figure 38 shows the nsFCS curve of hybridised DNA-D23, the data is fit with equation (55). There is a clear antibunching peak present at 0ns, it is fitted as 1.7ns for the donor dye and 3.3ns for the

acceptor dye. The donor dye ATTO 550 and the acceptor ATTO 647N have an expected average lifetime of 3.6ns and 3.5ns respectively. The acceptor lifetime is as expected. The low lifetime of the donor can be explained by FRET, the lifetime of a fluorophore decreases in presence of an acceptor fluorophore. Therefore, the found lifetime of the donor dye is realistic.
To exclude that the found lifetime of the donor dye is an error of the fit, it is compared to the lifetime of the donor dye found in the smFRET measurement. The mean lifetime of the donor in presence of an acceptor is 1.5ns. This is close to the value found with nsFCS, therefore it is concluded that the nsFCS fits the fluorescent lifetime correctly.

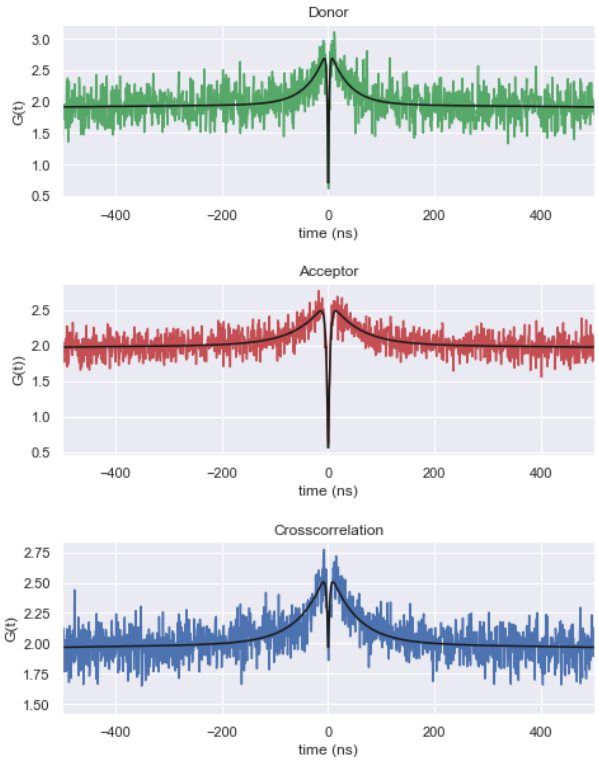

Figure 38: nsFCS curve of DNA-D23, The coloured lines represent the data, and the black line is the fit
Green is donor correlation, red acceptor and blue presents the cross-correlation
Fitted values are τ_{ab} donor = 1.7 ns τ_{ab} acceptor= 3.3 ns, τ_{cd} donor = 35 ns, τ_{cd} acceptor = 29 ns, τ_{cd} cross correlation = 35 ns

In Figure 38 a clear bunching peak is present, around 30ns, for both the donor and acceptor as for the cross-correlation, which was not as expected. The present bunching peaks of the donor and the acceptor can be explained by dye linker flexibility[55]. The fluorescent label is attached to the DNA by a short linker. This linker can move and thereby add flexibility to the dyes. This added flexibility can influence the dyes in two manners. First, a fluctuation in photon emission can arise because the distance between the FRET labels changes slightly in time. Second, fluctuations in photon emission can arise from environmental quenching due to a change in the environment as a result of the movement of the dye[55].
It is expected that in the case of fluctuations in FRET efficiency due to distance changes, a negative correlation arises at the cross-correlation, blue data in Figure 38. A positive cross-correlation indicates that the donor and acceptor signal increase and decrease simultaneously, which is impossible in the case of FRET where the radiative emission of the donor decreases as the emission of the acceptor increases due to energy transfer.
Linker flexibility can explain the observed bunching via varying environmental quenching. Due to the flexibility of the linker, the fluorophore moves and can interact with its environment. This can lead to a fluctuating radiative and FRET energy transfer due to local quenching. In the case of quenching, there is an additional component through which non-radiative energy relaxation can occur. This

competes with FRET. More quenching of the donor fluorophore leads to less energy transferred to the acceptor fluorophore and thus a decrease in emission of both donor and acceptor fluorophores. This leads to the observed positively correlated intensity fluctuations between donor and acceptor.

In the smFRET experiments shown in chapter 5.1 smFRET, the inter-dye distance based on lifetime r(τ) and intensity r(I) differ slightly. The difference in mean inter-dye distance, $\Delta r = r(\tau) - r(I)$, gives an idea of the radius of the dye's accessible volume[56]. r(τ) and r(I) can be calculated by using equations (16), (17) and (18). For the DNA-D23 sample, the radius of the dye's accessible volume is 0.5nm, so this is the freedom of the dye. Since this is a small distance, it is plausible that the fluctuations in FRET intensity are less of an influence than the fluctuations in intensity that arise from environmental quenching.

Sindbert et al. have investigated four types of alkenyl linkers on their dynamics and have shown experimentally that the dyes have a fast component around 0.5 ns and a slow component of 10 to 60ns depending on the linker[55]. The fast component is said to be due to the local reorientation of the dye and the slow component is due to the global motions of the dye and the linker. The radius of the dye's accessible volume is shown to be 0.6 to 1.6 nm, which differs between linker types.
The linker that attaches the dye to the D23 sample probed in this thesis is a C-linker, thus the exact values of the dynamics and the radius of the accessible volume do not apply. However, the linkers are comparable. The found dynamics of the dyes are 35ns for the donor and 29 ns for the acceptor, which is in a comparable timescale to other linkers. The radius of the dye's accessible volume as defined by smFRET is 0.5 nm, which is within a comparable size to the other linkers.
This shows that the observed dynamics in the nsFCS measurement are due to the flexibility of the dye linker, which causes uncertainty in dye position and quenching environment.

The hybridised DNA sample D23 shows dye-chain interaction and is therefore not suitable as a control of a rigid FRET labelled molecule. The observed phenomena do represent the dynamics of the sample, so this shows that the nsFCS analysis performs well.
On a positive note, this experiment shows that nsFCS is suitable for the determination of the occurrence of dye-linker interaction and the reconfiguration time of the linker.

5.2.4 Validation of reconfiguration time analysis

Polyethylene glycol (PEG) and single-stranded DNA (ssDNA) are used to get an initial idea of the influence of viscosity on chain dynamics in molecules that do not experience internal friction. PEG represents an ideal gaussian chain with equal FRET efficiency as the αS sample of interest so that it is a representative control for measuring αS chain dynamics. The properties of ssDNA are similar to polymer chains, therefore it is used as an initial measure to see the effect of viscosity on the chain dynamics of a non-rigid structure[57].

5.2.4.1 PEG

The PEG sample is not measured due to labelling problems, see the appendix A for an elaborate overview.

5.2.4.2 ssDNA

To probe changes in chain dynamics of a molecule as a function of viscosity, the single-stranded DNA sample described in chapter 3.1 Samples are used. ssDNA is disordered, to assess its agreement with the Gaussian chain model, a smFRET measurement is performed.

Figure 39 shows the burst plot of ssDNA, it is seen that the mean FRET efficiency over lifetime is above the static reference line, but below the gaussian chain line. This shows that ssDNA is indeed

not a static molecule, however it does not behave following the Gaussian chain model. This could be due to the intrachain interaction of the nucleotides.

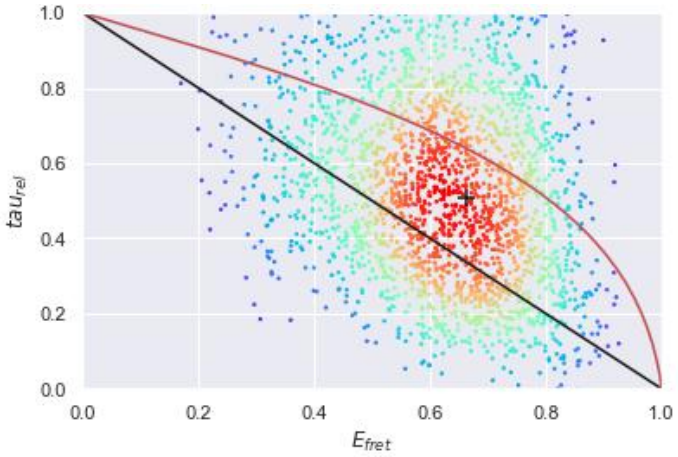

Figure 39: 2D cloud plot of FRET efficiency against the relative lifetime of ssDNA, the colour cloud coding is from red to blue for most to least frequent bursts, the back line is the static reference line, and the red line is the Gaussian chain reference, the 'plus' sign shows the mean FRET efficiency, 0.66, and the mean relative lifetime, 0.51

Since ssDNA is not a rigid molecule, it is expected that the dynamics of the ssDNA slow down in a more viscous solution, due to an increase in solvent friction. A longer reconfiguration time is expected.
Generally the shorter a DNA strand, the less sensitive it is to the solvent viscosity[58]. The ssDNA strand that is probed has a length of 27 nucleotides, which is considered as long and therefore should be sensitive to the solvent viscosity.

Two nsFCS measurements are performed, one in only buffer and one in buffer containing 30v% glycerol. The nsFCS graphs are fitted with equation (55) the reconfiguration time of the ssDNA is determined both in simple buffer and in 30v% glycerol.
Figure 40 shows the influence of the viscosity on the chain dynamics of ssDNA, it can be seen that the reconfiguration time increases slightly in a viscous solvent.
This validation experiment indicates that the chain dynamics of a non-rigid molecule are slowed down in a more viscous solvent and that this can be measured by the proposed setup and analysis method.

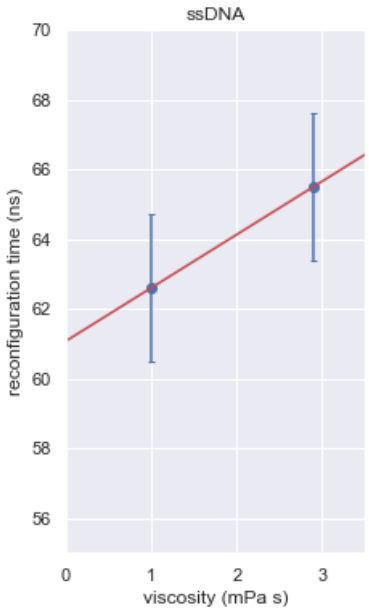

Figure 40: Influence of viscosity on chain dynamics of ssDNA, the blue dots are the datapoints and the blue lines give the standard deviation, the red line is the fit of the data

5.2.5 Assessing dye-chain interactions

It has been observed that the fluorescent dye can interact with the sample it is attached to. When assessing the chain dynamics of labelled αS it should be made sure that any photon bunching is caused by the dynamics of the protein and not by other processes such as dye interaction or interaction between proteins. Therefore, αS is labelled with a single dye to assess the dye-protein interaction. AF488, AF568 and AF594 are used since these are known to exhibit minimal dye-chain interaction.

In Figure 41 the donor nsFCS curve is shown for αS labelled with AF488 at position 140, the data is fit with equation (55). There is no acceptor present so the acceptor and cross-correlation are not shown. There is no photon bunching observed, indicating the absence of dye chain interaction. There is a reconfiguration time fitted at 140ns, this is not associated with chain dynamics but with the triplet or a not completely corrected pile-up.
The fitted lifetime of the donor signal, 3.7ns, is close to the expected average lifetime of free dye, 4.1ns. This further supports that there is no dye-chain interaction between AF488 and αS.

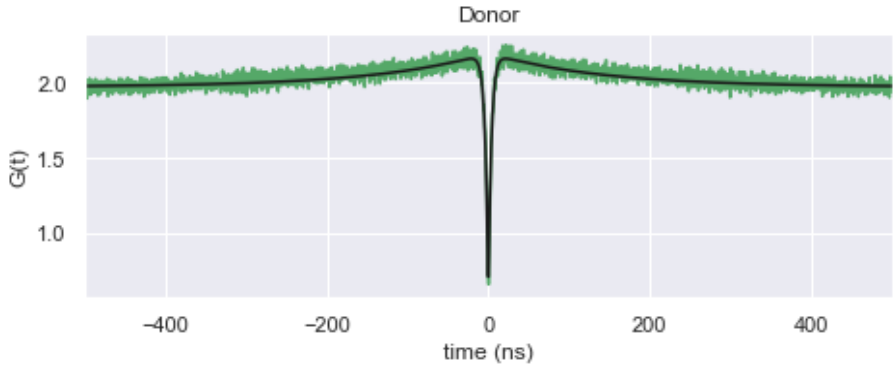

Figure 41: nsFCS curve for αS single labelled with AF488, , Fitted τ_{ab} donor= 3.7 ns, τ_{cd}= 140ns

In Figure 42 the nsFCS curve for αS labelled with AF568 is seen. There is a clear photon bunching peak present, fitted with a time of 16ns. The found reconfiguration time is in a comparable timescale

to flexible dye linkers. This indicates that there is an occurrence of interaction between the chain and the dye. The dye undergoes interaction with the side groups of the αS chain causing local quenching.

The lifetime of the dye is fitted as 2.6ns, whereas the expected average lifetime is 3.6 ns. This difference could be due to dye chain interaction, as explained in chapter 5.2.3 hybridised DNA. Due to linker flexibility, the dye is locally quenched by the side groups of αS, causing the lifetime to decrease. So there is dye-chain interaction between AF568 and αS.

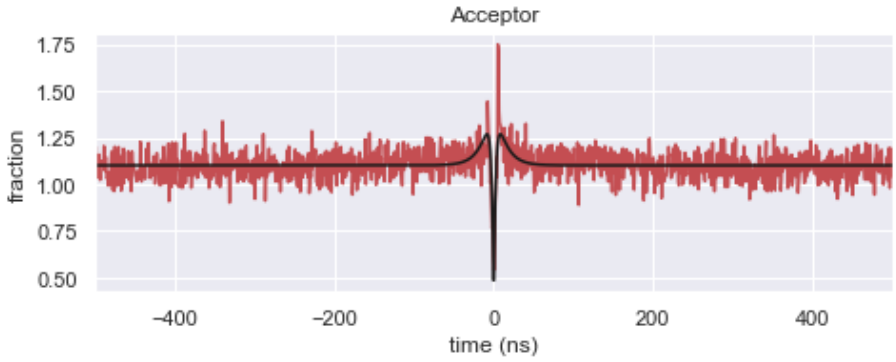

Figure 42: nsFCS curve for αS single labelled with AF568, Fitted τ_{ab} = 2.6 ns and τ_{cd}= 16 ns

In Figure 43 the nsFCS curve of αS labelled with AF594 can be seen. Here virtually no photon bunching can be observed so it can be stated that there is no interaction of the dye with the protein. There is a reconfiguration time fitted at 100ns, this is not associated with chain dynamics but with the triplet or a not completely corrected pile-up.
The lifetime of the dye is fitted as 3.6 ns, which is close to the expected average lifetime of 3.9ns. This reinforces the absence of dye-chain interaction. So there is no dye-chain interaction between AF594 and αS.

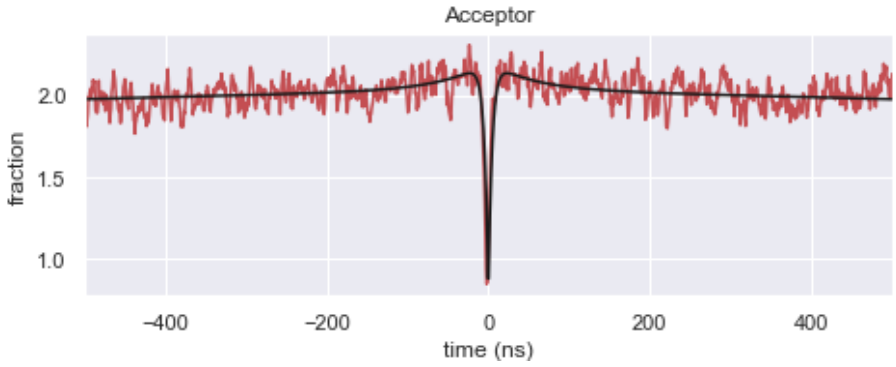

Figure 43: nsFCS curve for αS single labelled with AF594, , Fitted τ_{ab} = 3.6 ns and τ_{cd}= 100 ns

From the three αS samples labelled with a single dye, it is seen that AF488 and AF594 do not interact with αS and thus have the least influence on the photon bunching part of the nsFCS curve. The dye AF594 does show a weak interaction. It is chosen to use AF488 and AF594 as the FRET pair for labelling and further experiments on the dynamics of αS.

5.2.6 Assessing inter-chain interactions

An extra validation is performed to assess the occurrence of interaction between αS proteins. It is expected that there is no interaction present between different αS proteins, due to the low concentration of protein present. However, it is good to confirm this hypothesis experimentally.

An nsFCS measurement is performed on a sample containing an equal concentration of single labelled αS with AF488 and single labelled αS with AF594, both labelled on position 140. The sample is excited in continuous wave with a laser of 488nm, as would be for an αS FRET labelled sample. The AF594 dye can thus only be excited when it is in very close proximity to the AF488 dye.

Figure 44 shows the resulting nsFCS graph. It is seen that no photon bunching peaks are present for the donor, acceptor and cross-correlation. In addition, the intensity time trace of the measurement showed no occurrence of FRET between single labelled αS. Therefore, it can be concluded that there is no detectable inter-chain interaction.

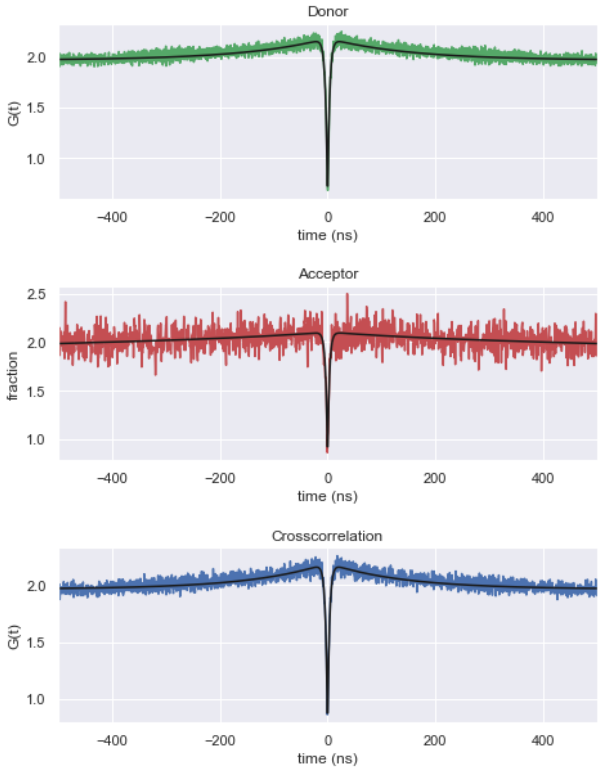

Figure 44: nsFCS curve for αS single labelled with AF488 and αS labelled with AF594
The coloured lines represent the data, the black line is the fit
Green is donor correlation, red acceptor and blue presents the cross-correlation
Fitted τ_{ab} donor = 3.7 ns τ_{ab} acceptor = 3.3 ns and τ_{ab} cross = 3.6 ns

In Figure 44, it is seen that there is some very noisy acceptor signal present. In a perfect situation, there should not be any signal in the acceptor channel, since when FRET does not occur, the acceptor fluorophores are not exited. The signal that is there is due to direct excitation of the AF594 dye by the laser and leakage from donor fluorophores to the acceptor channel. The signal of the acceptor channel is 1% of the donor channel, it can be stated that the signal at the acceptor channel will not be significant in comparison to the actual acceptor signal in measurement with FRET labelled molecules.

From this experiment, it can be concluded that there is no interaction between αS proteins. Due to the absence of both dye-protein and inter-protein interaction for AF488-594 FRET labelled αS it can be stated with certainty that when performing nsFCS measurements any seen bunching is caused by the protein chain dynamics.

6. smFRET and nsFCS on FRET labelled αS

The measurement setup and analysis for smFRET and nsFCS measurements are validated. This allows performing nsFCS measurements on FRET labelled αS to determine the reconfiguration time of αS. Chain dynamics are probed across three different parts of the protein, with the samples αS 9-69, 42-90 and 90-140.

First, the FRET labelling ratio of each sample is determined to define if sufficient FRET labelled molecules are present to conduct smFRET and nsFCS measurements.

Next, smFRET measurements are performed to characterize the average FRET efficiency and the relative lifetime of each sample.

Lastly, nsFCS is performed in a simple buffer to assess the reconfiguration time of αS.

6.1 Sample FRET labelling efficiency

For the determination of the labelling ratio of all αS samples an FCCS analysis is performed, following the method in chapter 3.6 FCCS measurements. The cRCC gives the fraction of fluorophores present that are in a FRET labelled conformation, see chapter 4.2 FCCS analysis[51]. A cRCC of 1 would be ideal. However, due to the labelling method, a value of 0.5 would statistically be expected. Table 8 shows the determined cRCC values for the FRET labelled αS samples used in this thesis.

Table 8: cRCC value of investigated αS samples

Sample	cRCC donor	cRCC acceptor
αS, 90-140	0.56	0.39
αS, 42-90	0.15	0.14
αS, 9-69	0.15	0.24

As can be seen, the cRCC values are not zero, thus there are double labelled conformations present. The lower the double labelling ratio, the fewer FRET bursts are recorded per unit of time for the same sample concentration, and thus longer measurements are required to obtain sufficient statistics for nsFCS analysis. For the samples αS, 42-90 and αS, 9-69 the cRCC is relatively low.

For each sample, a 300s smFRET measurement is performed to investigate the number of FRET bursts per second. The concentration is equal for all samples, namely 0.3nM. Upon reviewing the time trace measurements it is seen that the sample gives sufficient FRET bursts to achieve enough statistics for smFRET and nsFCS studies, namely 4 per second for the αS 42-90 and αS 9-69 sample and 15 for αS 90-140.

Figure 45 shows the time trace of the acceptor signal during donor excitation for each sample, which is associated with FRET bursts. The top panel is the time trace of αS 90-140 the middle of αS 42-90 and the bottom of αS 9-69. This time trace nicely reflects the FRET labelling efficiency, the higher the cRCC the more FRET bursts occur per second.

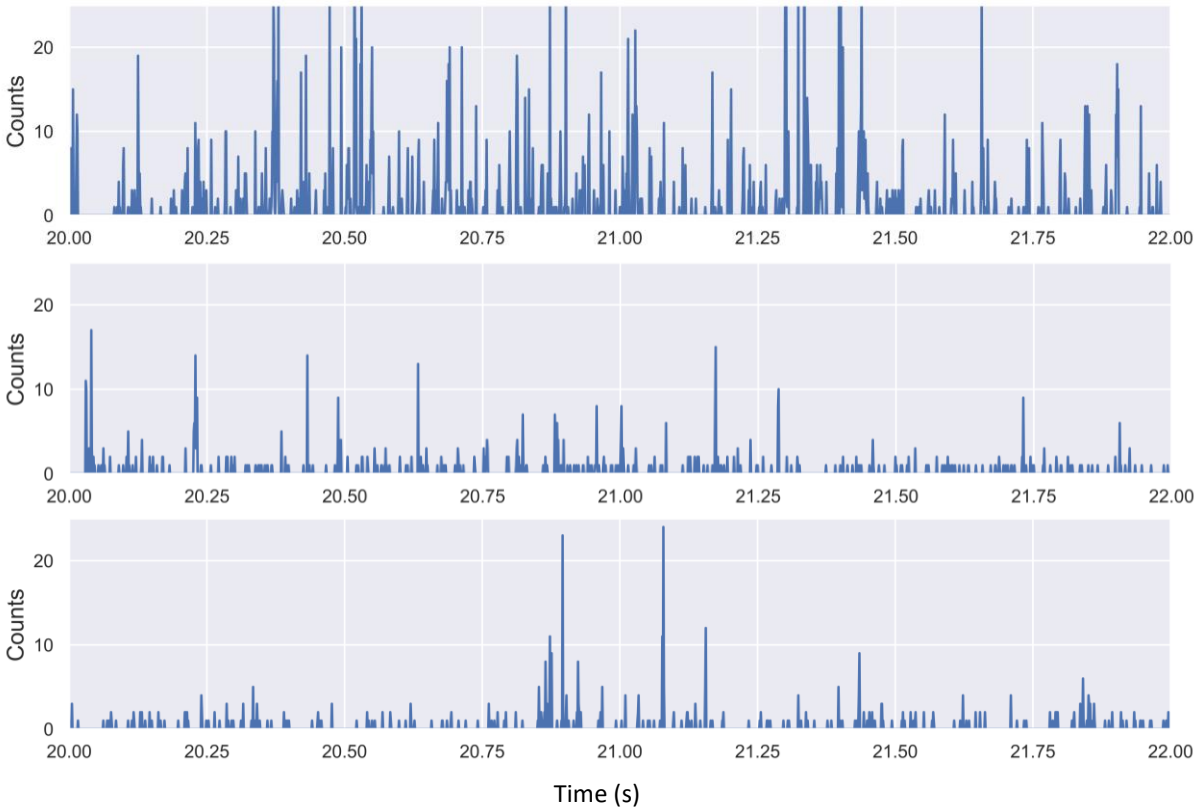

Figure 45: Time Trace of smFRET measurements, the top shows the time trace of αS 90-140 the middle of αS 42-90 and the bottom of αS 9-69.

6.2 Determining the mean FRET efficiency of αS with smFRET

smFRET measurements are performed to characterize the average FRET efficiency and relative lifetime of each sample. The measurements are performed as described in chapter 3.7 smFRET measurements.

All samples have an equal concentration of 0.3nM. For all measurements, the upper and lower bounds for selecting FRET bursts are set equally, respectively to 1000 and 10 counts per burst.

Figure 46 shows the resulting burst plot of the three αS samples. The mean FRET efficiency of αS 9-69 is 0.62, of αS 42-90 it is 0.68 and of αS 90-140 it is 0.55.

The mean points of the relative lifetime and FRET efficiency of all three samples are close to the line described by the Gaussian chain model, so the behaviour of aS can indeed be modelled as a Gaussian chain, which is in agreement with earlier findings[7,59]. The mean points of the αS 9-69 sample and αS 90-140 sample are slightly below the gaussian line. This could suggest a small deviation from the model, for αS 9-69 this is in line with earlier found results[7,59].

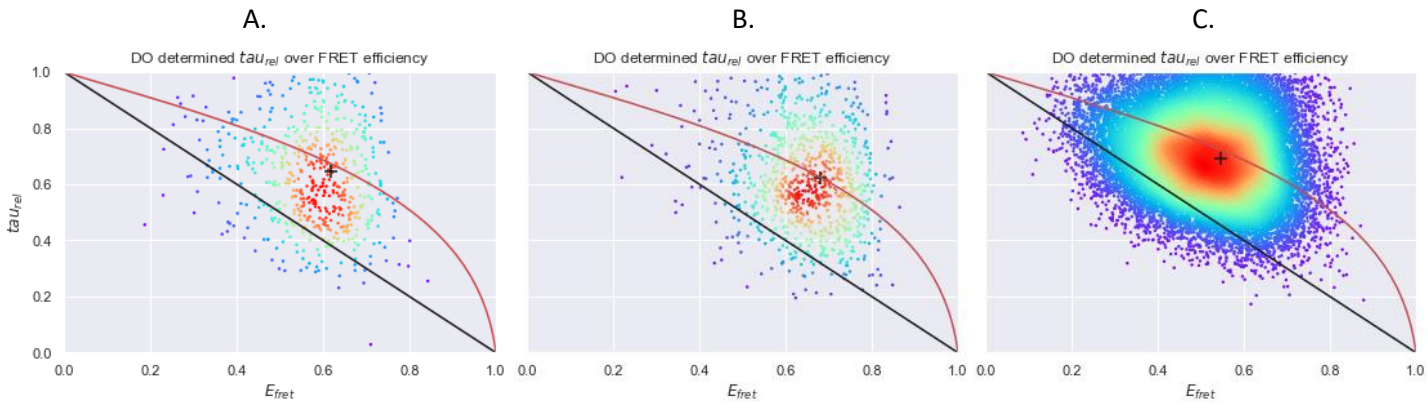

Figure 46: FRET efficiency over the relative lifetime of αS, colour coding is from red to blue for most to least frequent events, the back line is the static reference, the red line the gaussian chain line and the plus symbol marks the mean FRET efficiency over the mean relative lifetime
A. αS 9-69, mean τ_{rel} = 0.65 and mean E_{FRET} = 0.62 B. αS-42-90, mean τ_{rel} = 0.62 and mean E_{FRET} = 0.68
C. αS 90-140, mean τ_{rel} = 0.6a and mean E_{FRET} = 0.55

It is seen that the αS 90-140 sample shows many more data points than the other two samples. This is explained by the FRET labelling efficiency. The 90-140 sample has a higher cRCC than the other two samples, around 0.5 compared to around 0.2, see chapter 6.1 Sample FRET labelling efficiency. During the same measurement time, more FRET bursts occur since there are relatively more FRET labelled samples present at the same sample concentration. The double labelling efficiency of αS 9-69 and αS 42-90 samples are roughly equal and show a comparable amount of FRET events. This is in line with the determined cRCC values.

From the determined mean FRET efficiency, the mean distance between the two FRET dyes on the labelled αS chain is calculated following equation (18). The Förster radius or the FRET pair AF488-594 is 6.0 nm[60].

$$E(r) = \frac{R_0^6}{R_0^6 + r^6} \qquad (18)$$

Table 9 shows the resulting inter-dye distance based on the observed mean FRET efficiency. Although the distance in amino acids differs for each sample, the difference in mean FRET efficiency between samples is not accordingly. This suggests that the global structure of each part of the protein differs in compactness. The ends of the N-terminus, αS 9-69, are relatively closest together, followed by the NAC region, αS 42-90 and the C-tail, αS 90-140.

Table 9: Inter-dye distance based on observed mean FRET efficiency

Sample	Distance (amino acids)	E_{FRET}	$\langle r^2 \rangle$ (nm)
αS 9-69	60	0.62	5.5
αS 42-90	48	0.68	5.3
αS 90-140	50	0.55	5.8

6.3 Determining the reconfiguration time of αS with nsFCS

To determine the reconfiguration time of αS, nsFCS measurements are performed on FRET labelled αS in simple buffer as described in chapter 3.8 nsFCS measurements.
In this chapter first the nsFCS measurement for FRET labelled αS 90-140 is shown and discussed. Afterwards, the results for αS 42-90 and 6-69 are shown and the reconfiguration time for the different parts of the protein are compared.

6.2.1 nsFCS on αS 90-140

Figure 47 shows the nsFCS graph of αS 90-140, the top panel gives the donor correlation, the middle the acceptor correlation and the bottom the cross-correlation.

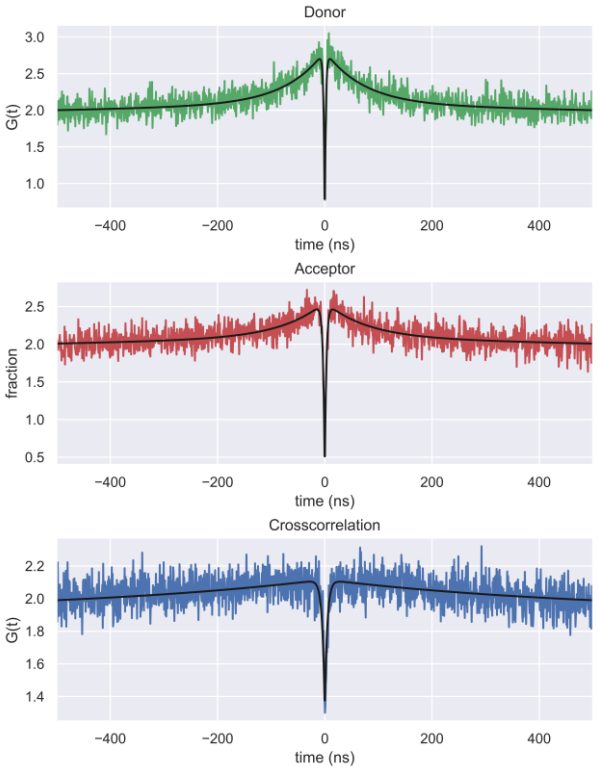

Figure 47: nsFCS curves for αS 90-140, The coloured lines represent the data, and the black line is the fit Green is donor correlation, red acceptor and blue presents the cross-correlation, fitted τab donor = 1.9 ns τab acceptor = 3.0ns tab cross =4.6 ns fitted τcd donor = 73.8 ns, τcd acceptor = 80.1 ns tcd cross = 502ns

For all three correlation curves, an antibunching dip at time 0 is seen. The fitted lifetime of the donor dye, 1.9ns, is lower than the expected average lifetime of the dye, 4.1ns. This can be explained by the occurrence of FRET as explained in chapter 2.6 Förster resonance energy transfer and 5.2.3 hybridised DNA. The fitted acceptor lifetime, 3.0ns, is relatively close to the expected lifetime of 3.9ns. The fitted lifetime of the cross-correlation is fitted as 4.6ns.
The donor and acceptor antibunching times are as expected, however, the values for the cross-correlation are larger than expected. An explanation for this will be given later.

The donor and acceptor correlations show a positive photon bunching peak around 70ns. The fitted values of the corresponding chain dynamics are close to each other, so it can be stated that the bunching is caused by the same phenomenon in both graphs.
In the cross-correlation graph, a negative bunching peak is expected due to the anticorrelation of the donor and acceptor signal. However, this is not present. What can be observed is that the antibunching for the cross-correlation is fitted slightly larger than the expected average lifetimes of

the dyes. In addition, the antibunching dip is broader than in the donor and acceptor graph. Figure 48 shows an overlay of the nsFCS corves for the donor and cross-correlation signal, with a smaller timescale on the x-axis. Here it is seen more clearly that the antibunching dip is broader for the cross-correlation than for the donor correlation.

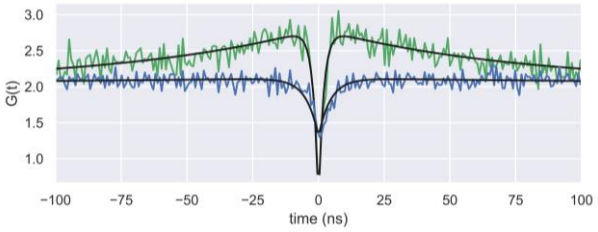

Figure 48: Overlayed nsFCS curves for donor and cross-correlation of αS 90-140
Green is donor correlation, blue presents the cross-correlation and the black lines are the fits of the data

From this observation can be concluded that there is a negative photon bunching peak present for the cross-correlation, only it is less prominent than expected. This can be explained by the following; Due to the use of a continuous wave in nsFCS instead of PIE, the bursts that are due to leakage of the donor signal cannot be determined and removed from the dataset. Therefore, the acceptor signal contains both acceptor excitation by FRET and donor leakage. This causes a minimal correlation between the detected donor and acceptor signal, which results in a less broad anticorrelation in the cross-correlation than expected. This causes the fit to incorrectly define the time of the anticorrelation as the antibunching time and to not fit the chain dynamics time properly.
In conclusion, there is anticorrelation between the donor and acceptor signal, only this is partly masked by correlation due to donor leakage to the acceptor channel.

From these observations, it can be stated that the photon bunching and anticorrelation are a result of fluctuation in the inter-dye distance. Therefore, it is shown that αS 90-140 exhibits chain dynamics, with a reconfiguration time in the order of 75ns.

6.2.2 Standard error

The standard error is calculated for the reconfiguration time defined by nsFCS analysis.
The reconfiguration time is calculated for three independent 12-hour nsFCS measurements of the same sample, αS 90-140 in simple buffer.
The mean and standard deviation of the determined reconfiguration time of these measurements is calculated. The resulting deviation is 2.1ns.
For a sample where fewer FRET bursts occur in time, it is expected that the standard error increases since the SNR decreases. Since determining the error for all samples is time-consuming, the error defined for αS 90-140 is set as the deviation for all measurements.

In later experiments, the viscosity of the solvent will be increased, this can affect the SNR and thus the error of the standard error of the reconfiguration time. In a more viscous environment, the number of molecules that pass the confocal volume is lower due to slower diffusion, this leads to fewer photons detected from separate proteins. On the other hand, due to the slower diffusion, the molecule spends a longer time in the confocal volume, which leads to more photons detected per passing protein. The resulting SNR depends on the number of detected photons per time unit, less detected photons cause a decrease and more photons an increase.
From experiments, it is seen that the SNR increases with increasing solvent viscosity. So it is assumed that the standard deviation increases. However, for the sake of time and simplicity, the error is assumed to be equal to the error for simple buffer.

6.2.3 nsFCS on αS 9-69 and 42-90

Figure 50 and Figure 49 show the nsFCS graph of αS 9-69 and αS 42-90, the top panel gives the donor correlation, the middle the acceptor correlation and the bottom the cross-correlation.

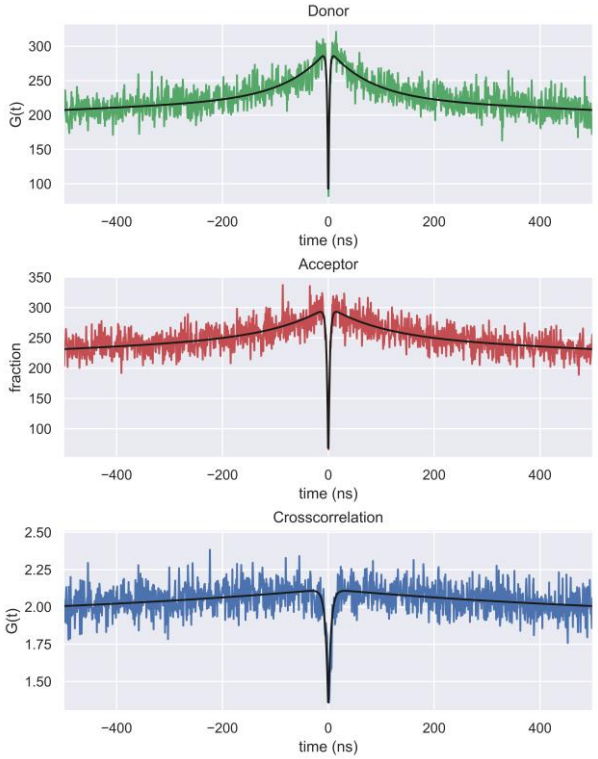

Figure 49: nsFCS curves for αS 9-69, The coloured lines represent the data, and the black line is the fit
Green is donor correlation, red acceptor and blue presents the cross correlation,
fitted τab donor = 1.9 ns τab acceptor = 2.8 ns tab cross =5.0 ns
Fitted τcd donor = 83.4 ns , τcd acceptor = 110.3 ns τcd cross = 685 ns

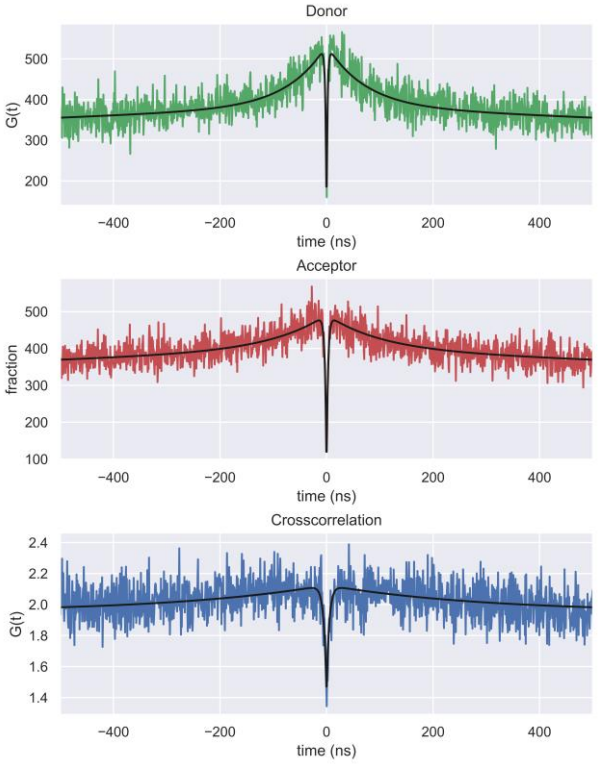

Figure 50: nsFCS curves for αS 42-90, The coloured lines represent the data, and the black line is the fit Green is donor correlation, red acceptor and blue presents the cross-correlation, fitted τab donor = 2.2 ns τab acceptor = 2.8 ns tab cross =4.6 ns τab cross = 5.0ns fitted τcd donor = 73.8 ns, τcd acceptor = 80.1 ns tcd cross = 295ns

The nsFCS graphs for αS 42-90 and 9-69 are similar to the nsFCS graph of αS 90-140.

The fitted lifetime of the donor is lower than the expected average lifetime for all samples, which can be explained by FRET. The fitted lifetime of the acceptor is generally close to the expected average lifetime. The fitted lifetime of the cross-correlation is generally higher than the expected average lifetime, as a result of correlation due to donor leakage which causes a narrower anticorrelation and leads to the fit to incorrectly define the time of the anticorrelation as the antibunching time.

All samples show a photon bunching peak for the donor and acceptor correlation and a slight anticorrelation in the cross-correlation. The fitted chain dynamics times for the donor and acceptor are all within the same timescale.
This shows that the αS exhibits chain dynamics over its whole length. For each part of the protein, the reconfiguration time differs, this can be the result of a difference in internal friction.
It is observed that the N-terminus, αS 9-69, moves slower than the NAC region and the C-tail, αS 42-90 and 90-140.

The found reconfiguration time of αS can be validated with literature. Razaei-Ghaleh et al. have reported nsFCS measurements on αS[3]. Here the αS was labelled at the locations 42-92, which is comparable to the investigated αS 42-90 sample. It would be expected that the found reconfiguration times are within the same range. Razaei-Ghaleh et al. found a reconfiguration time of 58 ns ±13 ns in buffer. In this thesis, a value of 75 ns is found for αS 42-90, which is within the error margins.

From all observed results, it can be concluded that the nsFCS measurements and analysis as used in this Thesis can be successfully used to study the chain dynamics in αS.

7. Chain dynamics of αS

In this chapter, the internal friction is probed for the three regions of αS. nsFCS measurements are performed to determine the reconfiguration time for αS with increasing solvent viscosity.
The found reconfiguration times are plotted over the solvent viscosity. It is expected that the reconfiguration time increases linearly with increasing viscosity, due to an increase in solvent friction. When a line is fitted for the reconfiguration time, the extrapolation to zero viscosity gives the timescale associated with internal friction. When performing this for all three regions of αS, the internal friction can be mapped over the protein.
In addition, the change in reconfiguration for a more and less compact conformation of αS is investigated by the use of the solvent additives HFIP and urea.
It is chosen to use the donor correlation for the determination of the reconfiguration time of the protein. The acceptor and cross-correlation signals contain donor leakage and are therefore not of best use.

7.1 Internal friction of αS

To probe the internal friction of αS, nsFCS measurements are performed on the three αS samples of interest, αS 6-69, 42-90 and 90-140, for increasing viscosity. The viscosity of the solvent is increased by adding glycerol to the solvent, the viscosities are calculated as described by Volk et al.[61].
All measurements are performed as described in chapter 3.8 nsFCS measurements and processed as described in chapter 4.5 nsFCS . The resulting values of the chain reconfiguration time, τ_{CD}, are plotted as a function of solvent viscosity and fitted with equation (9), see Figure 51.

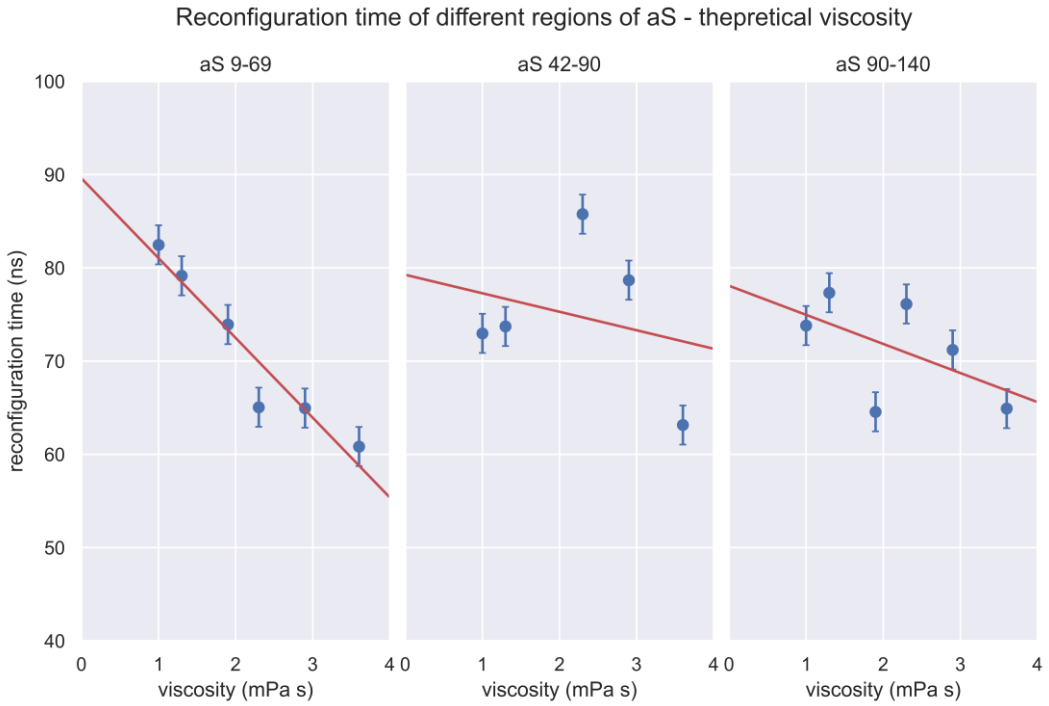

Figure 51: Reconfiguration time of different regions of αS for increasing viscosity, the blue dots are the data points, the blue lines give the standard deviation and the red line is the fit of the data

Figure 51 shows that the influence of the viscosity on the chain dynamics of the αS protein is not as expected. Since αS is an IDP it was expected that an increase in solvent viscosity would lead to an increase in solvent friction, hence, slower dynamics and thus higher chain reconfiguration times.

For αS 9-69 an inverse relation is seen, αS 42-90 shows an initial increase, followed by a decrease in reconfiguration time and 90-140 shows no overall change in reconfiguration time with increasing solvent viscosity. This results that the internal friction, at zero viscosity, cannot be extrapolated.
The observed behaviour would indicate that glycerol does not only increase the solvent viscosity but also interacts with αS in another manner. Causing a change in both solvent and internal friction. Two possible effects could be the induction of protein compaction or a deviation in viscosity in the direct environment of αS compared to the bulk[18,62].
It is known that proteins with a more compact structure are less influenced by the viscosity of the solvent. If glycerol induces protein compaction, αS would be less influenced by the solvent and thereby not show a linear relation in reconfiguration time upon increasing viscosity[63]. However, compaction of αS is only known to be induced at a concentration above 5M of glycerol, and the highest concentration of glycerol used is 4.8M[18]. Therefore this explanation seems less plausible.
A deviation in environmental viscosity of αS could be induced by the osmophobic effect[61]. The osmophobic effect is an unfavourable interaction between an osmolyte and the functional groups or backbone of a protein. This causes the osmolyte to be preferentially excluded from the protein environment[64].
The presence of both effects is investigated in the upcoming chapters.

7.2 Influence of glycerol on protein compactness

Changes in protein compactness of αS due to the presence of glycerol are assessed by determining the mean FRET efficiency and the hydrodynamic radius for increasing glycerol molarity.
If glycerol alters the protein compaction, it is expected to see a change in the mean FRET efficiency of αS upon the addition of glycerol to the solvent. It is expected that the hydrodynamic radius of the protein changes consistent with any change in FRET efficiency.

Additionally, it is investigated if glycerol changes the aggregational behaviour of αS. An aggregation experiment is performed with αS in solvent containing increasing glycerol concentrations, see appendix B for more information. It is seen that glycerol induces αS aggregation due to the preferential exclusion of glycerol from the αS environment. The aggregation experiments are performed at a sample concentration of mM while the nsFCS experiments are performed at a concentration of pM, therefore the behaviour of αS in aggregation experiments can not be directly related to nsFCS experiments.

7.2.1 mean FRET efficiency

The mean FRET efficiency of αS upon the addition of glycerol to the solvent is investigated. In Figure 52 the mean FRET efficiency defined by nsFCS measurements of all three αS samples is shown. The most left graph is for αS 9-69, the middle for αS 42-90 and the most right for αS 90-140.
The error is calculated by taking the full with half maximum of the mean FRET efficiency for the αS 90-140 sample in simple buffer. It is assumed that this does not differ largely for increasing sample viscosity and between samples. For simplicity, this is set as the error for all measurements.

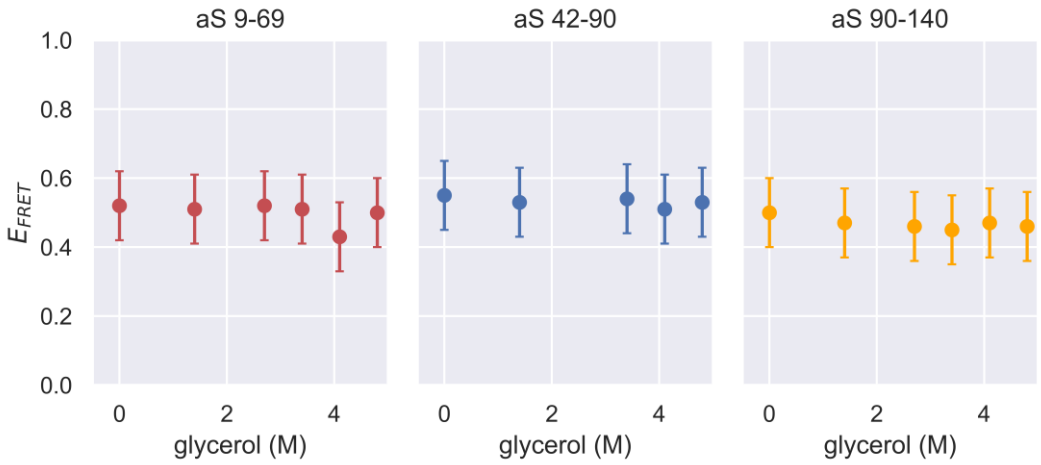

Figure 52: mean FRET efficiency of αS for increasing glycerol concentration

It is seen that the FRET efficiency remains constant for all three αS samples for increasing solvent glycerol concentration. The slight deviations in FRET efficiency are smaller than 0.1, this is probably the result of measurement variability, and not due to a change in protein structure.
Based on the FRET efficiency it is concluded that the protein does not show a change in protein compaction in the presence of glycerol. Therefore the first proposed interaction between glycerol and αS does not hold.

7.2.2 Hydrodynamic radius

In the previous subchapter, it is shown that αS does not change its global structure in the presence of glycerol. This means that the hydrodynamics radius of αS should remain the same for different solvent viscosities[65]. The hydrodynamic radius, R_h, of a particle is the spherical shape that it occupies in space and can be calculated following the Stokes-Einstein equation[66]:

$$D = \frac{k_B T}{6\pi\eta R_h} \tag{58}$$

With D the diffusion coefficient, k_B Boltzmann's constant, T absolute temperature, η viscosity and R_h the hydrodynamic radius of the particle.

The diffusion coefficient of αS is determined with FCS measurements, before nsFCS measurements. The same sample is used for both experiments to reduce parameter variability. The diffusion determined by FCS is the diffusion coefficient of the whole protein. The only difference between the three αS samples is the labelling location of the fluorophores, therefore the diffusion coefficient and any derived parameters are expected to be similar for the three samples. Small deviations can occur due to measurement or calibration variability.
If the hydrodynamic radius of αS does not remain the same for increasing sample viscosity, it means that the determined viscosity is not equal to the actual viscosity of the αS environment.

Figure 53 shows the hydrodynamic radius calculated following equation (58), with the diffusion coefficient as determined by FCS and the viscosity of the solvent, based on the glycerol concentration. The error is calculated based on the error of the diffusion coefficient, as defined by FCS.

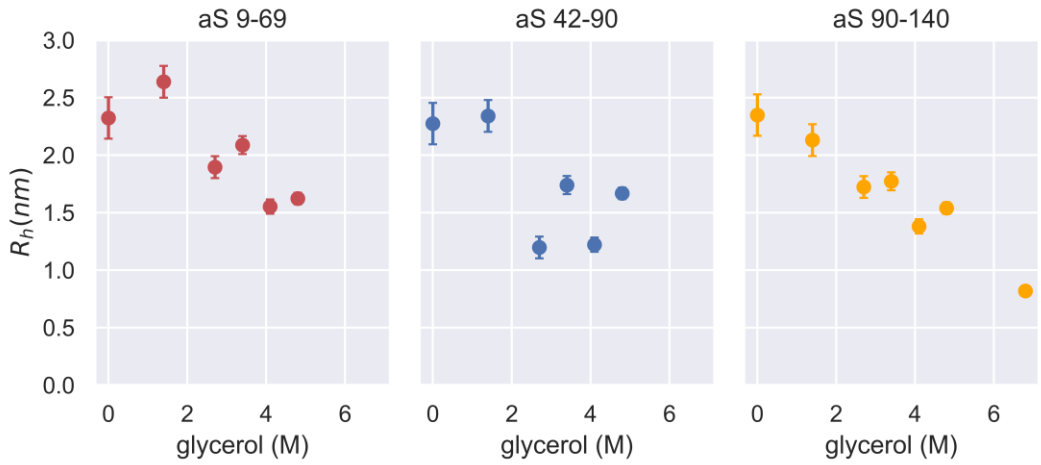

Figure 53: Hydrodynamic radius of αS for increasing glycerol concentration

It is seen that the hydrodynamic radius decreases in the presence of glycerol. This would suggest that protein compaction occurs. However, this is in contradiction to the findings of the mean FRET efficiency, which shows no change in global protein structure. An explanation would be that the viscosity of the solvent around αS is not equal to the viscosity of the bulk.
Verma et al. have shown the osmophobic effect of multiple osmolytes on αS[62]. They have found that glycerol is preferentially excluded from the environment of αS. This causes the local viscosity of αS to be lower than the viscosity of the bulk. This explains the apparent decrease in hydrodynamic radius since this is computed with the incorrect viscosity.
This finding can be used to calculate the correct environmental viscosity of αS, and show the correct relationship with the determined reconfiguration time.

7.3 Viscosity of αS environment

The correct viscosity of the environment of αS can be computed with equation (58). It is assumed that for αS in simple buffer, the environmental viscosity is equal to the viscosity of the bulk. Therefore, the R_h determined in simple buffer is assumed to remain constant with the addition of glycerol. The diffusion coefficient resulting from FCS measurement is used to compute the viscosity for each solvent containing increasing glycerol molarity.
It is expected that the environmental viscosity is equal for each sample at the same glycerol concentration. Small deviations can occur due to measurement or calibration variability.
If the theory of preferential exclusion of glycerol from the αS environment holds, then it is expected that the environmental viscosity of αS is lower than the theoretical viscosity of the bulk.

Figure 54 shows the environmental viscosity of αS, compared to the theoretical viscosity of the bulk. It is seen that the computed viscosity is lower compared to the theoretical viscosity. In addition, the environmental viscosity of αS is approximately equal for each sample at the same glycerol concentration. An extra FCS measurement is performed to assess the environmental viscosity of αS at a higher glycerol concentration, of 6.8M, 50v% glycerol. This shows that the computed viscosity increases minimally for a significantly higher glycerol concentration.
Additionally, errors in the solvent viscosity can arise due to slight deviations of environmental temperature or not perfect calibration of the used pipet and scale. However, the difference between the theoretical and calculated viscosity is too large to be due to measurement errors. The errors would need to be a 5°C increase in temperature or an error of 45% in pipetting volume or 30% in measured weight. These large deviations are highly unlikely, therefore the difference in theoretical and determined viscosity is not due to measurement errors.

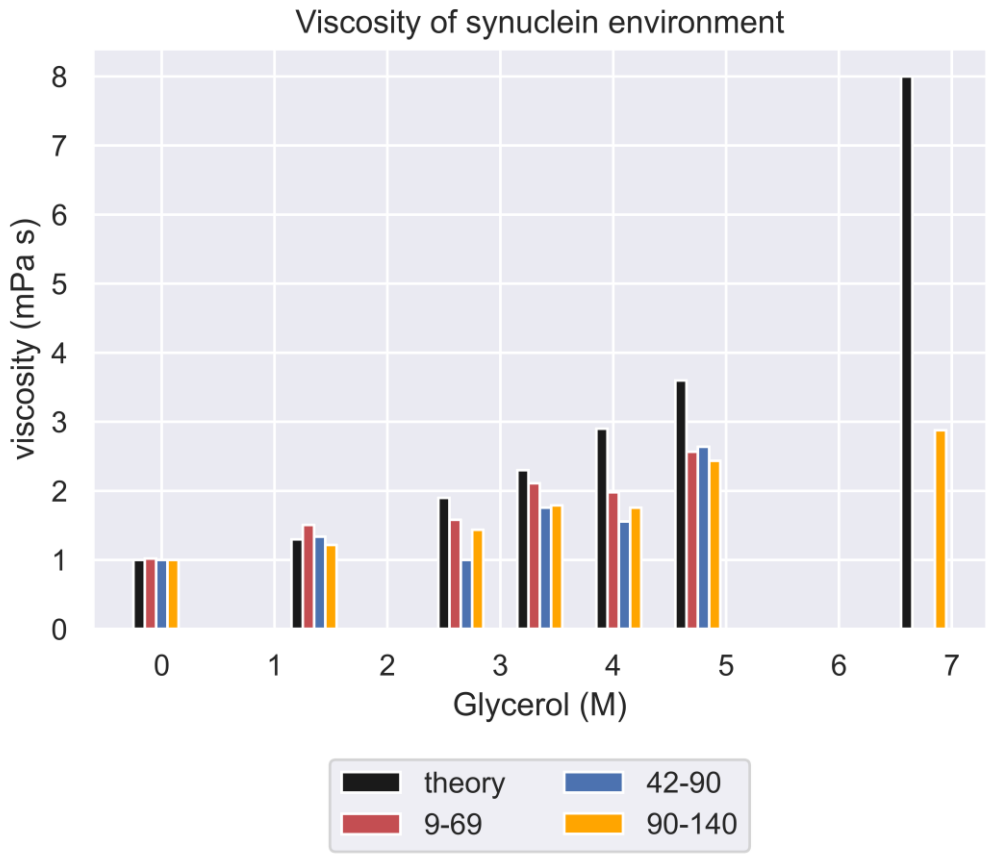

Figure 54: The computed viscosity of the αS environment with extra high glycerol measurement, the black bar is the theoretical viscosity of the bulk, red is 9-69, blue is 42-90 and orange is 90-140

These observations suggest that αS preferentially excludes glycerol from its environment, causing the environmental viscosity of αS to be lower than the viscosity of the bulk. Thus the reconfiguration time of αS should be plotted against the computed environmental viscosity and not the bulk viscosity.

7.4 Viscosity corrected influence on chain dynamics

In this chapter, it is investigated if the unexpected influence of the viscosity on the chain dynamics of αS, shown in Figure 51, can be accounted to the incorrectly defined viscosity.
The values of the chain reconfiguration time of αS, shown in Figure 51 are plotted as a function of the determined solvent viscosity shown in Figure 54.

Figure 55 shows the resulting graphs, they are fitted with equation (9) as a guide to the eye.

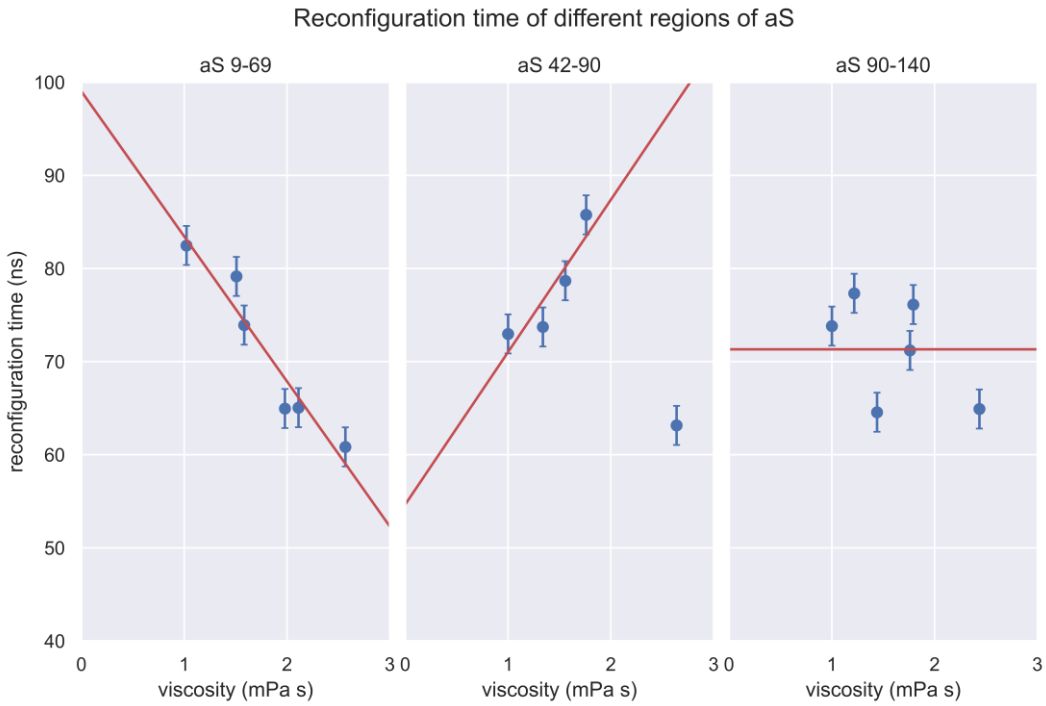

Figure 55: Reconfiguration time of different regions of αS for corrected viscosity, the blue dots are the data points, the blue lines give the standard deviation and the red line is the fit of the data, the reconfiguration time associated with internal friction is 99ns for αS 9-69, 55ns for αS 42-90 and 80ns for 90-140

It is seen that upon plotting the reconfiguration time of αS over the solvent viscosity, the trends for αS 9-69 and αS 90-140 do not change. For αS 42-90, there is now an increase in reconfiguration time with increasing solvent viscosity. So the unexpected trends can not be accounted to the incorrectly defined viscosity for all samples.

For αS 9-69 the trend remains unchanged, for increasing viscosity the reconfiguration time decreases. This could be due to the effect of glycerol on the amphipathic part of the protein. Amphipathic means that the molecular structure contains both polar and non-polar parts. However, the decrease in chain reconfiguration time can not be explained by any literature, so its origin remains unclear.
αS 42-90 shows an increase in reconfiguration time for increasing viscosity, so a realistic internal friction component is fitted, of 55ns. At a viscosity of 2.5mPa s the reconfiguration time drastically decreases, this cannot be explained with literature. This value may be the result of an inaccurate fit, for example, due to a low SNR.
αS 90-140 shows no overall change in reconfiguration time with increasing solvent viscosity. It is possible that this part of the protein is less sensitive to the solvent or is shielded from the solvent and thereby does not show a clear change in reconfiguration time in a more viscous environment.

7.5 Influence of solvent additives on protein dynamics

Even though the internal friction can not be quantified for all regions, it is still of interest to assess the change in change dynamics when αS is subjected to different solvent additives that can alter its secondary structure. Mainly changes in the configuration dynamics of the NAC region are of interest since this region is associated with aggregation.

The αS 42-90 sample probes the NAC region, therefore, the experiments shown in this chapter are performed on this sample. The change in chain dynamics is investigated for both a more compact conformation of αS and a denatured situation.

To look at the behaviour of αS with increased secondary structure the influence of HFIP on the reconfiguration time is investigated. It is known that upon the addition of HFIP, αS starts to form alpha-helixes which increase the presence of secondary structure by the formation of hydrogen bonds within the protein[25]. This is expected to introduce more internal friction and slow down the reconfiguration time.

To look at the behaviour of completely unfolded αS, the influence of viscosity on αS with 8M urea is investigated. The αS protein has been shown to have a smaller radius of gyration than a perfect random coil[67]. This suggests that αS is not completely unfolded but has a slight globular structure. In a solvent of 8M urea, it has been shown that αS is completely unfolded[68]. Therefore, upon denaturation of αS with urea, a decrease in the internal friction is expected which leads to faster chain dynamics.

7.4.1 HFIP

HFIP is known to increase the presence of secondary structure in αS by inducing alpha-helixes formation[25]. Therefore it is expected to lead to compaction and slow down chain dynamics.

αS is shown to form α-helixes at concentrations of 3 to 10v% of HFIP[25]. Therefore it is chosen to add 10v% of HFIP to the solvent.

Upon addition of 10v% of HFIP to the solvent, aggregates were seen in the intensity time trace of the sample, see Figure 56. Due to the aggregation, it was not possible to determine the reconfiguration time from the nsFCS measurements for this sample.

It is remarkable that aggregation occurs, since the concentration of αS is in the order of 500pM it has an extremely low probability to aggregate. The fact the aggregates were formed at such low protein concentration suggests that HFIP induces alpha-helix formation that causes the protein to be in a highly aggregation-prone conformation.

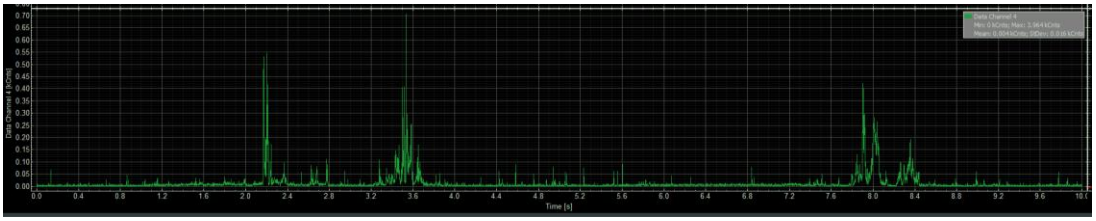

Figure 56: Intensity time trace of αS 42-90 with the addition of 10% HFiP

Since a concentration of 10v% HFIP is not suitable for nsFCS measurements a lower concentration of 2v% is chosen.

The mean FRET efficiency in the absence and presence of HFIP is determined to check whether the αS chain changes compaction. In absence of HFIP, the mean FRET efficiency of αS 42-90 is 0.56, in the presence of 2v% HFIP it is unchanged. Therefore it can be concluded that 2v% of HFIP does not induce protein compaction. No or little α-helix flormation is induced at this low concentration of HFIP.

It was still of interest to see if any changes in the reconfiguration time of αS 42-90 occur with the addition of 2v% HFIP. The resulting chain reconfiguration time is shown in Figure 57.
It is seen that the addition of 2v% HFIP to the solvent significantly slows down the dynamics of the protein. HFIP does not change the viscosity of the solvent, so since the solvent friction only depends on the viscosity, it can be assumed that HFIP leads to an increase in internal friction.
Even though no change in protein compaction is seen, this suggests the induction of α-helix formation, which causes the presence of secondary structure to limit the dynamics of the chain. No experiments are performed with the addition of glycerol due to time limitations.

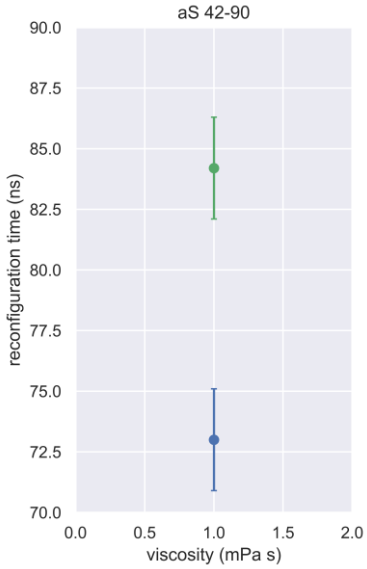

Figure 57: Influence of solvent additives on the reconfiguration time of αS 42-90. The blue data point shows the reconfiguration time in absence of HFIP, the green data point shows the reconfiguration time with the addition of 2v% HFIP

From the observed data, it can be concluded that HFIP slows down the reconfiguration time of αS. 10% of HFIP is shown to induce aggregation even at sub mM concentration.

7.4.2 Urea

The αS protein can be denatured with the addition of 8M urea to the solvent. This is expected to completely unfold the protein, and decrease or even remove internal friction, so τ_i is expected to be zero or close to zero.

The unfolding of αS is expected to show a decrease in the mean FRET efficiency and an increase in the hydrodynamic radius of the protein. The reconfiguration time of αS 42-90 in 8M urea as a function of viscosity is probed to assess the influence of urea on the internal friction. In addition to αS 42-90 also αS 9-69 is probed to see if the effect is the same for other parts of the protein.

Figure 58A shows the mean FRET efficiency and hydrodynamic radius of αS 42-90 and αS 9-69 upon the addition of 8M urea. It is seen that the presence of urea decreases the mean FRET efficiency and increases the hydrodynamic radius of αS. From this observation, it can be concluded that urea causes expansion of αS.

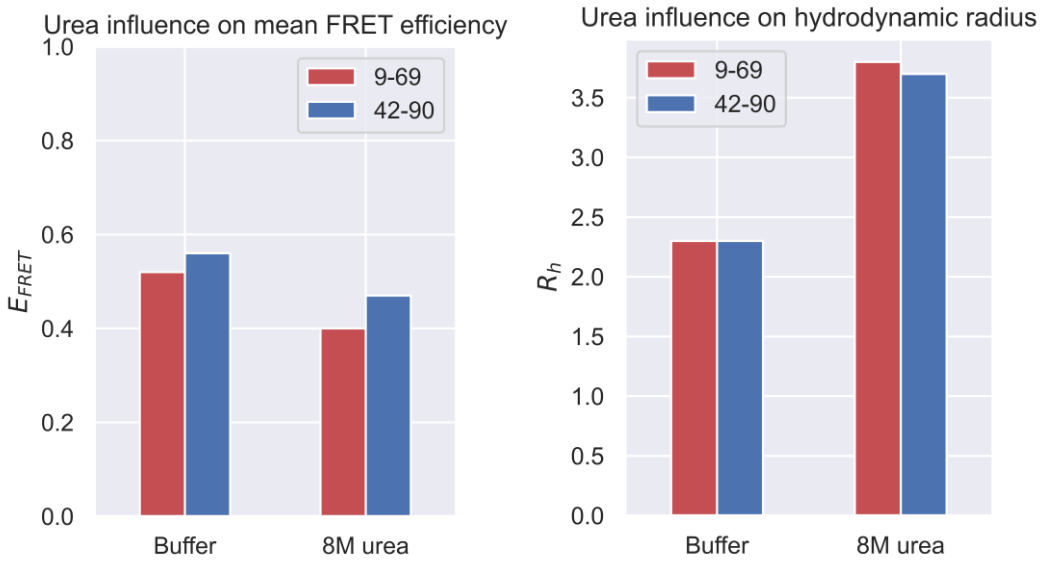

Figure 58: Influence of 8M urea on compaction of αS, red is αS 9-69 and blue is αS 42-90
On the left, the effect on the mean FRET efficiency is shown, on the right, the effect on the hydrodynamic radius is shown

It is checked if the mean FRET efficiency of αS 42-90 in presence of 8M urea changes upon the addition of glycerol, this is shown in Figure 59.

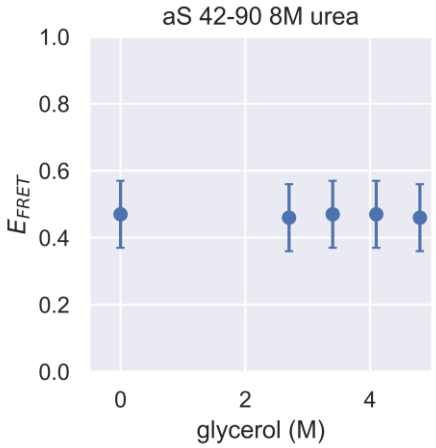

Figure 59: mean FRET efficiency of αS 42-90 with 8M urea for increasing glycerol concentration

It is seen that the mean FRET efficiency does not change with increasing glycerol concentration, so the hydrodynamic also radius remains the same. The viscosity of the αS environment can be corrected in the same manner as discussed in chapter 7.3 Viscosity of αS environment. Figure 60Figure 54 shows the resulting environmental viscosity of αS 42-90, compared to the theoretical viscosity of the bulk.

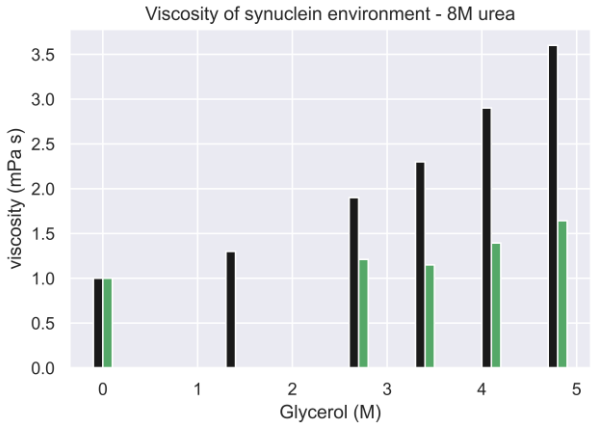

Figure 60: The computed viscosity of the αS environment with extra high glycerol measurement, the black bar is the theoretical viscosity of the bulk, the green bar of αS 42-90 with 8M urea

To assess the influence of urea on the reconfiguration time of different parts of the protein, an nsFCS measurement is made for αS 42-90 and αS 9-69 in buffer with 8M urea. The resulting reconfiguration time is compared to the reconfiguration time in absence of urea, see Figure 61.
It is seen that the reconfiguration time of αS 9-69 and αS 42-90 are almost identical in presence of 8M urea. This could suggest that all protein regions behave the same in complete denaturation, however, due to a lack of more data points no hard conclusion can be drawn.

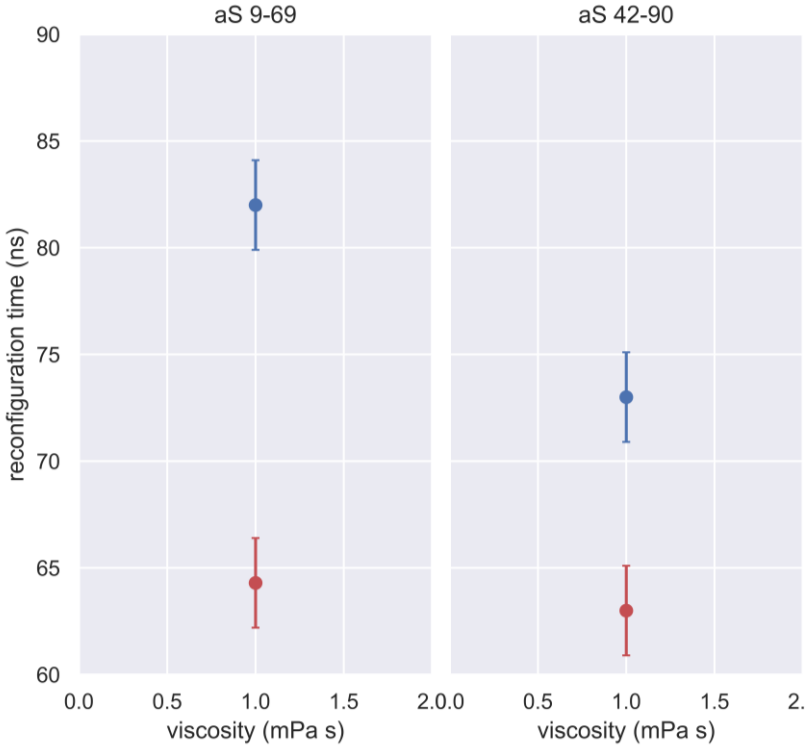

Figure 61: The influence of 8M urea on the reconfiguration time in simple buffer of αS 9-69, left graph, and 42-90, right graph. The blue data points are without the addition of urea, and the red data points are with the addition of 8m urea

The internal friction of αS in presence of 8M urea is determined for only αS 42-90 since only for this part of the protein the internal friction is known in absence of urea.
Figure 62 shows the reconfiguration time as a function of corrected viscosity for αS 42-90 both in the absence and presence of 8M urea. It is seen that the overall reconfiguration time of αS decreases in presence of 8M urea. This could be due to the absence of secondary structure, this causes a decrease or even absence of internal friction, resulting in a decrease in total reconfiguration time.
Figure 62 shows that the reconfiguration time initially increases with increasing viscosity and thereafter decreases suddenly for glycerol concentrations above 4M. There is no clear reasoning behind this behaviour that can be supported by the literature.
8M of urea is expected to completely denature αS, so no secondary structure should be present. It is expected that the internal friction is zero or close to zero, and that protein dynamics are slowed down in a more viscous solvent.
For the initial increase in reconfiguration time, the red line, the internal friction at zero viscosity, τ_i, is fitted at 24ns. The green line gives a τ_i of 39ns. Both values are significantly lower than the found τ_i of 55ns in absence of urea. This shows that urea lowers the internal friction of αS, as was expected. However, urea does not completely denature the protein, this could be the consequence of interaction with glycerol.

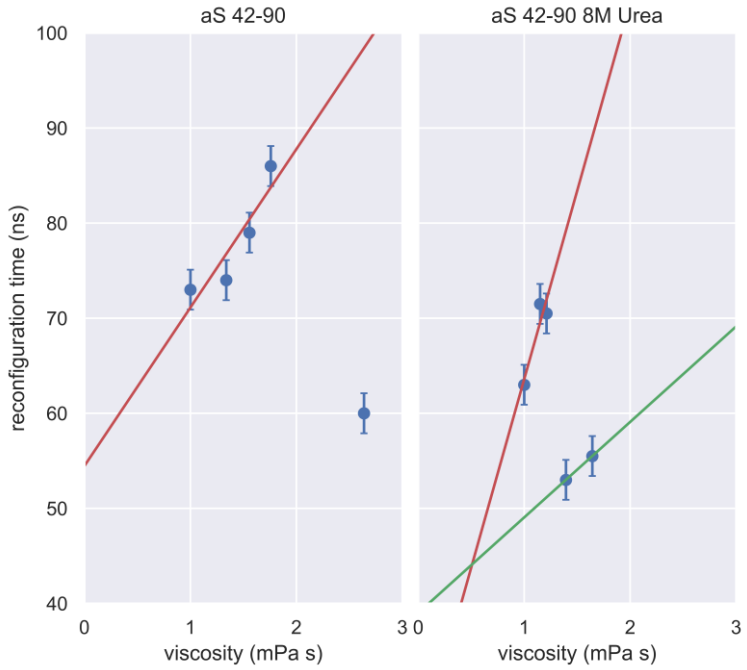

Figure 62: The influence of 8M urea on the reconfiguration time of αS 42-90, the left panel is without the addition of urea, the right panel is with 8M urea added to the solvent, and the red line is the fit of the first three data points and the second line the fit of the last two data points, the reconfiguration time associated with internal friction 55ns in absence of urea, in presence of urea it is 24 ns for the red line and 39ns for the green line

Additionally, it is seen that the overall viscosity of the αS environment is lower in presence of urea compared to the absence of urea. All measurements are performed with the same glycerol concentration series, therefore a difference in environmental viscosity is attributed to a difference in αS interaction with the solvent. The more unfolded a protein is, the more it is exposed to the osmolyte present in the solvent. This causes a stronger preferential exclusion of the osmolyte from the protein environment[64]. This could explain the behaviour of αS in presence of both 8M urea and glycerol. Because the protein is completely denatured, the preferential exclusion of glycerol from the protein environment is more prominent. This results in a lower environmental viscosity of αS.

From the experiment performed with 8M urea, it can be stated that nsFCS poses a suitable manner to determine the change in reconfiguration time of αS upon denaturation of the protein. It is shown that the internal friction of αS decreases with denaturation.

8. General conclusion and discussion

This thesis aimed to study the conformational chain dynamics of αS. The technique nsFCS is used to determine the chain reconfiguration time and the internal friction of αS for the C terminus, NAC region and the N-terminus. The change in reconfiguration time due to denaturation and secondary structure formation is also studied.

αS exhibits a different behaviour in reconfiguration time upon exposure to glycerol for each part of the protein.
For the N-terminus, it is observed that the reconfiguration time decreases with increasing viscosity, a fact that could not be explained by the theory.
For the NAC region, the reconfiguration time does increase with increasing viscosity. This part of the protein behaves like a random coil where solvent-dependent friction increases with increasing solvent viscosity.
The C-terminus shows no overall change in reconfiguration time for increasing viscosity. This could be the result of less surface exposure to the solvent, leading to a minimal or absence of change in solvent-dependent friction.

Changes in the configuration dynamics of the NAC region are of great interest since this region is associated with aggregation. The change in chain dynamics is investigated for a less and more compact conformation of αS. The NAC region shows a decrease in reconfiguration time when it is completely denatured and an increase in reconfiguration time when secondary structure is induced.
The NAC region shows a decrease in reconfiguration time in presence of urea, which corresponds to faster dynamics. This is attributed to the denaturing properties of urea, less secondary structure leads to less internal friction.
The NAC region shows an increase in reconfiguration time in presence of HFIP, which corresponds to slower dynamics. This is attributed to the formation of α-helical structure in the protein, this induction of secondary structure leads to more internal friction.

An additional observation is that glycerol is preferentially excluded from the αS environment, leading to a local decrease in the environmental viscosity of αS. In addition, the expansion of the protein by denaturation leads to a higher preferential exclusion of glycerol, causing an even lower environmental viscosity of αS.

It is observed that HFIP induces aggregation, even at unexpectedly low concentrations of aS, in the pico Molar range.

During the validation of the measurement setup and analysis, it is also shown that nsFCS allows for the determination of dye-linker dynamics time.

Even though the internal friction of αS could not be quantified for all parts of the protein, the results do give insight into the configuration dynamics of αS and the change in different solvents. It is proven that the technique of nsFCS in combination with smFRET poses a promising way to study the effect of different solvents and situations on the dynamics of the intrinsically disordered protein alpha-synuclein.

9. Outlook and recommendations

In this thesis, the chain reconfiguration times across different parts of αS are probed as a function of solvent viscosity to study chain dynamics and quantify internal friction.

The behaviour of αS is more complex than initially thought. The main drawback of this experiment is that the compound used to change the solvent viscosity, glycerol, influences αS also in other manners. Glycerol is preferentially excluded from the αS environment, which lowers the environmental viscosity. For some regions of αS, it was not possible to probe the internal friction component.

To study only the changes in chain dynamics as a function of the viscosity and no other parameters, an alternative manner of altering solvent viscosity can be investigated in the future. This could be done by altering the temperature or adding another chemical compound.

To put the observed behaviour of the chain dynamics more into perspective it is advised to study the influence of 8M urea on both the 9-69 and the 90-140 at increasing solvent viscosity. In addition, the influence of other solvent additives, like a high salt concentration, could be of interest to study the change in chain dynamics.

In the future, it is interesting to observe the influence of several binding partners on the dynamics of the αS protein and relate this with aggregation behaviour. For example, the N-protein and τ-protein since these are known to decrease the lag time of αS aggregation[69]. In this manner, a better fundamental understanding can be created of the relation between protein dynamics and the propensity to aggregate.

For future studies, it is advised to use samples with a high labelling efficiency since this results in higher SNR of the data. In addition, zero-mode waveguides can be used. These can drastically shorten the measurement time, from 12 hours to 30 minutes, while also increasing the number of bursts of interest[70].

Bibliography

1. FN E. Alpha-synuclein structure, functions, and interactions. *J Res Med Sci*. 2016;21(2). doi:10.4103/1735-1995.181989

2. Volpicelli-Daley LA, Luk KC, Patel TP, et al. Exogenous α-Synuclein Fibrils Induce Lewy Body Pathology Leading to Synaptic Dysfunction and Neuron Death. *Neuron*. 2011;72(1):57-71. doi:10.1016/J.NEURON.2011.08.033

3. Rezaei-Ghaleh N, Parigi G, Soranno A, et al. Local and Global Dynamics in Intrinsically Disordered Synuclein. *Angew Chemie Int Ed*. 2018;57(46):15262-15266. doi:10.1002/anie.201808172

4. Semerdzhiev S. HIERARCHICAL SELF-ASSEMBLY OF ALPHA-SYNUCLEIN: FROM DISEASE TO MATERIALS. 2016.

5. Wang C, Zhao C, Li D, et al. Versatile structures of α-synuclein. *Front Mol Neurosci*. 2016;9(JUNE):48. doi:10.3389/FNMOL.2016.00048/BIBTEX

6. Brodie NI, Popov KI, Petrotchenko E V., Dokholyan N V., Borchers CH. Conformational ensemble of native α-synuclein in solution as determined by short-distance crosslinking constraint-guided discrete molecular dynamics simulations. *PLOS Comput Biol*. 2019;15(3):e1006859. doi:10.1371/JOURNAL.PCBI.1006859

7. Marseille MJ. Conformation and flexibility of the intrinsically disordered protein. 2020.

8. Grosberg AY, Khokhlov AR, de Gennes PG. Giant molecules: Here, there, and everywhere, second edition. *Giant Mol Here, There, Everywhere, Second Ed*. January 2010:1-322. doi:10.1142/7199

9. (PDF) Conformations of Polymer Chains Lecture manuscripts of the 39th Spring School 2008: "Soft Matter - From Synthetic to Biological Materials", Eds.: J.K.G. Dhont, G. Gompper, G. Nägele, D. Richter, R.G. Winkler, pages C1.1 - C1.23. https://www.researchgate.net/publication/259601416_Conformations_of_Polymer_Chains_Lecture_manuscripts_of_the_39th_Spring_School_2008_Soft_Matter_-_From_Synthetic_to_Biological_Materials_Eds_JKG_Dhont_G_Gompper_G_Nagele_D_Richter_RG_Winkler_pages_C11_. Accessed November 26, 2021.

10. B S, A S, H H, D N. Single-Molecule FRET Spectroscopy and the Polymer Physics of Unfolded and Intrinsically Disordered Proteins. *Annu Rev Biophys*. 2016;45:207-231. doi:10.1146/ANNUREV-BIOPHYS-062215-010915

11. Radiom M, Paul MR, Ducker WA. Dynamics of single-stranded DNA tethered to a solid. 2016. doi:10.1088/0957-4484/27/25/255701

12. Soranno A, Zosel F, Hofmann H. Internal friction in an intrinsically disordered protein—Comparing Rouse-like models with experiments. *J Chem Phys*. 2018;148(12):123326. doi:10.1063/1.5009286

13. Zheng W, Hofmann H, Schuler B, Best RB. Origin of Internal Friction in Disordered Proteins Depends on Solvent Quality. *J Phys Chem B*. 2018;122(49):11478-11487. doi:10.1021/acs.jpcb.8b07425

14. Soranno A, Holla A, Dingfelder F, Nettels D, Makarov DE, Schuler B. Integrated view of internal friction in unfolded proteins from single-molecule FRET, contact quenching, theory, and simulations. *Proc Natl Acad Sci U S A*. 2017;114(10):E1833-E1839. doi:10.1073/PNAS.1616672114/SUPPL_FILE/PNAS.1616672114.SAPP.PDF

15. Golden M, Garcia-Portugués E, Sørensen M, Mardia K V., Hamelryck T, Hein J. A Generative Angular Model of Protein Structure Evolution. *Mol Biol Evol*. 2017;34(8):2085-2100. doi:10.1093/MOLBEV/MSX137

16. Egorov A V., Lyubartsev AP, Laaksonen A. Molecular dynamics simulation study of glycerol-water liquid mixtures. *J Phys Chem B*. 2011;115(49):14572-14581. doi:10.1021/JP208758R/ASSET/IMAGES/LARGE/JP-2011-08758R_0008.JPEG

17. Soranno A, Buchli B, Nettels D, et al. Quantifying internal friction in unfolded and intrinsically

disordered proteins with single-molecule spectroscopy. *Proc Natl Acad Sci U S A*. 2012;109(44):17800-17806. doi:10.1073/pnas.1117368109

18. Gertjan Veldhuis AA and VS. INDUCED FOLDING OF THE INTRINSICALLY DISORDERED PROTEIN ALPHA-SYNUCLEIN: ROLE OF OSMOLYTES. 31(0):1-34.

19. Glycerol. https://stringfixer.com/nl/Glycerol. Accessed April 6, 2022.

20. Zou Q, Habermann-Rottinghaus SM, Murphy KP. Urea Effects on Protein Stability: Hydrogen Bonding and the Hydrophobic Effect. *Proteins*. 1998;31:107-115. doi:10.1002/(SICI)1097-0134(19980501)31:2

21. Halonen S, Kangas T, Haataja M, Lassi U. Urea-Water-Solution Properties: Density, Viscosity, and Surface Tension in an Under-Saturated Solution. *Emiss Control Sci Technol*. 2017;3(2):161-170. doi:10.1007/S40825-016-0051-1/TABLES/5

22. Urea - American Chemical Society. https://www.acs.org/content/acs/en/molecule-of-the-week/archive/u/urea.html. Accessed April 5, 2022.

23. Sixty Solvents: http://www.chem.rochester.edu/notvoodoo/pages/sixty_solvents.php?page=hexafluoroisopropanol. Accessed May 23, 2022.

24. Gast K, Siemer A, Zirwer D, Damaschun G. Fluoroalcohol-induced structural changes of proteins: some aspects of cosolvent-protein interactions. *Eur Biophys J*. 2001;30(4):273-283. doi:10.1007/S002490100148

25. Munishkina LA, Phelan C, Uversky VN, Fink AL. Conformational behavior and aggregation of α-synuclein in organic solvents: Modeling the effects of membranes. *Biochemistry*. 2003;42(9):2720-2730. doi:10.1021/BI027166S/ASSET/IMAGES/LARGE/BI027166SH00001.JPEG

26. 1,1,1,3,3,3-Hexafluoro-2-propanol = 99 920-66-1. https://www.sigmaaldrich.com/NL/en/product/aldrich/105228. Accessed April 6, 2022.

27. Khatri BS, McLeish TCB. Rouse Model with Internal Friction: A Coarse Grained Framework for Single Biopolymer Dynamics. *Macromolecules*. 2007;40(18):6770-6777. doi:10.1021/MA071175X

28. Sanderson MJ, Smith I, Parker I, Bootman MD. Fluorescence microscopy. *Cold Spring Harb Protoc*. 2014;2014(10):1042-1065. doi:10.1101/pdb.top071795

29. Molecular Expressions Microscopy Primer: Specialized Microscopy Techniques - Fluorescence - Basic Concepts in Fluorescence. https://micro.magnet.fsu.edu/primer/techniques/fluorescence/fluorescenceintro.html. Accessed November 19, 2021.

30. Fluorochrome Spectra | Chroma Technology Corp. https://www.chroma.com/knowledge-resources/about-fluorescence/introduction-to-fluorescence/fluorochrome-spectra. Accessed December 17, 2021.

31. Jain A, Blum C, Subramaniam V. Fluorescence Lifetime Spectroscopy and Imaging of Visible Fluorescent Proteins. *Adv Biomed Eng*. January 2009:147-176. doi:10.1016/B978-0-444-53075-2.00004-6

32. Fluorescence Microscopy: In-Line Illumination with Imaging Filters. https://www.edmundoptics.eu/knowledge-center/application-notes/microscopy/fluorescence-microscopy-in-line-illumination-with-imaging-filters/. Accessed December 16, 2021.

33. Ishikawa-Ankerhold HC, Ankerhold R, Drummen GPC. Advanced Fluorescence Microscopy Techniques—FRAP, FLIP, FLAP, FRET and FLIM. *Molecules*. 2012;17(4):4047-4132. doi:10.3390/molecules17044047

34. The basic principles of fluorescence and FRET. (A) Jablonski diagram,... | Download Scientific Diagram. https://www.researchgate.net/figure/The-basic-principles-of-fluorescence-and-FRET-A-Jablonski-diagram-explaining-the_fig1_283239055. Accessed November 26, 2021.

35. Roy R, Hohng S, Ha T. A practical guide to single-molecule FRET. *Nat Methods 2008 56*. 2008;5(6):507-

516. doi:10.1038/nmeth.1208

36. Ries J, Schwille P. Fluorescence correlation spectroscopy. *BioEssays*. 2012;34(5):361-368. doi:10.1002/BIES.201100111

37. MicroTime 200 | PicoQuant. https://www.picoquant.com/products/category/fluorescence-microscopes/microtime-200-time-resolved-confocal-fluorescence-microscope-with-unique-single-molecule-sensitivity. Accessed May 23, 2022.

38. File:FCCS Simulations.svg - Wikimedia Commons. https://commons.wikimedia.org/wiki/File:FCCS_Simulations.svg. Accessed June 27, 2022.

39. PicoQuant. Photon Counting and Timing Reliable and easy to use modules with high-end performance.

40. The Principle of Time-Correlated Single Photon Counting.

41. Daniel Nettels, Armin Hoffmann and, Schuler* B. Unfolded Protein and Peptide Dynamics Investigated with Single-Molecule FRET and Correlation Spectroscopy from Picoseconds to Seconds†. *J Phys Chem B*. 2008;112(19):6137-6146. doi:10.1021/JP076971J

42. Nettels D, Hoffmann A, Schuler B. Unfolded Protein and Peptide Dynamics Investigated with Single-Molecule FRET and Correlation Spectroscopy from Picoseconds to Seconds †. 2008. doi:10.1021/jp076971j

43. Nettels D, Gopich I V., Hoffmann A, Schuler B. Ultrafast dynamics of protein collapse from single-molecule photon statistics. *Proc Natl Acad Sci*. 2007;104(8):2655-2660. doi:10.1073/PNAS.0611093104

44. Antibunching | PicoQuant. https://www.picoquant.com/applications/category/metrology/antibunching. Accessed November 16, 2021.

45. Hellenkamp B, Schmid S, Doroshenko O, et al. Precision and accuracy of single-molecule FRET measurements—a multi-laboratory benchmark study. *Nat Methods*. 2018;15(9):669-676. doi:10.1038/s41592-018-0085-0

46. Fakhree MAA, Nolten IS, Blum C, Claessens MMAE. Different Conformational Subensembles of the Intrinsically Disordered Protein α-Synuclein in Cells. *J Phys Chem Lett*. 2018;9(6):1249-1253. doi:10.1021/ACS.JPCLETT.8B00092/SUPPL_FILE/JZ8B00092_SI_001.PDF

47. Zeba™ Spin Desalting Columns, 7K MWCO, 5 mL. https://www.thermofisher.com/order/catalog/product/89891. Accessed June 29, 2022.

48. SPCM-AQRH-TR, Single Photon Counting Module for Time Resolution. https://www.excelitas.com/product/spcm-aqrh-tr. Accessed June 17, 2022.

49. MicroTime 200 A versatile platform for time-resolved confocal microscopy. www.picoquant.com. Accessed November 19, 2021.

50. Pulsed Interleaved Excitation (PIE) | PicoQuant. https://www.picoquant.com/applications/category/life-science/pulsed-interleaved-excitation-pie. Accessed October 12, 2021.

51. Sadaie W, Harada Y, Matsuda M, Aoki K. Quantitative In Vivo Fluorescence Cross-Correlation Analyses Highlight the Importance of Competitive Effects in the Regulation of Protein-Protein Interactions. *Mol Cell Biol*. 2014;34(17):3272. doi:10.1128/MCB.00087-14

52. Heesink G, Boamfa A. Analysis of smFRET and nsFCS experiments with Python 3.9. 2021.

53. Cherny DI, Eperon IC, Bagshaw CR. Probing complexes with single fluorophores: Factors contributing to dispersion of FRET in DNA/RNA duplexes. *Eur Biophys J*. 2009;38(4):395-405. doi:10.1007/S00249-008-0383-Z/FIGURES/7

54. scipy.stats.gaussian_kde — SciPy v1.8.1 Manual.

https://docs.scipy.org/doc/scipy/reference/generated/scipy.stats.gaussian_kde.html. Accessed June 12, 2022.

55. Sindbert S, Kalinin S, Nguyen H, et al. Accurate distance determination of nucleic acids via förster resonance energy transfer: Implications of dye Linker length and rigidity. *J Am Chem Soc*. 2011;133(8):2463-2480. doi:10.1021/JA105725E/SUPPL_FILE/JA105725E_SI_001.PDF

56. Sindbert S, Kalinin S, Nguyen H, et al. Accurate distance determination of nucleic acids via förster resonance energy transfer: Implications of dye Linker length and rigidity. *J Am Chem Soc*. 2011;133(8):2463-2480. doi:10.1021/JA105725E/SUPPL_FILE/JA105725E_SI_001.PDF

57. Latinwo F, Schroeder CM. Model systems for single molecule polymer dynamics. *Soft Matter*. 2011;7(18):7907. doi:10.1039/C1SM05298E

58. Uzawa T, Cheng RR, Cash KJ, Makarov DE, Plaxco KW. The Length and Viscosity Dependence of End-to-End Collision Rates in Single-Stranded DNA. *Biophys J*. 2009;97(1):205-210. doi:10.1016/J.BPJ.2009.04.036

59. Boamfa A. Modelling alpha-synuclein as a Gaussian chain. 2021;(equation 1).

60. R<0> values for some Alexa Fluor dyes—Table 1.6 | Thermo Fisher Scientific - US. Thermo Fisher Scientific. //www.thermofisher.com/uk/en/home/references/molecular-probes-the-handbook/tables/r0-values-for-some-alexa-fluor-dyes.html. Accessed February 1, 2022.

61. Volk A, Kähler CJ. Density model for aqueous glycerol solutions. *Exp Fluids*. 2018;59(5):1-4. doi:10.1007/S00348-018-2527-Y/FIGURES/2

62. Verma G, Singh P, Bhat R. Disorder under stress: Role of polyol osmolytes in modulating fibrillation and aggregation of intrinsically disordered proteins. *Biophys Chem*. 2020;264:106422. doi:10.1016/J.BPC.2020.106422

63. Zheng W, Hofmann H, Schuler B, Best RB. Origin of Internal Friction in Disordered Proteins Depends on Solvent Quality. *J Phys Chem B*. 2018;122(49):11478-11487. doi:10.1021/ACS.JPCB.8B07425/SUPPL_FILE/JP8B07425_SI_001.PDF

64. Bolen DW, Baskakov I V. The osmophobic effect: natural selection of a thermodynamic force in protein folding. *J Mol Biol*. 2001;310(5):955-963. doi:10.1006/JMBI.2001.4819

65. Lobanov MY, Bogatyreva NS, Galzitskaya O V. Radius of gyration as an indicator of protein structure compactness. *Mol Biol 2008 424*. 2008;42(4):623-628. doi:10.1134/S0026893308040195

66. Ahmed MC, Crehuet R, Lindorff-Larsen K. Computing, analyzing and comparing the radius of gyration and hydrodynamic radius in conformational ensembles of intrinsically disordered proteins. *bioRxiv*. August 2019:679373. doi:10.1101/679373

67. Uversky VN, Li J, Souillac P, et al. Biophysical Properties of the Synucleins and Their Propensities to Fibrillate: INHIBITION OF α-SYNUCLEIN ASSEMBLY BY β- AND γ-SYNUCLEINS. *J Biol Chem*. 2002;277(14):11970-11978. doi:10.1074/JBC.M109541200

68. Bertoncini CW, Jung YS, Fernandez CO, et al. From the Cover: Release of long-range tertiary interactions potentiates aggregation of natively unstructured α-synuclein. *Proc Natl Acad Sci U S A*. 2005;102(5):1430. doi:10.1073/PNAS.0407146102

69. Semerdzhiev SA, Fakhree MAA, Segers-Nolten I, Blum C, Claessens MMAE. Interactions between SARS-CoV-2 N-Protein and α-Synuclein Accelerate Amyloid Formation. *ACS Chem Neurosci*. 2022;13(1):143-150. doi:10.1021/ACSCHEMNEURO.1C00666/SUPPL_FILE/CN1C00666_SI_001.PDF

70. Nü Esch MF, Ivanović,Ivanović, MT, Claude J-B, et al. Single-molecule Detection of Ultrafast Biomolecular Dynamics with Nanophotonics. *J Am Chem Soc*. December 2021:jacs.1c09387. doi:10.1021/JACS.1C09387

71. Polyethylene Glycol (PEG) Selection Guide. https://www.sigmaaldrich.com/NL/en/technical-documents/technical-article/materials-science-and-engineering/drug-delivery/polyethylene-glycol-

selection-guide. Accessed March 31, 2022.

72. HS-PEG5K-NH2 HCl Salt, average Mn 5,000 HS-PEG-NH2. https://www.sigmaaldrich.com/NL/en/product/aldrich/jka5145?gclid=Cj0KCQjwg_iTBhDrARIsAD3Ib5h4SCl7r9_ZgmR7hLFm36I2x34nx9zJNGo78gh_YrIwZfipOgbPz-saAo10EALw_wcB. Accessed May 24, 2022.

73. Sephadex G-10 | Cytiva. https://www.cytivalifesciences.com/en/us/shop/chromatography/resins/size-exclusion/sephadex-g-10-p-05610. Accessed June 20, 2022.

74. ÄKTA pure | Cytiva. https://www.cytivalifesciences.com/en/us/shop/chromatography/chromatography-systems/akta-pure-p-05844. Accessed June 20, 2022.

75. Giehm L, Lorenzen N, Otzen DE. Assays for α-synuclein aggregation. *Methods*. 2011;53(3):295-305. doi:10.1016/J.YMETH.2010.12.008

76. Biancalana M, Koide S. Molecular Mechanism of Thioflavin-T Binding to Amyloid Fibrils. *Biochim Biophys Acta*. 2010;1804(7):1405. doi:10.1016/J.BBAPAP.2010.04.001

77. Arosio P, Knowles TPJ, Linse S. On the lag phase in amyloid fibril formation. *Phys Chem Chem Phys*. 2015;17(12):7606. doi:10.1039/C4CP05563B

78. Munishkina LA, Cooper EM, Uversky VN, Fink AL. The effect of macromolecular crowding on protein aggregation and amyloid fibril formation. *J Mol Recognit*. 2004;17(5):456-464. doi:10.1002/JMR.699

79. Uversky VN, Li J, Fink AL. Evidence for a partially folded intermediate in alpha-synuclein fibril formation. *J Biol Chem*. 2001;276(14):10737-10744. doi:10.1074/JBC.M010907200

Appendix A - Labelling of PEG

A polyethene glycol sample (PEG) was chosen as a control to look at the influence of viscosity on the chain dynamics of an ideally disorderly behaving structure. However, due to labelling issues of the PEG, it was not possible to conduct this experiment. Here the steps and troubleshooting of the labelling methods are proposed.

PEG is a hydrophilic polymer that is synthetically polymerised to the desired molecular weight, see Figure 63[71]. A double labelled PEG chain with a molecular weight of 5000 is expected to have a FRET efficiency in a comparable range as the αS samples of interest. The PEG sample has an average molecular weight of 5000, this is assumed to be normally distributed around the mean. The range of weight, and thus size distribution is a result of the polymerisation inaccuracy.

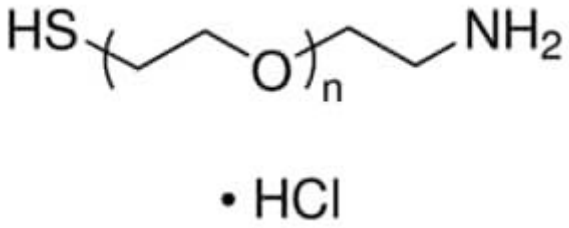

Figure 63: chemical structure of PEG[72]

The samples used are HS-PEG3K-NH2 and HS-PEG5K-NH2 from Sigma-Aldrich[72]. This is a PEG chain with a thiol and an amine functional group attached to either end and has a molecular weight of 3 or 5kDa. The labelling of this sample has probed a lot of issues, the protocol for PEG labelling and the investigation of the origin of the problem are discussed below.

First of all, PEG with two functional groups was chosen, since this should give a high ratio of double FRET labelled sample. The functional groups in question are thiol and amine.

Labelling of HS-PEG3K-NH2

First PEG with a molecular weight of 3kDa was chosen since this has an equal length to 60 amino acids of αS. Upon revision, this sample does not correspond 1 on 1 with the probed distances on aS, the FRET efficiency of the sample seemed to be too high.

For the first labelling try, the 3kDA PEG was labelled using the dyes AF488 with an ester group and AF568 with a maleimide group, since these were readily available.

In general, for labelling procedures filtering is performed with spin columns that have a molecular cut-off, molecules larger than the cut-off size pass the filter and small molecules, like free dye, remain in the filter. However, all available spin columns had a molecular cut-off larger than the size of the PEG which makes them unusable for this application.

A new filtering procedure is set up, where a gravity separation column and a chromatography column are used. The gravity column consists of a gel filtration resin, Sephadex G10[73]. This filter is based on size separation, small molecules pass the filter quicker than large molecules.
For column chromatography, the column Superdex 75 and the Äkta pure system are used[74].

First, the PEG is dissolved in PBS pH 7.4 in a concentration of 1mg/ml. This sample is diluted to 5mM. The PEG contains disulfide bonds that cause trouble with labelling Thiol groups, dithiothreitol (DTT) is used to reduce the disulfide-thiol bonds prior to labelling.

2µL of 1mM DTT is added to a 30µL 5mM PEG sample and incubated for 30 minutes. Then the sample is put on the gravity separation column to remove the excess of unbound DTT. To make sure that all DTT is removed, the filtrate was collected in separate batches of two consecutive drops that came out of the filter. DTT has a distinct absorption peak around 230 nm, the absorption spectrum measured for each batch. The batches that showed a peak at 230 nm contained DTT, so these were discarded. DTT is a smaller molecule than PEG, so it passes the filter quicker. The filtrate that follows the DTT can contain PEG, these batches were combined for further use. Since PEG does not have a clear absorption spectrum it cannot be determined if the PEG is present.
To the filtrate containing PEG, 2µL of 20mM AF488-NHS ester and 50µl of 1.1mM AF568-maleimide dye are added, and incubated for two hours. The PEG and dyes are present in a 1:1:1 molar ratio. After incubation, the free dye is removed from the sample with the Superdex 75 column.

The Äkta pure system showed that more AF568 dye was bound to the PEG dan AF488. This could be because the dye was over 10 years old, after a long time the dye can degrade and the functional group where the dye is attached can unbind.
Only free AF488 dye was observed and no AF594, this could be due to total binding of the dye or due to a smaller size causing it to not come out of the filter so soon.

When looking at the FCS curve of the dye a diffusion coefficient corresponding to free dye was found. In addition, no correlation was seen between the donor and acceptor signal, an indication of the absence of FRET labelled PEG.

It was chosen to not use this sample further due to suboptimal labelling and because the FRET efficiency of the structure is close to one, causing a low donor signal. This is not optimal for nsFCS measurements where both the donor and acceptor signal should be detectable.

Labelling of HS-PEG5K-NH2

A new different PEG sample was chosen with a higher molecular weight, HS-PEG5K-NH2 from Sigma-Aldrich[72]. This polymer, with dyes attached to its ends, is expected to give a FRET efficiency of around 0.6. It was chosen to use fresh dyes, to omit the problem of old dyes. ATTO550-maleimide and ATTO647-NHS ester are used.

The same measurement procedure as explained previously is performed. 2µL 1mM DTT is added to 500µL 0.20mM PEG and incubated for 30 minutes. The unbound DTT is filtered from the sample with the gravity column. Then 81µL 100nM ATTO500-maleimide and 85µL 100nM ATTO647-NHS ester are added to the filtered PEG sample and incubated for 2 hours. Lastly, the free dye is filtered from the sample with the Superdex 75 column.

The Äkta pure system showed that there was no double labelled sample present.
In Figure 64 a picture of a part of the Superdex 75 separation column is shown, here multiple dye bands can be seen. These bands remained in that exact location on the filter. The dye seems to have an affinity with the filter material, which causes it to remain unmoved on the filter.
The manufacturer of the dyes was contacted to report the problem, they stated that no similar problem was reported before.

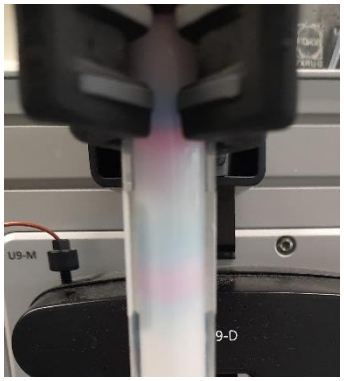

Figure 64: Dye bands on Superdex 75 separation column

The diffusion coefficient is found to be the same as for free dye. It can be concluded that the PEG was not labelled, this was attributed to the interaction between the dye and the Superdex 75 column.

Since the Superdex 75 column cannot be used to filter the free ATTO dye from the sample another method is employed, which uses a filter that consists of another material. The Viva spin 500, 3kMWCO is used for filtering. This is a concentrator that lets small molecules pass the filter, and large molecules not.

The same labelling procedure is performed as described before, except that for both filtering steps the concentrator is used.
2µL 1mM DTT is added to 500µL 0.20mM PEG and incubated for 30 minutes. The unbound DTT is filtered from the sample with the Viva spin 500. Then 81µL 100nM ATTO500-maleimide and 85µL 100nM ATTO647-NHS ester are added to the filtered PEG sample and incubated for 2 hours. Lastly, the free dye is filtered from the sample with the Viva spin 500.

When the free dye is filtered from the sample it is observed that the dye also attaches to the filter of the Viva spin 500, see Figure 65.

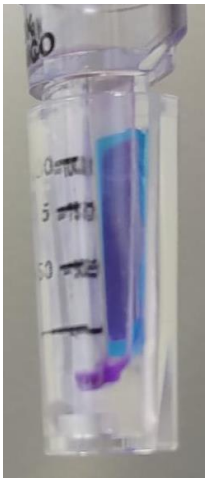

Figure 65: Vivaspin 500 3kMWCO with dye attached to filter

An FCS measurement is performed on the filtrate, the fitted diffusion coefficient is again found to be the same as for free dye. So again the labelling of the PEG was not successful.

There are three possibilities where the problem for the labelling can reside. Either there is a problem with the dye, or with the PEG, or with the filter that the PEG attached to it, so there is no PEG left in the sample.

Troubleshooting

To exclude a problem with the dye, the labelling of another molecule can be assessed.
It was chosen to label BSA with the ATTO647-NHS ester dye since BSA has many NH2 groups where the due can bind. ATTO647-NHS ester binds best in a pH between 8.5 and 9, compared to the used pH of 7.8. Therefore labelling is performed with both pHs in parallel.

To omit the filtering steps a sample with 5x molar excess of BSA is prepared, at this high excess, it is probable that no free dye remains. 25mg/ml BSA was prepared in PBS with a pH of 7.8 and 8.8. 5µL of 1mg/ml ATTO647 was added to 1mL of the BSA solution. The sample is incubated for 2 hours and an FCS is performed. Both samples show a diffusion coefficient of 55, which corresponds to BSA and not free dye. Therefore it can be concluded that the ATTO647 dye is functional.

To exclude a problem with the filter membrane the same labelling procedure is repeated with SH-PEG5k-NH2. For both samples is different pH the FCS-defined diffusion coefficient corresponds to free dye and not PEG. This indicates that the dye was not able to conjugate to PEG.

From the performed experiments it is concluded that the used SH-PEG5k-NH2 is not able to conjugate with dye. This could be due to a manufacturing problem of the PEG itself or due to any unknown different problem.
The problem was reported to the manufacturer, they did not know of similar recurring problems and offered a new product. However, this did not arrive in time to be measured and included in this thesis.

Appendix B - Influence of glycerol on αS aggregation

As an additional experiment to put the behaviour of αS into perspective, the influence of glycerol on αS aggregation is investigated. In the following chapter, a brief explanation is given on the manner of aggregation assays. The results of the influence of glycerol on aggregation behaviour are presented and discussed.

Measuring aggregation

For the detection and investigation of αS aggregation, a simple method is used. The fluorescent dye Thioflavin T (ThT) is used, this dye binds strongly to beta-sheets that are present in amyloid fibrils and experiences a change in fluorescent behaviour upon binding[75]. ThT in free solution emits only a very low fluorescent signal due to self-quenching[76]. The fluorescence is so weak that is below the limit of detection for most microscopes. When ThT attaches to αS fibrils the molecule stabilises and no longer quenches itself, therefore, the fluoresce intensity increases significantly.
ThT is added to samples containing αS, where aggregates are formed, where it attaches to the fibrils and increases the fluorescence intensity of the sample. By measuring the fluorescent intensity over time the process of aggregation can be monitored.

Here the lag time is the parameter of interest, the lag time is the fined as the time where the signal intensity is increased to 10% of the baseline[77]. This is defined as the time of aggregation initiation.

For aggregation to occur there must be a high concentration of αS present. The proteins need to be able to interact or collide with each other to form aggregates. When the αS concentration is extremely low, as in the case of the single-molecule experiment, the chances of collision are small. Therefore, in aggregation experiments, high concentrations are used, in the order of 100µM.

Measurement procedure

To investigate the influence of glycerol on the aggregation of synuclein several samples are prepared. 100µM αS in buffer is used as the control. Samples containing 100µM αS and 11µM ThT with 20, 25, 30 and 35% glycerol are prepared. The samples are placed on a polysterine 96 well plate with a non-binding surface and measured in triplet. The experiment was performed at 37°C. The aggregation process is followed over a time period of 523 hours.

Results and discussion

Figure 66 to Figure 70 and Table 10 show the influence of glycerol on the aggregation lag time of αS. It is seen that with the addition of glycerol the lag time of aggregation is lower than for the control. This suggests that the presence of glycerol creates an aggregation-prone environment for αS.

For increasing glycerol concentration, at 30 and 35%, the lag time increases in comparison to 20 and 25% of glycerol but is still shorter than for the control. It could be that here the viscosity of the sample starts to play a role. Aggregation is diffusion dependent, the αS proteins need to collide with each other to aggregate. In a highly viscous solvent, the proteins diffuse slower and thus fewer collisions occur which causes a longer aggregation lag time.

The observed behaviour of αS is in line with other research, Munishkina et al. showed that 40% and 50% of glycerol shorten the lag time of fibril formation[78]. They also reported longer lag times with increasing glycerol concentration with above 60% an absence of aggregation. The slow down and absence of aggregation behaviour is also attributed to the increased viscosity of the solvent.

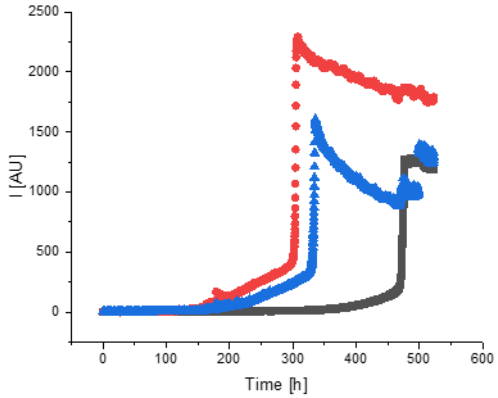

Figure 66: Aggregation assay - control

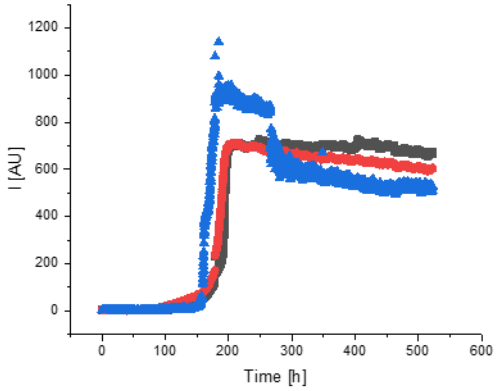

Figure 67: Aggregation assay - 20v% glycerol

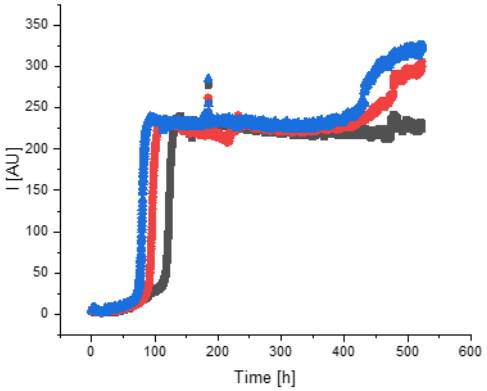

Figure 68: Aggregation assay - 25v% glycerol

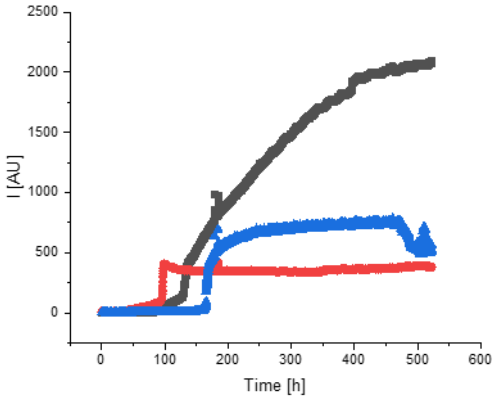

Figure 69: Aggregation assay - 30v% glycerol

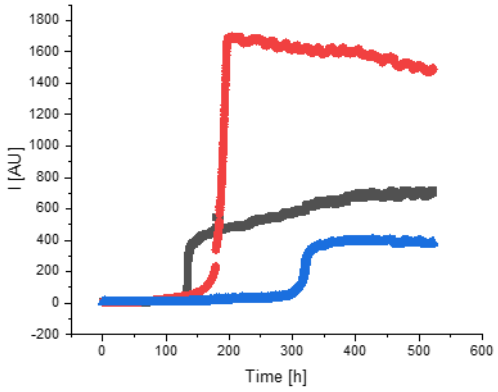

Figure 70: Aggregation assay - 35v% glycerol

Table 10: Aggregation lag time of αS

Sample	Average lag time (h)
Control	113
20v% glycerol	102
25v% glycerol	56
30v% glycerol	74
35v% glycerol	93

The decrease in lag time αS aggregation in presence of glycerol can be explained by the preferential exclusion of glycerol from the αS environment[62,79]. Figure 71 shows a graphical representation of the effect. The exclusion of glycerol causes a thermodynamically unfavourable condition. A solution is to reduce the protein surface that is exposed to the solvent, which can be accomplished by protein aggregation. Thus the presence of glycerol enhances αS aggregation. At higher concentrations of glycerol, the viscosity effect dominates, as stated previously.

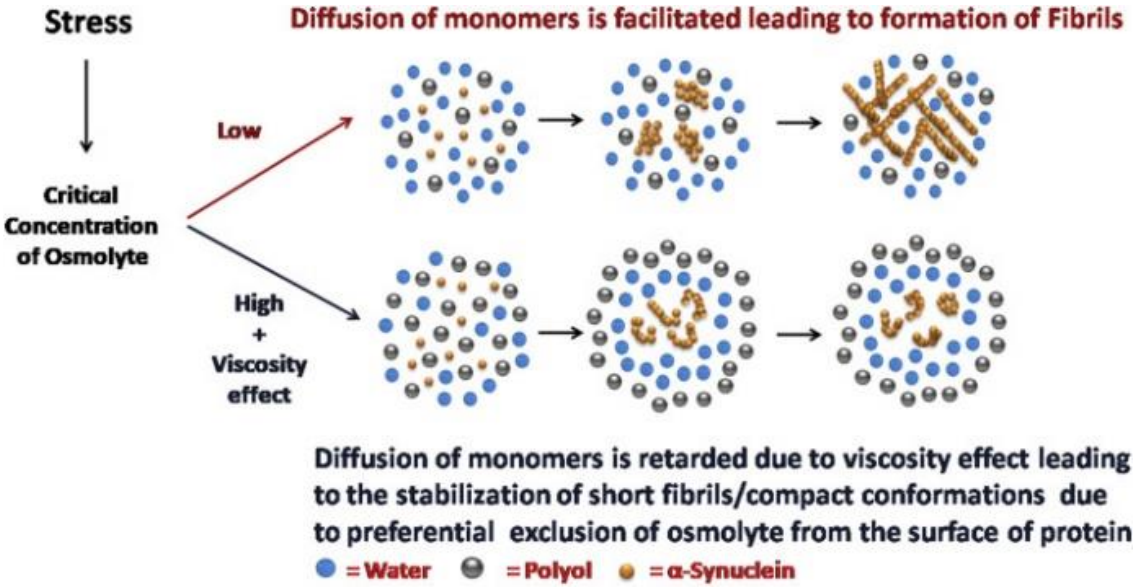

Figure 71: Representation of effect of a polyol, e.g. glycerol, on aggregation facilitation[62]

In conclusion, glycerol is excluded from the direct environment of αS due to the osmophobic effect. At low concentrations of glycerol, this facilitates faster protein aggregation, at higher glycerol concentrations the viscosity effect dominates and aggregation initiation is delayed.